Cardiff
Catalysis Institute

Sefydliad Catalysis
Caerdydd

Photocatalytic Nitrate Reduction under Solar-Simulated Light Using Modified TiO_2

Thomas Caswell

September 2017

Abstract

The purpose of this project is to enhance the photocatalytic activity of TiO_2 for the photocatalytic reduction of aqueous nitrates for application as a solar-catalytic treatment of polluted water. The aim is also to establish a better understanding of the mechanisms by which noble metals enhance the activity of TiO_2. Mono-metallic and bi-metallic Au, Ag and other M-TiO_2 catalysts were prepared with the aim of improving charge-carrier separation, these catalysts were then characterised by XRD, BET and TEM. Preparation method variables such as calcination temperature and metal loading were investigated and found to have a large effect on catalytic activity.

Metal loadings of between 0.3 and 0.4% were found to give the highest activity and this was concluded to be due to an optimum amount of surface coverage by small metal nanoparticles. The catalysts were found to be very selective towards nitrogen with Au catalysts tending to form ammonia at high conversions and Ag catalysts forming nitrite at low conversions. Bimetallic AuAg catalysts were prepared that had higher activities than their mono-metallic equivalents with 100% selectivity to N_2. These catalysts were found to be highly reusable.

None of the prepared M-TiO_2 catalysts were found to have any visible-only activity for nitrate photo-reduction and the enhancement of photo-activity with the deposition of metals was concluded to be due to increased charge-carrier separation effects.

Attempts were made at visibly-active TiO_2 by N-doping but although UV-visible DRS analysis showed a redshift in the adsorption band of these catalysts and XRD found the anatase to rutile ratio to be near ideal no reproducible visible-light activity was achieved.

Acknowledgements

Firstly I would like to thank the UK Catalysis Hub and my project supervisor Professor Graham John Hutchings for giving me the wonderful opportunity to study at the Cardiff Catalysis Institute.

I would also like to thank my post-doctoral supervisor Peter Miedziak for his invaluable support over the course of my study.

I also extend my thanks to the many students and researchers who made study at the CCI fun, even during the toughest of times.

I must express my utmost gratitude to my family and my partner Amber, not only for their unending love and support in all my endeavours but also for igniting in me a passion for all things scientific.

Chapter 1

Chapter 2

CHAPTER 1

1.1 **The Problem of Nitrates**

Safe drinking water, free from contaminants is essential to the function of all of society. It is for this reason that bodies such as the World Health Organisation (WHO) propose guidelines and limits on the concentrations of hundreds of chemical species. These recommendations are based on research undertaken at lead institutions across the globe and are enforced by government legislation. The WHO state that one of their prime principles is that "all people, whatever their stage of development and their social and economic conditions, have the right to have access to an adequate supply of safe drinking water".

Nitrates (NO_3^-) and Nitrites (NO_2^-) are naturally occurring anions that are part of the nitrogen cycle, they are also common contaminants in drinking water and present a significant health hazard if their concentrations are not controlled. Nitrates can become present in drinking water through contamination of ground water, a major source of drinking water. This leeching of nitrates into ground water is most acute in areas of intense agriculture, where highly soluble nitrogen-based fertilisers are used heavily [1]. Studies show that nitrites combine with haemoglobin in the body to form methaemoglobin resulting in the medical condition methaemoglobinemia, or "blue baby syndrome" which, as the name implies, is particularly dangerous in infants. Links between nitrates and cancer have also been established in these studies [2-4]. Compounding this problem is the fact that even if present in harmful concentrations, nitrates and nitrites remain undetectable to human senses as they possess no smell or taste and do not cause discoloration of water. In addition to health risks, high levels of nitrates in natural water sources such as rivers and lakes can cause uncontrolled algal growth that results in deoxygenation of the water and death of large portions of aquatic life. In order to limit human exposure to aqueous nitrates in drinking water, the World Health Organisation (WHO) suggested concentrations of 50mg/L and 3mg/L for nitrate and nitrite ions in water respectively [5].

1.2 Current Solutions

1.2.1 Non-Treatment Options

In many cases, the first course of action when high levels of nitrate are detected in a water source is often a non-treatment option. Non-treatment options include:

- Drilling a new well.
- Better protecting the water source to nitrate contamination.
- Combining of water streams or blending.

The most effective of these options is blending. This simple solution involves blending the nitrate-rich water source with nitrate-lean water from another source to yield water that meets nitrate level standards. In some situations this can be the most cost effective method of solving this problem compared to installing water treatment systems. However there are many cases in which, for various reasons it is not cost effective to blend with other water sources and water treatment options are required [6].

1.2.2 Ion Exchange

Ion exchange is currently the most popular water treatment option for nitrate removal [7]. The principle of ion exchange is that unwanted dissolved aqueous ions can be exchanged using an ion exchange resin for less harmful ions of the same charge. An example of this is the process of water softening in which +2 cations such as Mg^{2+} and Ca^{2+} are exchanged for "softer" cations such as Na^{+} and K^{+} which are stored in the exchange resin.

Nitrates can be removed in a similar manner using strong-base anion exchange resins which are categorised into two types:

- Type 1 resins that use trimethylamine functional groups.
- Type 2 resins that work by using dimethylethanolamine functional groups.

The order of affinity for some common anions found in drinking water are shown below.

Sulphate > Nitrate > Chloride > Bicarbonate

These types of resins are non-selective in that they do not target a specific anion to be removed. Nitrate-selective resins have become available which preferentially remove nitrates

over sulphate or chloride ions. This is achieved by swapping methyl groups on the nitrogen atom of Type 1 trimethylamine function groups for bulkier groups, making it more difficult for divalent anions such as sulphate to be exchanged.

One of the main issues with Ion Exchange technologies is the saturation of exchange resins with the target ion or ions. For example; if a type 1 or 2 exchange resin is run to exhaustion the resin with continue to take up sulphate from the inlet water and dump nitrate into the outlet stream because of sulphate's stronger affinity for these resins over nitrate. To avoid this, these resins must be regenerated by flushing sodium chloride brine through the system which flushes out the accumulated nitrates. This concentrated nitrate brine waste is stored in a dry well or septic tank where some denitrification occurs via anaerobic bacteria. The disposal of this brine waste is one of the major downsides to Ion Exchange as it cannot be disposed of simply [8].

1.2.3 Reverse Osmosis

Reverse Osmosis (RO) technology uses a semi-permeable membrane and high pressure to reverse the process of osmosis and remove dissolved ions, molecules or particles from water [9]. This means that rather than the natural osmatic flowing of water from areas of low concentration of solute to areas of higher concentrations the process is reversed by forcing the solvent (water) using high pressure (2-17 bar for fresh water) from an area of high concentration of solute to an area of low concentration of solute [10]. This technique, developed largely in the 1950's for the desalination of seawater is capable of removing up to 98% of all dissolved inorganic species [11]. Reverse Osmosis is a totally non-selective technique that removes all contaminants including particles in suspension and even bacteria, this makes RO an excellent technique for certain industrial applications in which very pure water is required [12]. In these situations reverse osmosis is often combined with electro-deionisation techniques to achieve nitrate levels below 2 ppm which is required in particular by European Pharmacopeia for water used for injection [13]. This lack of selectivity actually becomes somewhat of a hindrance for purification of drinking water as is it essential for some safe salts to be present when consumed by humans, without these salts a dangerous medical condition known as hyponatremia can occur in which the concentration of sodium in the blood becomes too dilute. Another disadvantage of this technology is the energy required to

generate the pressures necessary to overcome natural osmotic pressure and achieve RO. Some of this spent energy can be recovered in larger RO applications by using turbines driven by the concentrate flow in larger applications or energy recovery pumps used in smaller systems. Although 50% of input energy can be recovered using these methods the process remains relatively costly in terms of energy and in small domestic RO systems only 5 to 15% of water entering the system is recovered with the rest flowing out with the waste water, thus making these systems inefficient. Much like Ion Exchange, a concentrated nitrate brine is produced as a waste product of reverse osmosis which has to be disposed of appropriately [14].

A key factor when considering the application of RO is the higher cost with respect to ion exchange.

1.2.4 Electrodialysis

Electrodialysis (ED) is a technology which has increased in usage over the last few years. ED is a process in which an electric current is used in conjunction with ion exchange membranes to remove dissolved ions from the water. Contaminated water is passed through a thin sheet as an electric current is applied and thus ions are attracted to their counter-charged electrodes, cationic and anionic membranes are placed between the water stream and the electrodes, trapping nitrate, nitrite and other dissolved contaminants [15].

1.2.5 Microbial Methods

Denitrification of water using nitrogen-digesting bacteria is a solution currently employed in many parts of Europe, including the United Kingdom. Its main advantage over ion exchange and RO systems is that biological reduction of nitrates yields mainly benign nitrogen gas as a "waste" product and so the problem of concentrated brines is circumvented. Bacterial denitrification can be separated in to two major categories which differ in the type of electron donor involved, namely heterotrophic and autotrophic processes.

Autotrophic denitrifiers utilise inorganic carbon compounds as the source of electrons for the reduction of nitrates whereas heterotrophic denitrifiers rely on organic carbon sources which are often exogenous (methanol, acetic acid) which increases the costs associated with the

process as well as increasing the toxicological risks associated with adding compounds such as methanol to the water stream [16].

As previously stated, bacterial denitrification methods hold some advantages over other techniques, such as the lack of brine waste, however this is counterbalanced with the increased costs of post-treatment filtration and disinfection associated with this method.

1.2.6 Thermo-catalysis

Pioneering work on thermo-catalytic solutions to the nitrate problem was conducted in 1989 by Vorlop and Tacke [17]. This work showed the effectiveness of bimetallic catalysts in reducing nitrates, specifically a noble metal/base metal combination such as Pd/Fe supported on alumina. From this initial work it was observed that Pd yielded the best results generally compared to other noble metals and so experiments were devised to optimise the activity of the catalyst as well as the selectivity to nitrogen by changing the noble metal : base metal ratio [18-20].

In these bimetallic systems, metal-metal contact is essential in achieving an active catalyst, when metal-metal proximities are close enough the low oxidation state of the promotor metal is more easily maintained by improved spillover from the noble metal; this is essential for activity. Although close metal proximities improve activity, alloy formation was found to decrease the selectivity and the activity of catalysts supported not only supported on alumina but also on zirconia, titania, tin oxide and carbon [21,22].

Although the majority of studies focus on alumina as a support material, studies of bimetallics on the different support materials mentioned above showed higher selectivity to nitrogen when carbon supports were used, largely due to better dispersion of supported metals [23,24].

The catalytic reduction of nitrates takes place in two distinct steps, first by the reduction to nitrite and then a second reduction of nitrite to nitrogen. A major challenge in the catalytic reduction of nitrate is the formation of ammonia from over-reduction, this problem becomes more prominent at higher conversions due to formation of OH^- ions and the subsequent increase in pH. A way to address this issue is to employ an acid additive to neutralise OH^- ions, CO_2 being the most frequently used [25]. Some successful efforts have been made in using formic acid which, upon decomposition, produces both CO_2 and H_2 providing pH control and a reducing agent [26,27].

Monometallic catalysts have also been studied to a lesser extent, with zero-valent iron being a promising early nitrate reduction catalyst [27-32]. In this system, metallic Fe^0 is utilised to reduce nitrate to N_2 with nitrite and ammonia as by-products as well as Fe^{2+} and Fe^{3+}. Although cheap and non-toxic, these iron-based systems require a reducing species to regenerate metallic iron and close the reaction cycle.

Work by Strukal e*t al* proposed the use of Pd-based monometallic catalysts with Sn-based supports being used as a promotor [33]. This work was followed upon later by Epron *et al* who used Pd-based catalysts on CeO_2 and TiO_2 supports [34]. Concerning these systems, the TiO_2 supported catalysts showed an advantage over those supported by CeO_2 in that they exhibited a higher tolerance for CO_2 which acts as a poison in the case of CeO_2. Although promising, these monometallic catalysts exhibited poorer performance than the leading bimetallic catalysts with the exception of work conducted by Pinna and co-workers who were able to achieve comparable results to bimetallics using a Pd/SnO_2 catalyst, attributing the improved activity to the low porosity of the support, negating mass transfer limitations [35].

1.3 Principles of Photocatalysis

A catalyst is defined as a substance that increases the rate of a chemical reaction without being consumed in said reaction by means of lowering the associated activation energy. A photocatalyst can therefore be defined as a catalyst that accelerates the rate of a photoreaction [36]. The use of photocatalysis in the destruction of aqueous nitrates is a relatively new area of research, an overview of which will be given in the next section with this section being used to define photocatalytic principles.

Eqn 1:
$$A + D \xrightarrow[\text{Light} \geq E_g]{\text{Semiconductor}} A^- + D^+$$

Equation 1 concisely sums the general principle of photocatalysis. In this equation E_g is the band gap energy of the semiconductor and A and B are electron accepting and donating species respectively. The equation illustrates the electronic excitation of a semiconductor by light of an energy greater than the band gap energy followed by the generation of reactive ionic species A^- and D^+ from adsorbed species A and D**. Figure 1.1** shows a more detailed representation of photon-induced excitation in semiconductors.

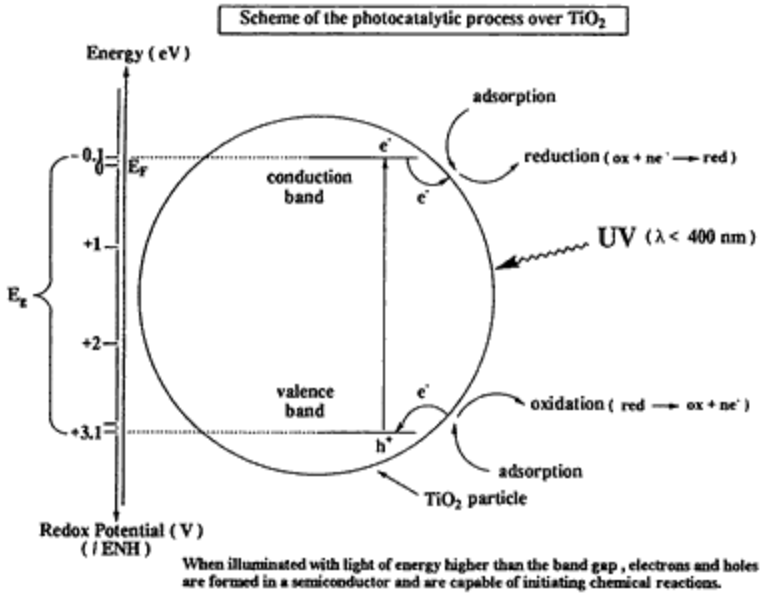

Figure 1.1: Energy band diagram of a spherical titania particle [37]

Unlike the electronic properties of a metal or an insulator, a semiconductor has a small energy gap between its valence band and conduction band. This is opposed to a metal, which has no energy gap between these bands, or insulators which have a very large energy gap between these bands. This inherent property of semiconductors means that when a photon with sufficient energy, I.E an energy greater than or equal to this band gap, strikes a semiconductor electrons residing in the valence band can absorb a photon and be excited to the valence band. This excitation of valence band electrons causes an electron deficiency in the valence band known as a hole, often represented as h^+ as well as an electron build-up in the conduction band represented as e^-. Following the generation of these electron-hole pairs the most common occurrence is their recombination, which is to say that the photo-generated conduction band electron relaxes into the valence band. This occurrence is undesirable in the context of photocatalysis as it prevents any further reactions taking place, a more desirable pathway would be for adsorbed species to react with these electrons and holes forming reduction and oxidation products respectively. The topic of how semiconductor catalysts can be modified to favour the latter pathway will be discussed later in this chapter.

A semiconductor's suitability to catalyse a given reaction is chiefly down to the energies of its conduction and valence band in relation to the redox potentials of the reactions relative to a standard electrode. For an electron donating species to be oxidised on the surface of a

photocatalyst its redox potential must be more negative (higher in energy) than the valence band of the semiconductor. Conversely, for an electron-accepting species to be reduced by a photocatalyst its redox potential must be more positive (lower in energy) than the conduction band of the semiconductor.

1.3.1 Hole-Scavenging Species

In the context of nitrogen reduction, a short-chained organic acid is often employed at the hole-scavenging species although there have been many studies exploring alternatives [38]. Short chained organic acids are justified in their use in this role because they are common side products of Advanced Oxidation Techniques (AOT) which aim to destroy more complex organic contaminants by oxidation. The organic species can either be oxidised directly by interaction with the hole or by interaction with hydroxide radicals formed by the oxidation of water at the hole site. Conversely, reduction can take place either by direct interaction of adsorbed species with photogenerated electrons or secondary reduction following interaction superoxide radicals formed from O_2 at the catalyst surface.

As stated previously, a huge variety of organic species have been explored for their use as hole scavenging species for photocatalytic reactions. Early work conducted by M.R. Prairie [39] investigated the performance of several organic species such as acetic acid, citric acid, EDTA, salicylic acid, ethanol and methanol as hole-scavengers for the photoreduction of aqueous chromate ions. This work highlighted citric acid as being the organic species that yielded the best reaction rate with EDTA also performing well, this was attributed to the chelating effect of these adsorbing species. More recent studies however contradict these findings such as the work conducted by Chenthamarakshan *et al* [40] on the reduction of Cd^{2+} ions. This work yielded the following order regarding the improvement of cadmium reduction rates; formate > methanol > ethanol > n – propanol. An explanation of this trend was given as the differences in the ease of hydrogen abstraction from the alpha position to the hydroxyl group between these species. These findings are corroborated by a large variety of papers such as the 2003 paper by Tan *et al* [38] which investigated various different hole scavengers for the reduction of selenium ions. Although species such as sucrose, acetic acid and salicylic acid were investigated, photocatalytic activity was only observed when using formic acid, methanol or ethanol. Of these activity-inducing scavengers, formic acid was

found to give the best activity for Se^{+} reduction followed by methanol and finally ethanol. Here the authors attribute the superiority of formic acid to its ease of mineralisation and the fact that it very quickly formed species such as $CO_2^{-\cdot}$ which were theorised to reduce nitrate upon interaction. This trend holds true for nitrate reduction also and has been observed in the work of Anderson in which formic and acetic acid along with their sodium salts were used as hole scavengers for the photoreduction of nitrate by a 1%Cu/TiO_2 catalyst under UV light [41]. In this study, formic acid was once again found to yield higher activities with 100% conversion achieved after 3h. It was noted that formic acid was the least selective of the hole scavengers tested with a selectivity of 67% with the major by-product being ammonia. The poor selectivity of formic acid was largely attributed to the higher conversions observed when using it compared to the other hole scavengers which all converted less than 20% of nitrate after the same 3h reaction time. This was confirmed by extending the reaction time when using the other hole scavenging compounds until similar conversions had been achieved and noting that the selectivities to N_2 were only slightly higher than that of formic acid.

1.4. TiO_2 as a Photocatalyst

Several materials meet the criteria to be effective photocatalysts, most of which are metal oxides such as ZnO_2 and CeO_2 as well as some metal sulphides such as ZnS. Of these semiconductor materials, TiO_2 has some desirable characteristics which make it the most widely researched photocatalyst in recent history. These characteristics include its low cost, thermal stability and lack of toxicity as well as, in relation to nitrate reduction, desirable valence and conduction band energies. The specific position of these bands makes titania a strongly oxidising and mildly reducing photocatalyst, a comparison between the valence and conduction band energies is shown in **figure 1.2** below.

The relative energies of the valence and conduction bands of titania make the following reactions thermodynamically feasible in the context of nitrate reduction.

$$E^{0}(NO_3^-/NO_2^-) = 0.49 \text{ V} \quad \textbf{(Eqn 1)}$$

$$E^{0}(NO_3^-/N_2) = 1.25 \text{ V} \quad \textbf{(Eqn 2)}$$

$$E^{0}(NO_2^-/N_2) = 1.23 \text{ V} \quad \textbf{(Eqn 3)}$$

And in an aqueous environment the following reaction with oxygen is possible which is in direct competition with the nitrate reduction reaction.

$$E^0(O_2/H_2O) = 1.23 \text{ V}$$ (**Eqn 4**)

From these equations it can be seen that the possible by-products formed from the photocatalytic reduction of nitrate by titania are nitrite from under-reduction of nitrate, ammonia from over-reduction, water from the competing oxygen reduction and the desired end-product nitrogen. Another observation that can be made from **figure 1.2** is the sizable band-gap in comparison to some of the other semiconductors presented.

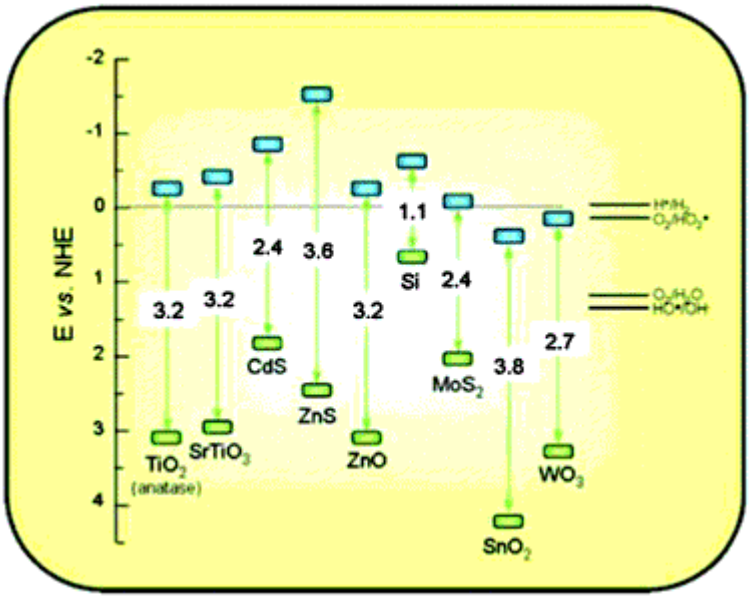

Figure 1.2: Band gaps (eV) for a variety of semiconductors [42]

This band gap of 3.2 eV eliminates photons in the visible-light regime from being able to excite a valence band electron in TiO_2, instead only a photon in the UV (B) region of the electromagnetic spectrum will suffice. This limits TiO_2 as a photocatalyst especially for solar applications because only around 6% of the suns radiation contains photons of a sufficient energy to induce catalysis.

Efforts to modify TiO_2 in order to broaden the range of photons available for catalysts have been made and will be discussed later in this chapter.

1.4.1 Structure and Properties of TiO_2

Titania exists in three main polymorphs; anatase, rutile and brookite. Of these three types, rutile is the most thermodynamically stable with the meta-stable anatase and brookite polymorphs transforming into rutile at temperatures around 600°C. Regardless of polymorph, the structure of titania remains the same with six oxygen atoms coordinating to a central Ti^{4+} cation forming chains of TiO_6 octahedra. The structural differences between anatase, rutile and brookite are in the linking together of these TiO_6 structures and work in the 1990's by Linsebigler *et al* describes in detail the differences between these structures and how these differences lead to electronic differences in the polymorphs [43]. This work shows that in anatase the octahedra share vertices in the 001 plane forming tetragonal structures while rutile TiO_6 structures share edges in the 001 plane, brookite octahedra share both edge and vertices forming an orthorhombic structure.

These differences in structure lead to a difference in electronic properties such as bandgap, which has been shown to be 3.2 eV for anatase, 3.0 eV for rutile, and 3.2 eV for brookite. In practice anatase and rutile are the most widely studied of the three polymorphs and so will be focused on more intensely during the course of this review. Of anatase and rutile, the former has been found to be the more active phase in general despite the lower band-gap of the latter. Although there is no strong consensus as to why this is the case it can be explained in part due to simple surface area effects as there is an increase in crystallite size from around 50 nm to around 200nm when moving from the anatase to the rutile phase [44]. Other more complicated suggestions have been made such as the probability of electron emission upon irradiation being proportional to the electron density near the Fermi energy. Computational studies conducted by Ju-Young Park *et al* using the DFT method concluded that the density of states within an energy window of ±1 eV of the Fermi energy was higher for anatase than rutile [45].

While this is true, the same study also found a higher density of states within the same energy window for the rutile phase, suggesting that on this basis alone it should be the more active of the phases. The reason this is not the case is because photocatalytic efficiency is not based solely around density of states near the Fermi energy. It is theorised in this paper that if the structural conditions of rutile were more similar to that of the other morphologies in this respect it would be the most photocatalytically efficient.

Other explanations of the superiority of anatase suggest the larger band gap may improve efficiency for certain reactions due to the increase in energy of the valence band [46]. While this increase in energy limits the amount of photons available to a narrower spectrum of light it also means the photogenerated electrons are of a higher energy and thus increases the reductive power of these electrons.

As mentioned previously, a photon-generated electron/hole pair must avoid undergoing recombination for them to participate in chemical reactions, it has been established by Riegel *et al* that there is a higher effective rate constant for recombination on the surface of rutile than on that of anatase, making the latter a more efficient photocatalyst [47]. Charge transfer also plays an important role in determining efficiency of a given morphology, when a hole/electron pair is generated in the bulk its ease of mobility to the surface is crucial to participating in reactions within its lifetime. Luttrell *et al* concluded in a recent paper that these charge transfer effects are highly important by comparing the photocatalytic activity of thin films of anatase and rutile of different thicknesses [48]. It was found that for thin films less than 2nm in depth the rutile morphology yielded the best activity, but while the activity with regards to rutile remained relatively unchanged with increasing thickness the activity of anatase increased up to a thickness of 5nm, proving that charge carriers for potential photocatalysis can be generated much deeper in the anatase phase than the rutile and thus explain its superiority as a photocatalyst.

From this then it can be seen that the effectiveness of a given phase of TiO_2 as a photocatalyst depends on its application and a variety of other factors as mentioned above with anatase being reported as being the most active phase in the vast majority of cases. The usefulness of the rutile phase however presented itself unexpectedly during the development of mixed phase titanias for use as paint pigments [49]. Of these mixed phase catalysts, an 80:20 anatase to rutile catalyst made by Degussa known as P25 showed an especially pronounced improvement over the single phases, making it the subject of a vast amount of study. The details of this synergy between phases is given in the next section.

1.5 Improving Titania

1.5.1 Reducing Charge Carrier Rates

Mixed-Phase Systems

One of the main ways in improving the activity of titania-based photocatalysts is minimising the rate at which electron/hole pairs recombine. This can be done in a variety of ways such as using metal nanoparticles as electron sinks, using a mixture of titania phases or using a composite system that utilises titania along with another compound such as CdS [50]. To begin we will discuss the use of mixed phase titania systems.

Early work exploring the improved activity of these early mixed phase catalysts, which in many cases outperformed pure anatase, attributed the higher activity to the transfer of photogenerated electrons from anatase to less energetic sites in the rutile phase conduction band, further improving the lifetimes of the charge carriers. This model is known as the "rutile sink" [51]. More recent research however has cast some doubt over this hypothesis by taking into account the energies of lattice and surface trapping sites which can have significantly lower energy than those of both anatase and rutile conduction bands [52]. A study by Huram and Rajh in 2003 used EPR spectroscopy to better understand the superior performance on P25 and proposed that rutile, contrary to acting as an electron sink, is actually a point of origin of photogenerated electron/hole pairs [53]. The paper suggests that there is then transfer of electrons from rutile to anatase lattice sites which subsequently migrate to surface trapping sites. This transfer of electrons means that rutile-originating holes that would normally suffer recombinations can also migrate to the surface and participate in oxidation reactions. The paper emphasises the importance of the small size of these rutile crystallites in enhancing photocatalytic activity through very intimate contact with anatase.

In conjunction with this enhanced charge separation the addition of rutile to anatase also increases the range of photoactivity into the visible region because of its smaller band-gap, these effects combine to form the "rutile antenna" model. **Figure 1.3a** illustrates the previously hypothesised role of rutile while **figure 1.3b** shows the mechanism proposed by the paper.

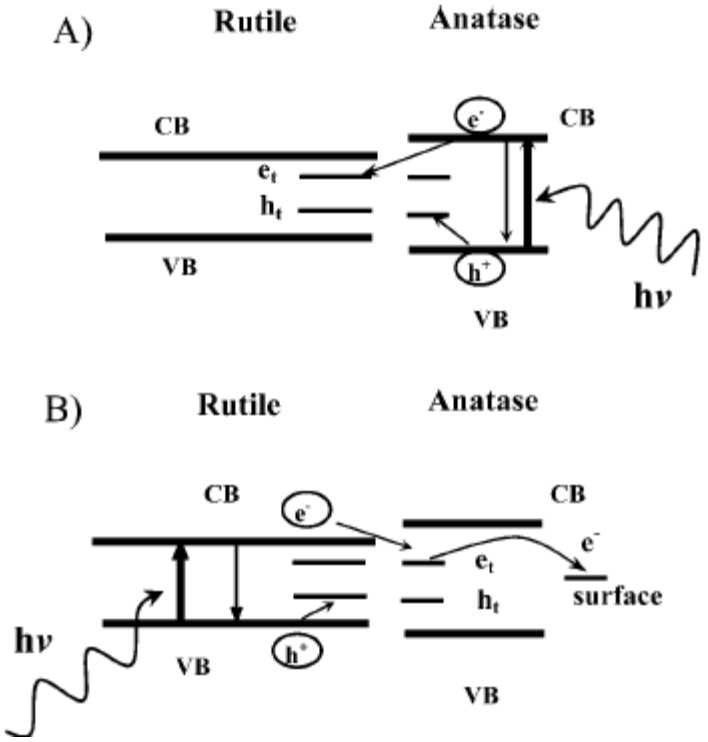

Figure 1.3: Diagrams illustrating A) the previously hypothesised role of rutile. B) The mechanism proposed by the authors. [53].

A third model proposed by Ranjith *et al* supports elements of both the "rutile sink" and "rutile antenna" models by suggesting that the roles of anatase and rutile are not the same under both UV and visible-light radiation [54]. Under equilibrium, there has been shown to be a barrier potential of 0.2 V between the anatase and rutile phases in the band-bending region [55]. Illumination of this system results in the equal probability of electron excitation to the interfacial conduction band from both phases and thus the band structure remains almost unchanged from equilibrium. Under these conditions, the lower energy rutile conduction band will draw electrons away from the anatase conduction band and the rutile will act as an electron sink. Conversely, under visible-only illumination the rutile phase is the sole absorber of photons resulting in a rearrangement to a band structure that favours electron transfer to anatase. Again the authors emphasise the importance of small rutile crystallite size as this is directly proportional to the size of the barrier potential region, the smaller the crystallite size, the easier the charge transfer to the surface.

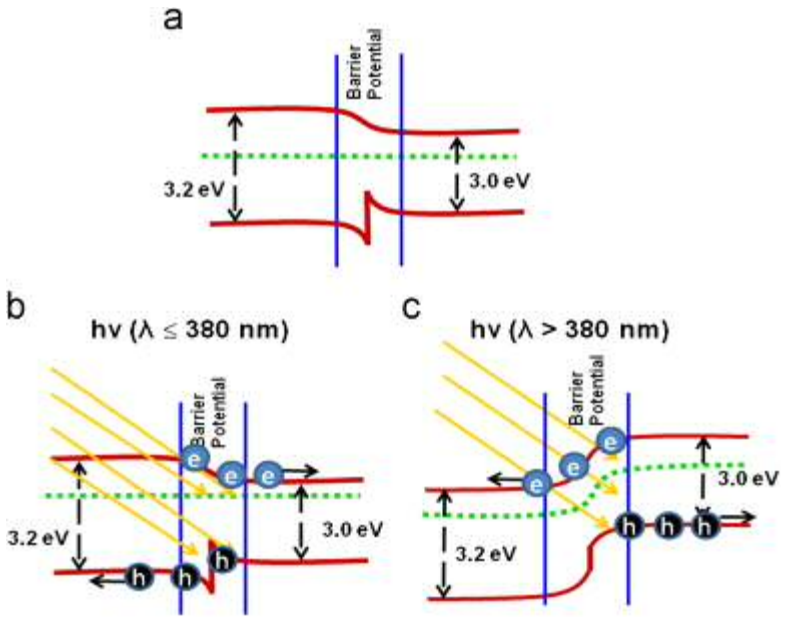

Figure 1.4: Diagrams illustrating; a) band structure of mixed-phase titania at equilibrium. b) The band structure when illuminated with U.V light. c) The band structure when irradiated with visible-only light [54].

As mentioned previously some promising improvements have been made to pure-phase titania catalysts by combining TiO_2 with other semiconductors. The aim of this is largely the same as that for adding rutile to anatase, which is to say that by employing a semiconductor with a lower band-gap the useful range of photons from sunlight can be extended. This method can also serve to improve charge carrier separation via the formation of hetero-junctions and Schottky barriers which send photogenerated electrons and holes in separate directions. With respect to nitrate reduction specifically this approach can have the beneficial effect of preventing the reduction of protons, a reaction which has been blamed for the excessive oxidation observed compared to stoichiometric values. This works via the transfer of electrons from the TiO_2 conduction band to a material with a lower band-edge [56]. Carbon nanotubes and C_{60} fullerenes are also examples of co-compounds that can be added to titania and improve charge-carrier separation [57-59].

Metal Co-Catalysts

There are many examples of increased photo-efficiency being achieved via the deposition of metal nanoparticles onto semiconductors [60-68]. The principle method by which this achieved is widely agreed to be due to improved charge-carrier lifetimes through the metal acting as an electron sink. This influx of electrons to the metal nanoparticle also serves to negatively shift the Fermi energy of the metal and increase the reductive power of the system [69].

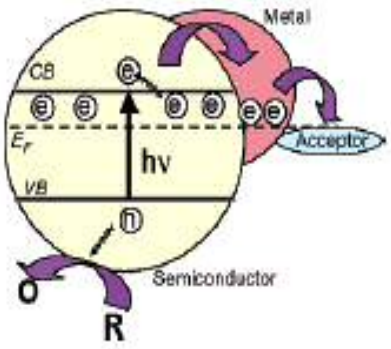

Figure 1.5: Enhancement of photocatalytic activity of TiO_2 with deposition of noble-metals via the SPR effect [69].

There is some conflict within the literature as to whether titania is active for the photo-reduction reaction with some reports stating that titania alone is completely inactive [70], and others reporting minimal activity with high selectivity to N_2 [71]. Regardless of this apparent discrepancy, it is well agreed upon that the addition of nanoparticular metal to titania results in a significant improvement in activity for a number of reactions, including nitrate reduction. Of the metals used to enhance the activity of titania, noble metal nanoparticles (NMNP's) are the most widely studied. An important characteristic of NMNP's are their absorption of visible-light via a phenomenon known as the surface-plasmon resonance (SPR) effect (**Figure 1.5**).

This effect has been credited with improving the activity of titania catalysts in a similar manner to the "rutile antenna" model discussed earlier; by extending the range of useful photons into the visible range. The SPR effect is a result of oscillations in the noble-metal surface electrons caused by an oscillating electro-magnetic field, the exact details of how these oscillations result in increased visible-light activity is debated in the literature. Tian *et*

al propose a charge-transfer mechanism in which metal surface-electrons are excited by visible light and are subsequently injected into the titania conduction band from which they are available to participate in chemical reactions [72]. An alternative mechanism by which plasmonic resonance enhances visible activity is based around the enhancement of local electric fields around NMNP's [73].

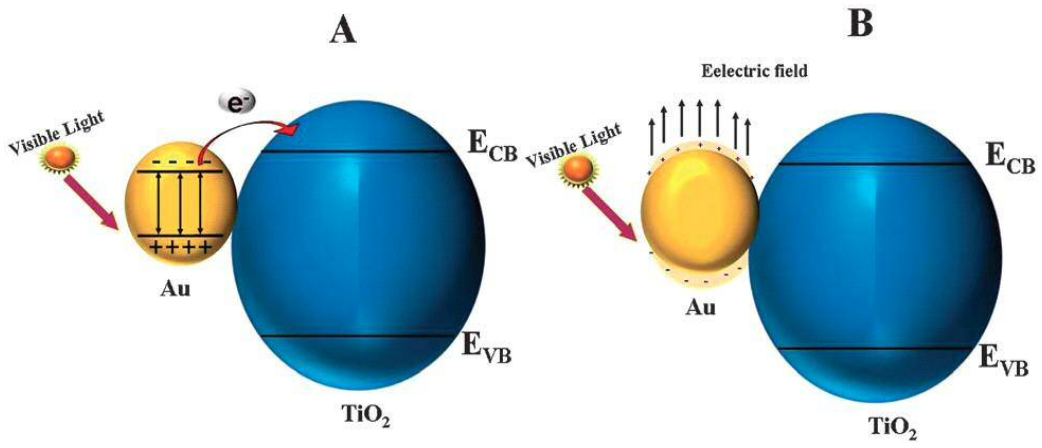

Figure 1.6: SPR enhancement of TiO_2 showing A) direct injection model and B) enhancement of local electric fields [73]

This idea proposes that the electronic oscillations caused by visible light results in large increases in the intensity of the electromagnetic fields at the metal-semiconductor interface and that this increase in electromagnetic field allows these electrons to become available for chemistry, rather than direct charge transfer. A comparison of these proposed mechanisms is illustrated in **Figure 1.6.** Simulations carried out by Liu *et al* gave credence to the electronic field enhancement mechanism [74].

As with the mixed-phase titania catalysts, the mechanism by which NMNP's enhance the activity of titania is different under different energies of irradiation. While under visible-light irradiation, NMNP's exhibit the SPR effect as described above. When excited with UV light however no SPR effect is present and instead the metal acts solely to reduce charge-carrier recombination rates (**Figure 1.7)**.

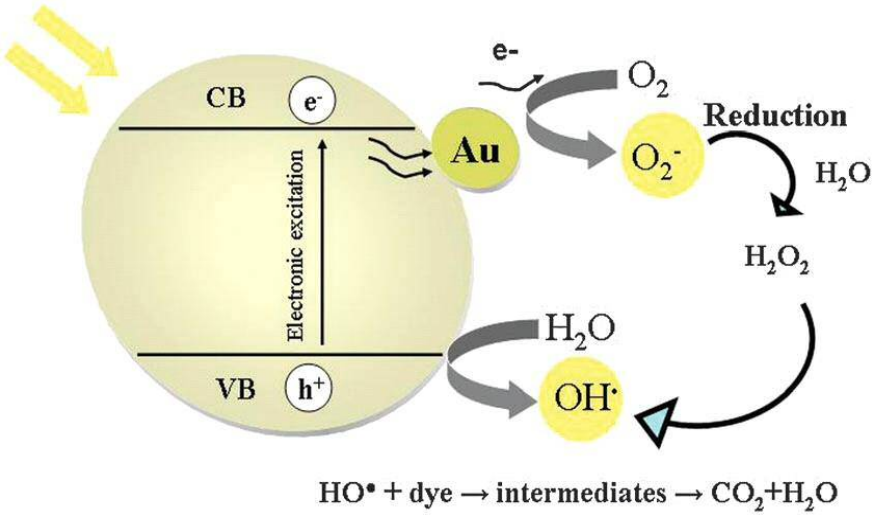

Figure 1.7: Enhancement of photocatalytic activity by metal doping via improved charge carrier separation [75]

This charge carrier separation is attributed to the formation of Schottky barriers at the metal/semiconductor interface [75]. A Schottky barrier is a potential energy barrier that an electron faces at a metal/semiconductor junction that causes a charge separation space, with electrons migrating to the negatively-charged metal surface which conversely leaves the titania surface with a positive charge. The transmission of charge-carriers across the Schottky barrier is determined by the barrier's height which is in turn dependent on factors such as the work function of the metal.

Factors Influencing Performance of NMNPs

There are several different factors that each play a part in determining the exact function of NMNPs on titania. These factors include have been subject to much investigation in the literature and include; particle size, morphology of particle and the metal dosage. In terms of particle size, the general consensus up until recently has been that that photo-catalytic activity increases with increasing NMNP size. In spite of this however, many studies present arguments to the contrary such as a 2003 study conducted by Subramanian *et al* in which the observed increase in photo-generated current with decreasing Au particle size was attributed

to a negative shift of the Fermi energy of the metal. This negative shift in the fermi energy of the Au is thought to increase the reductive efficiency of the catalyst. Other studies are in agreement with the work of Subramanian such as work by Bumajdad *et al* who noted an increase in the rate of the photocatalytic degradation of Safranin-O with decreasing nanoparticle size [76]. As well as citing decreasing metal fermi energy as an explanation of this phenomenon, Bumajdad also mentions several other factors that could lead to smaller metal nanoparticles being more active than larger ones, the most obvious of these being the increase in Au surface area with smaller particles.

In a relatively recent study Murdoch *et al* observed that the photocatalytic activity of 1%Au/TiO_2 catalysts increased with increasing Au particle size within the range of 3- 12 nm [77]. When normalised to give activity per atom of Au however the activity was found to be independent of particle size within this range. A drop in the specific activity per atom of Au was observed when the particles became bigger than this range, this was simply attributed to there being fewer metal-semiconductor interfaces per atom compared to catalysts with smaller Au particles. An interesting observation was also made about the nature of Au nanoparticles on different phases of titania, it was found that the mean particle size of Au on anatase was smaller than that for rutile (**Figure 1.8**). This effect was attributed to the greater interaction of anatase with Au nanoparticles because of its higher Fermi level, which in turn inhibits Au agglomeration during calcination.

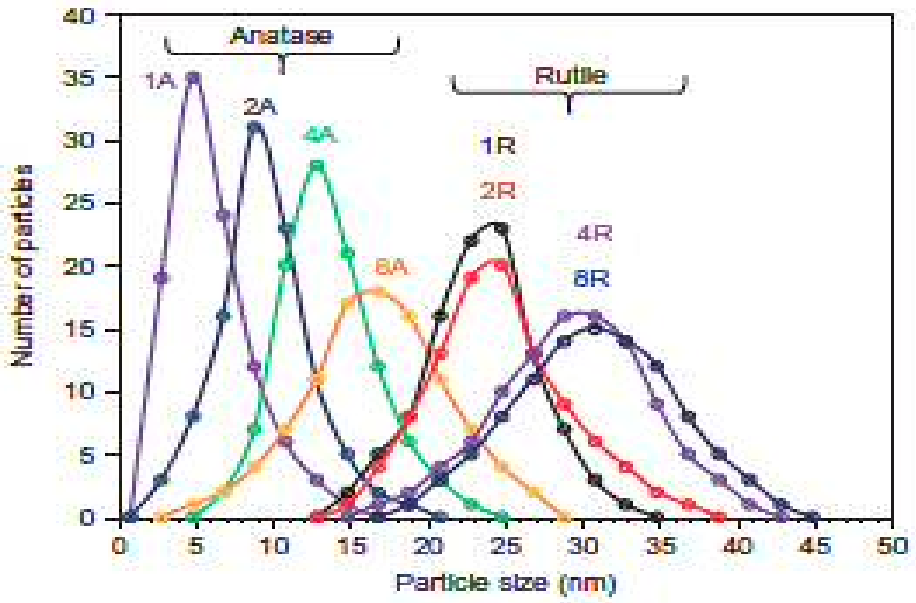

Figure 1.8: Au particle size distribution with increasing metal loading [77]

The dose of metal used is also an extremely important factor in determining its effect on photoactivity. As a general rule, photoactivity increases with increasing metal content up to a certain point after which certain detrimental effects start to dominate.

1.5.2 Band-gap Modification

As mentioned previously, the problem of titania's large band-gap can be somewhat remedied by using mixed phase systems and the "rutile antenna" effect. Similarly, gold nanoparticles have been shown to be able to extend the useful range of photons utilising visible-light to generate photo-electrons via the SPR effect. There are however a variety of other ways in which the band-gap problem has been tackled; these fall into the following categories:

- metal-ion doping
- Non-metal doping
- Dye sensitisation

The first of these methods is a widely studied field with metals such as Cr, Co, V and Fe typically being used [78-80]. As opposed to the use of metal co-catalysts, this method introduces the transition metals directly into the lattice structure of titania, typically using the sol-gel method, resulting in atomic distribution of dopant into the lattice. The goal here is to

effectively lower the band-gap of titania by introducing metals that have redox energy states between that of the valence and conduction bands of titania, creating intraband states near the valence or conduction bands. These intraband states allow for visible-light excitations and thus a red-shift in the observed band gap of the semiconductor.

When considering the choice of transition metals it has been found to be preferable to use elements with partially filled electronic shells rather than elements with closed-shell configurations. More specifically Choi *et al* showed in their 1994 paper that closed-shell dopants failed to improve the activity of the catalyst for the photolysis of carbon tetrachloride over plain titania (Li^+ , Mg^{2+}, Al^{3+}, Zn^{2+}, Ga^{3+}, Zr^{4+}, Sn^{4+}, Sb^{5+}), whereas dopants with partially-filled shells showed only a little improvement in activity [81]. More considerable increases in activity were observed however when using dopants with a half-filled shell configuration such as Fe^{3+}.

The paper theorised that as Fe^{3+} encounters a photo-generated electron or hole it is reduced or oxidised to Fe^{2+} and Fe^{4+} respectively. Crystal field theory shows these oxidation states of iron to be unstable and thus the charge can be easily passed on from these ions to adsorbed oxygen/hydroxyl groups. In addition to effectively lowering the band-gap of titania, metal-ion doping is also theorised to improve the activity of titania by promoting the existence of Ti^{3+} states. These Ti^{3+} states have been shown to promote the adsorption of oxygen to the catalyst surface by creating oxygen defects within the lattice [82]. These oxygen defects help form O^{2-} radicals from adsorbed oxygen which can then go on to reduce target compounds. While Fe^{3+} showed a marked improvement over other dopants, the low pH environment resulting from the use of organic acids meant that leaching of Fe became a significant problem. A common benchmark reaction for determining the activity of photo-catalyst is the degradation of organic dyes such as methylene blue or methyl orange. Khairy *et al* tested the performance of Zn and Cu-doped catalysts prepared using the sol gel method for methyl orange degradation under visible and UV illumination [83]. It was found that the addition of metal ions into the TiO_2 lattice improved the activity of titania both under UV and visible-only light, with pure titania showing almost no activity under visible-only irradiation. Cu^{2+} was found to increase the photocatalytic efficiency more than Zn^{2+} although the paper did not offer an explanation as to why Cu^{2+} outperformed Zn^{2+}. UV-visible absorption

spectroscopy revealed a red-shift in the absorption edge for both the Cu and Zn-modified catalysts.

As well as metal-ion doping some non-metal elements have been the focus of scientific study for the purpose of band-gap alteration in titania. Of these elements the most widely studied are S and N, although many of the p-block elements have been studied in recent times [84-86]. These non-metal dopants are expected to effectively lower the band-gap of titania by means of substituting an oxygen atom in the titania lattice, the 2p orbital of an element like nitrogen will then lie between the valence and conduction bands of the titania, enabling visible light absorption; the lower the atomic number of the dopant element, the higher in energy these 2p states are. Unlike metal dopants however, non-metal dopants do not act in an electron-trapping way and thus do not improve charge-carrier separation in the catalyst.

As well as substituting an oxygen atom, these elements can bind to lattice atoms, occupying interstitial positions rather than replacing atoms in the lattice. This gives rise to slightly different electronic effects but crucially still gives rise to the formation of extra states within the band-gap.

The methods upon which these elements are introduced into the lattice vary, with some using "dry" methods such as partial oxidation of TiO_2 precursors such as TiN and others using "wet" chemical techniques such as sol-gel synthesis. It is interesting to note that N-TiO_2 was initially produced by heat treating TiO_2 at high temperatures under a stream of ammonia gas [87].

Often times, a combination of methods is used to try and boost the efficiency of titania as a photocatalyst. A combination of dopants that has been particularly scrutinised is nitrogen-iron codoping [88-90]. These studies all agree on an observed red-shift in the absorbance of titania post-doping and attribute the improvement in activity to extra intraband energy levels created by substituting oxygen atoms with nitrogen atoms, with the iron either contributing by adding intraband levels of its own if incorporated into the lattice or improving charge-carrier separation as an oxide if deposited on the surface. A recent example of this type of codoping is displayed in Arman Sikirman and Jagannathan Krishnan's 2015 paper, in which a combination of nitrogen and iron doping was used to enhance the activity of a sol-gel titania catalyst for the degradation of methylene blue [91]. As a result of the doping, the authors

noted an increase in the surface area of the resulting catalysts over plain titania, with the surface area as determined by BET analysis of N-Fe-TiO_2, N-TiO_2, Fe-TiO_2, and pure TiO_2 were found to be 88, 74.72, 42.96, and 42.82m^2/g, respectively. As well as a surface increase the authors noted an increase in absorption edge as determined by UV-Visible diffuse reflectance spectroscopy, with the band gap energy for N, Fe-codoped TiO_2, N-doped TiO_2, and Fe-doped TiO_2 are 2.33, 2.88, and 3.17 eV, respectively. From this data it can be seen that both the nitrogen and the iron contribute to the formation of intraband states that serve to lower the band-gap, with nitrogen contributing much more than iron in this regard. The paper speculated that the synergy observed between these two dopants in this respect was due to N 2p orbitals mixing with O 2p orbitals to form a new valence band level while the iron 3d orbitals (Fe^{3+}) served to effectively form a new (lower) conduction band.

Under visible-light irradiation the plain titania showed no activity for methylene blue degradation, unlike the doped catalysts of which the co-doped N-Fe-TiO_2 was the most active, destroying around 80% of the dye after 240 minutes of reaction time. It is unclear whether the superiority of the co-doped catalyst is due to changes in the titania band-gap or the increase in catalyst surface area.

As well as metal/non-metal co-doped catalysts a popular modification of titania is with non-metal/noble metal co-modification. In this method nitrogen is doped into the titania lattice while the noble-metal is deposited on the surface. An elegant preparation of an Ag/N-TiO_2 catalyst can be found in a recent paper by Sun *et al* in which TiN precursor is sonicated in a beaker full of $AgNO_3$ solution for 2h followed by drying and heat treatment at 500°C. The results of this experiment showed that the co-modified catalyst showed a 6.5 fold increase in visible light activity for the degradation of methylene blue over plain titania and a 3 fold increase in activity over N-TiO_2. The enhanced photoactivity of the co-modified catalyst was attributed to a combination of increased visible-light response and increased electron/hole separation due to a synergistic interaction between Ag and N.

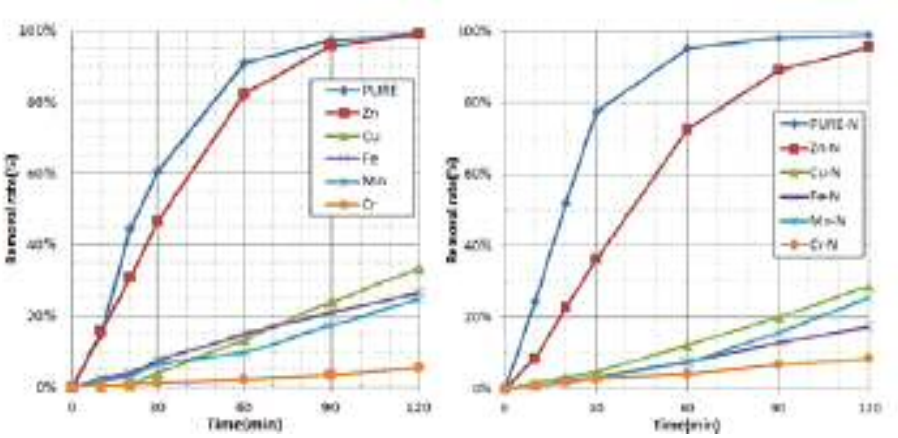

Figure 1.9: Activity of metal and N co-doped ZnO for photodegredation of organic dyes [92]

There is a counter argument to this line of investigation that says that non-metal impurities introduced into the TiO_2 lattice act as centres for charge-carrier recombination. In a 2014 paper by Wan-Su Kim *et al* transition metal-doping using Chromium, manganese, iron, copper, and zinc was carried out in conjunction with nitrogen doping in an effort to improve the UV(A) activity of these catalysts [92]. Metal-only-doped catalysts were prepared along with the dual metal-nitrogen-doped catalysts, the catalysts were prepared by a sol-gel method that utilised metal nitrate salts to incorporate the desired metal ions and urea to introduce nitrogen into the lattice.

From the activity data (**Figure 1.9**) it can be seen that pure titania is the most active of all the catalysts tested, and that while Zn-doped titania performs similarly to plain titania, the addition of metal and non-metal dopants seems to have a detrimental effect on activity.

1.6 Project Objectives

The objective of this project is to enhance the photocatalytic activity of TiO_2 for the reduction of aqueous nitrates under solar simulated radiation for the purpose of water-treatment primarily using metal-modification

In Chapter 3 the operational parameters that affect the activity of M-TiO_2 catalysts such as reaction temperature, reactant concentration and catalyst loading are investigated and the results of blank reactions are reported. The incipient wetness preparation method is systematically optimised by investigating factors like calcination temperature and metal loading and characterisation techniques such as XRD, BET and TEM are used to derive explanations to the effects observed. The reusability of these catalysts is also investigated.

In Chapter 4 the use of alternative metals to gold is explored and once again the dependence on weight loading is investigated. Bimetallic catalysts are investigated to ascertain if synergistic effects are present when depositing more than one metal on titania. The effect of catalyst poisoning by Cl^- and SO_4^- is investigated to test the catalyst applicability in real world water systems.

Efforts are made into the improving of the visible-light activity of titania by doping with nitrogen, the results and subsequent characterisation by UV-Vis DRS and XRD are detailed in this chapter.

Finally, Chapter 5 summarises the results obtained from all experiments and gives details of proposed future works.

1.7 References

[1] Pyriproxyfen in Drinking-water: Use for Vector Control in Drinking-water Sources and Containers
Background document for development of WHO Guidelines for Drinking-water Quality

[2] Report from the Commission to the Council and the European Parliament. On implementation of Council Directive 91/676/EEC concerning the protection of waters against pollution caused by nitrates from agricultural sources based on Member State Reports for period. 2004–2007, 2011.

[3] Nitrate in Drinking Water, Gregory D. Jennings and Ronald E. Sneed, Biological & Agricultural Engineering, Published by: North Carolina Cooperative Extension Service Publication Number: AG 473-4

[4] Bosch, H.M., A.B. Rosefield, R. Huston, H.R. Shipman and F.L. Woodward. 1950. Methemoglobinemia and Minnesota well supplies. J. Am. Water Works Assoc. 42: 161-170.

[5] C Mary, Cancer epidemiology, biomarkers & prevention: a publication of the American Association for Cancer Research, cosponsored by the American Society of Preventive Oncology Volume: 22 Issue: 9 Pages: 1637 DOI: 10.1158/1055-9965.EPI-13-0641 Published: 2013-Sep, PubMed ID: 23833123

[6] Nitrate and Nitrite in Drinking-water, Background document for development of WHO Guidelines for Drinking-water Quality World Health Organization 2011.

[7] Desilva, FJ. (April 2003). Water and Wastes Digest.

[8] Department of New Hampshire, Environmental Fact Sheet (2009)

[9] Jensen V, Darby, J. (2009). Technical Report 6: Addressing Nitrate in California Drinking Water. Report for the State Water Resources Control Board Report to the Legislature.

[10] Crittenden, J; Trussell, R; Hand, D; Howe, K; Tchobanoglous, G (2005). Water Treatment Principles and Design, Edition 2. John Wiley and Sons. New Jersey. ISBN 0-471-11018-3

[11] Glater, J. (1998). Desalination. 117: 297–309. doi:10.1016/S0011-9164(98)00122-2.

[12] Jollibee, Merci (29 September 2015). "History of Reverse Osmosis System"

[13] Henrik Bilidt (1985). Desalination. Volume: 53. Issues: 1–3. Pages 225–230

[14] SUEZ environnement Water Purification Systems UK Purite Ltd, "Nitrates and the Quality of Water" article (2015)

[15] Weber, Walter J. (1972). Physicochemical Processes for Water Quality Control. New York: John Wiley & Sons. p. 320

[16] A.Rozanska, J.Wisniewski (2003) Institute of Environment Protection Engineering Wroclaw University of Technology Wybrzeze Wyspianskiego.

[17] Mohseni-Bandp, A; Elliott, D; Zazouli, M. J Environ Health Sci Eng. 2013; 11: 35

[18] K.D. Vorlop, T. Tacke Chem. Ing. Tech., 61 (1989), pp. 836–837

[19] S. Horold, T. Tacke, K.D. Vorlop Environ. Technol., 14 (1993), pp. 931–939

[20] S. Horold, K.D. Vorlop, T. Tacke, M. Sell. Catal. Today, 17 (1993), pp. 21–30

[21] F. Gauthard, F. Epron, J. Barbier. J. Catal., 220 (2003), pp. 182–191

[22] F. Deganello, L.F. Liotta, A. Macaluso, A.M. Venezia, G. Deganello. Appl. Catal. B: Environ., 24 (2000), pp. 265–273

[23] O.S.G.P. Soares, J.J.M. Órfão, J. Ruiz-Martínez, J. Silvestre-Albero, A. Sepúlveda-Escribano, M.F.R. Pereira. Chem. Eng. J., 165 (2010), pp. 78–88

[24] Y. Yoshinaga, T. Akita, I. Mikami, T. Okuhara. J. Catal., 207 (2002), pp. 37–45

[25] O. Soares, J. Órfão, M. Pereira. Catal. Lett., 139 (2010), pp. 97–104

[26] A. Pintar, M. Setinc, J. Levec, J. Catal., 174 (1998), pp. 72–87

[27] A. Garron, F. Epron. Water Res., 39 (2005), pp. 3073–3081

[28] U. Prusse, M. Kroger, K.D. Vorlop. Chem. Ing. Tech., 69 (1997), pp. 87–90

[29] M.J. Alowitz, M.M. Scherer. Environ. Sci. Technol., 36 (2002), pp. 299–306

[30] I.F. Cheng, R. Muftikian, Q. Fernando, N. Korte. Chemosphere, 35 (1997), pp. 2689–2695

[31] S. Choe, Y.-Y. Chang, K.-Y. Hwang, J. Khim. Chemosphere, 41 (2000), pp. 1307–1311

[32] C.-P. Huang, H.-W. Wang, P.-C. Chiu. Water Res., 32 (1998), pp. 2257–2264

[33] P. Westerhoff, J. James. Water Res., 37 (2003), pp. 1818–1830

[34] R. Gavagnin, L. Biasetto, F. Pinna, G. Strukul. Appl. Catal. B: Environ., 38 (2002), pp. 91–99

[35] F. Epron, F. Gauthard, J. Barbier. J. Catal., 206 (2002), pp. 363–367

[36] M. D', Arino, F. Pinna and G. Strukul, Appl. Catal., B, 2004, 53, 161–168

[37] A. Mills and S. Le Hunte, J. Photochem. Photobiol., A, 2000, 108, 1–35.

[38] J. Herrmann, Catal. Today, 53, 115–12979

[39] T. Tan, D. Beydoun, R. Amal, Journal of Photochemistry and Photobiology A: Chemistry 159 (2003) 273–280

[40] M.R. Prairie, L.R. Evans, B.M. Stange, S.L. Martinez. Environ. Sci. Technol. 27 (9) (1993) 1776–1782.

[41] C.R Chenthamarakshan, Hui Yang, Yong Ming, Krishnan Rajeshwar. Journal of Electroanalytical Chemistry, Volume 494, Issue 2, 15 December 2000, Pages 79–86

[42] J. Sa *et al*. Applied Catalysis B: Environmental 85 (2009) 192–200

[43] A. L. Linsebigler, G. Lu and J. T. Yates, Chem. Rev., 1995, 95, 735–758

[44] Miguel Pelaez, Nicholas T. Nolan, Suresh C. Pillai, Michael K. Seery, Polycarpos Falaras, Athanassios G. Kontos, Patrick S.M. Dunlop, Jeremy W.J. Hamilton, J.Anthony Byrne, Kevin O'Shea, Mohammad H. Entezari, Dionysios D. Dionysiou. Applied Catalysis B: Environmental, Volume 125, 21 August 2012, Pages 331-349

[45] Park J.Y, Lee I. H. Journal of Nanomaterials Volume 2014 (2014), Article ID 250803

[46] Pan, J., Liu, G., Lu, G. Q. & Cheng, H.-M.. Angew. Chem., Int. Ed. 50, 2133–2137 (2011)

[47] Riegel, G. Bolton, J. R. *J. Phys. Chem.* 1995, *99*, 4215

[48] Luttrell, T. Halpegamage, S. Tao, J. Kramer, A. Sutter, E. Batzill, M. *Scientific Reports* **4**, Article number: 4043 (2014)

[49] Bacsa, R. P.; Kiwi, J. *Appl. Catal. B* 1998, *16*, 19

[50] Tian Y, Fu J, Chang B, Xi F, Dong X. Materials Letters. 2012 vol: 81 pp: 95-98

[51] Bickley, R. I., *et al*. *J. Solid State Chem.* 1991, *92*, 178

[52] Leytner, S.; Hupp, J. T. *Chem. Phys. Lett.* 2000, *330*, 231

[53] Hurum D, Agrios A, Gray K, Rajh T, Thurnauer M. J. Phys. Chem. B 2003, 107, 4545-4549

[54] Nair R, Paul S, Samdarshi S. Solar Energy Materials and Solar Cells. 2011. vol: 95 (7) pp: 1901-1907

[55] G. Li, K.A. Gray, Chem. Mater., 19 (2007), pp. 1143–1146

[56] W. Zhao, W. Ma, C. Chen, J. Zhao and Z. Shuai, J. Am. Chem. Soc., 2004, 126, 4782–4783

[57] Y. Yao, G. Li, S. Ciston, R. M. Lueptow and K. Gray, Environ. Sci. Technol., 2008, 42, 4952–4957

[58] Y. Yu, J. C. Yu, C.-Y. Chan, Y.-K. Che, J.-C. Zhao, L. Ding, W.-K. Ge and P.-K. Wong, Appl. Catal., B, 2005, 61, 1–11. B.

[59] Ahmmad, Y. Kusumoto, S. Somekawa and M. Ikeda, Catal. Commun., 2008, 9, 1410–1413

[60] Iliev, V; Tomova, D; Bilyarska, L; *et al*. Applied Catalysis B-Environmental Volume: 63 Issue: 3-4 Pages: 266-271

[61] Zhu, Shuying; Liang, Shijing; Gu, Quan; *et al*. Applied Catalysis B-Environmental Volume: 119 Pages: 146-155

[62] Wang, Xingdong; Caruso, Rachel A. Journal of Materials Chemistry Volume: 21 Issue: 1 Pages: 20-28 Published: 2011

[63] Zielinska-Jurek, Anna; Kowalska, Ewa; Sobczak, Janusz W *et al*. Applied Catalysis-B Environmental Volume: 101 Issue: 3-4 Pages: 504-514 Published: JAN 14 2011

[64] Subramanian, V; Roeder, RK; Wolf, EE. Ind. Eng. Chem. Res., 2006, 45 (7), pp 2187–2193

[65] Zhang F Pi Y Cui J Yang Y Zhang X Guan N. J. Phys. Chem. C, 2007, 111 (9), pp 3756–3761

[66] A. Valentine Rupa D. DivakarT. Sivakumar. Catalysis Letters September 2009, Volume 132, Issue 1, pp 259–267

[67] Wang, Xingdong; Waterhouse, Geoffrey I. N.; Mitchell, David R. G.; *et al*. Chem. Cat. Chem.Volume: 3 Issue: 11 Pages: 1763-1771 Published: NOV 2011

[68] Gomathi Devi L Kavitha R. Applied Surface Science. 2016. vol: 360 pp: 601-622

[69] V. Subramanian, E. E. Wolf and P. V. Kamat, J. Am. Chem. Soc. 2004, 126, 4943–4950

[70] R. Jin, W. Gao, J. Chen, H. Zeng, F. Zhang, Z. Liu and N. Guan, J. Photochem. Photobiol., A, 2004, 162, 585–590

[71] F. Zhang, R. Jin, J. Chen, C. Shao, W. Gao, L. Li and N. Guan, J. Catal., 2005, 232, 424–431. 82 Y. Li and F. Wasgestian, J. Photochem. P

[72] Y. Tian and T. Tatsuma, Chem. Commun., 2004, 1810–1811

[73] H. Wang, T. You, W. Shi, J. Li and L. Guo, J. Phys. Chem. C, 2012, 116, 6490–6494

[74] Z. Liu, W. Hou, P. Pavaskar, M. Aykol and S. B. Cronin Nano Lett., 2011, 11, 1111–1116

[75] A. L. Linsebigler, G. Lu and J. T. Yates, Chem. Rev., 1995, 95, 735–758

[76] A. Bumajdad, M. Madkour, Y. Abdel-Moneam and M. El-Kemary, J. Mater. Sci., 2014, 49, 1743–1754

[77] Murdoch, M.; Waterhouse, G. I. N.; Nadeem, M. A. Nature Chemistry. Volume: 3 Issue: 6 Pages: 489-492 Published: JUN 2011

[78] Serpone. N. J. Phys. Chem. B 2006, 110, 24287-24293

[79] Dvoranová D Brezová V Mazúr M Malati M. Applied Catalysis B: Environmental 2002 vol: 37 (2) pp: 91-105

[80] Wilke K Breuer H. Journal of Photochemistry and Photobiology A: Chemistry 1999 vol: 121 (1) pp: 49-53

[81] Choi, W.; Termin, A.; Hoffmann, M. R. J. Phys. Chem. 1994, 98, 13669–13679

[82] Li, F. B.; Li, X. Z. Appl. Catal. A: Gen. 2002, 228, 15–27

[83] Khairy M Zakaria W. Egyptian Journal of Petroleum 2014 vol: 23 (4) pp: 419-426

[84] Devi L Kavitha R. Applied Catalysis B: Environmental 2013 vol: 140 pp: 559-587

[85] Dozzi M.V, Selli. E. Journal of photochemistry and photobiology. , 2013, Vol.14, p.13-28

[86] Dozzi. M, Selli. E. Materials Science in Semiconductor Processing 2016 vol: 42 pp: 36-39

[87] R. Asahi, T. Morikawa, T. Ohwaki, K. Aoki, Y. Taga. Science, 293 (2001), p. 269

[88] Dolat, D., Mozia, S., Ohtani, B., and Morawski, A. W. (2013). Chem. Eng. J., 225, 358–364.

[89] Shen, X.-Z., Guo, J., Liu, Z.-C., and Xie, S.-M. (2008). Appl. Surface Sci., 254 (15), 4726–4731.

[90] Hu, S., Li, F., Fan, Z., and Chang, C.-C. (2011). Appl. Surface Sci., 258(1), 182–188

[91] Gomathi Devi L Kavitha R. Applied Surface Science 2016 vol: 360 pp: 601-622

[93] W -S Kim, G Jang, Jieun Lee, Dongseok Rhee, Energy Procedia 61 (2014) 2456 – 2459

CHAPTER 2

2.1 Introduction

The photocatalytic experiments carried out in this project were conducted in the manners and using the equipment described in this chapter unless otherwise stated.

2.2 Experimental Set-Up for Solar-Simulating Reactions

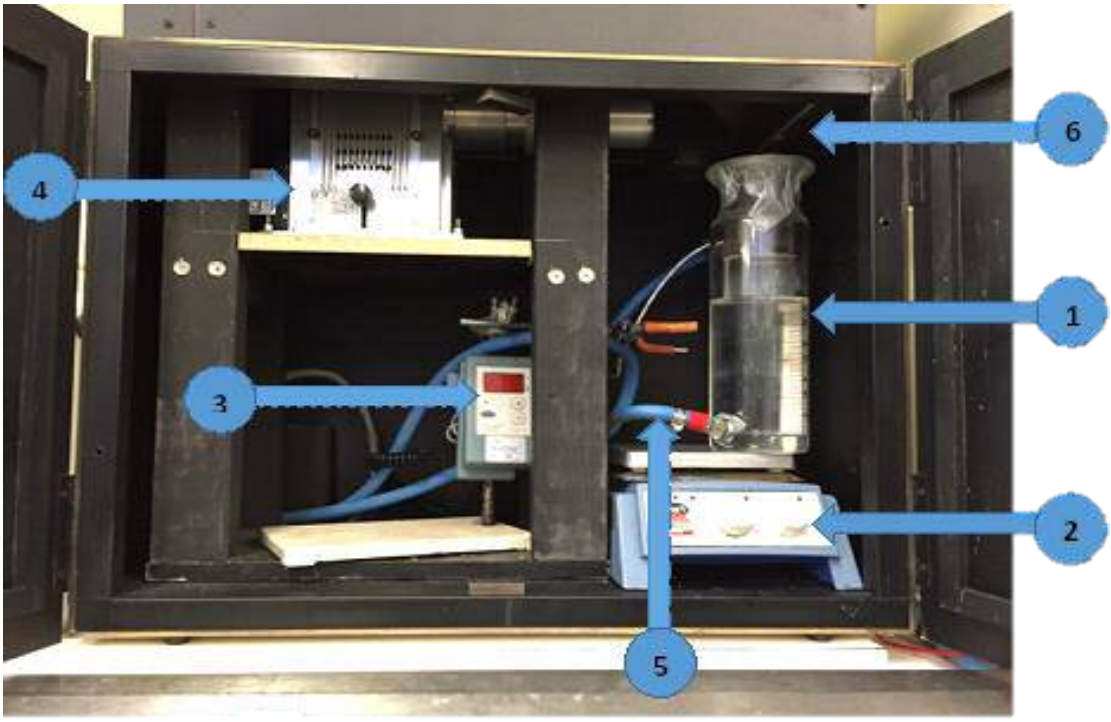

Figure 2.2: Photograph of reaction showing following components: 1) 500 ml jacketed glass reaction vessel, 2) hotplate and magnetic stirrer, 3) thermocouple, 4) xenon arc lamp, 5) hoses connecting reaction vessel outer jacket to temperature-controlled water bath, 6) darkened box.

The equipment used for assessing the photcatalytic reactions is shown in **figure 2.1** above. A 500 ml open-topped jacketed glass reactor is used as a reaction vessel and thus the source of illumination must come from the top. To achieve this an angled mirror attachment is used to angle the beam 90° downwards. Temperature control of the reaction is achieved by flowing water from a thermo-regulated water bath through the inlet port in the outer jacket of the vessel which then returns from the outlet port to the water bath in a cycle. A thermocouple suspended just above the bottom of the vessel used as a means

of monitoring reaction temperature; thermal equilibrium of the reaction solution is confirmed when the readout of the reaction thermocouple matches the readout on a second thermocouple located on the water bath unit. Stirring is achieved using a single magnetic stirrer bar, with the same bar being used for all experiments. The stirrer speed was selected as the speed that sufficiently agitates the suspension of catalyst and prevents any settling while avoiding the formation of a vortex or any visible change to the shape of the surface of the reaction solution. A wooden box with a metal frame and matt black interior paint was used to prevent the entry or exit of light into the system while the reaction was running, a simple U-bend vent was fitted to the rear of the box to allow the venting of warm air and to prevent possible build-up of photo-generated ozone. For this reason the reaction setup was located inside a fume hood. In cases where the introduction of gasses is desired, a plastic tube fitted with a small metal diffuser was connected to a gas line inside the fume hood and suspended above the bottom of the reactor using a clamp stand to allow stirring. The xenon arc lamp used for illumination is elevated on a shelf and the power supply is fed through the U-bend to allow control while the box is sealed.

2.2.1 Solar Simulating Xenon Arc Lamp

The source of illumination for the solar-simulating reactions was conducted using a LOT LS0306300 W xenon arc lamp chosen because of its output spectra which mimics natural daylight and includes UVA, UVB, visible and infra red components in proportions similar to that of solar light. The irradiance of the lamp is 1000W/m^2 which closely mimics the average solar irradiance at sea level on the earths surface on a clear day.

2.2.2 Experimental Setup of Visible Light-Only and UV-Only Reactions

Due to the angling mirror being necessary for top-down illumination the application of optical filters is hindered in the reaction setup shown above. For this reason reactions requiring the use of optical filters such as visible light-only and UV-only reactions was carried out on another reaction setup which utilised a 100 ml pyrex three-necked round-bottomed flask as a reaction vessel with a mercury thermometer on one neck and on the others loosely-fitted glass stoppers to allow the escape of gasses while preventing excessive loss of solvent. Stirring was again achieved with magnetic stirring by a stirrer bar and hotplate/stirrer. Temperature control was achieved via the hotplate. Illumination in this setup was achieved by shining another xenon arc lampside-on to the reaction

vessel. Once again a matt-black box was used to contain the reaction equipment and prevent the entry or exit of light during the reaction.

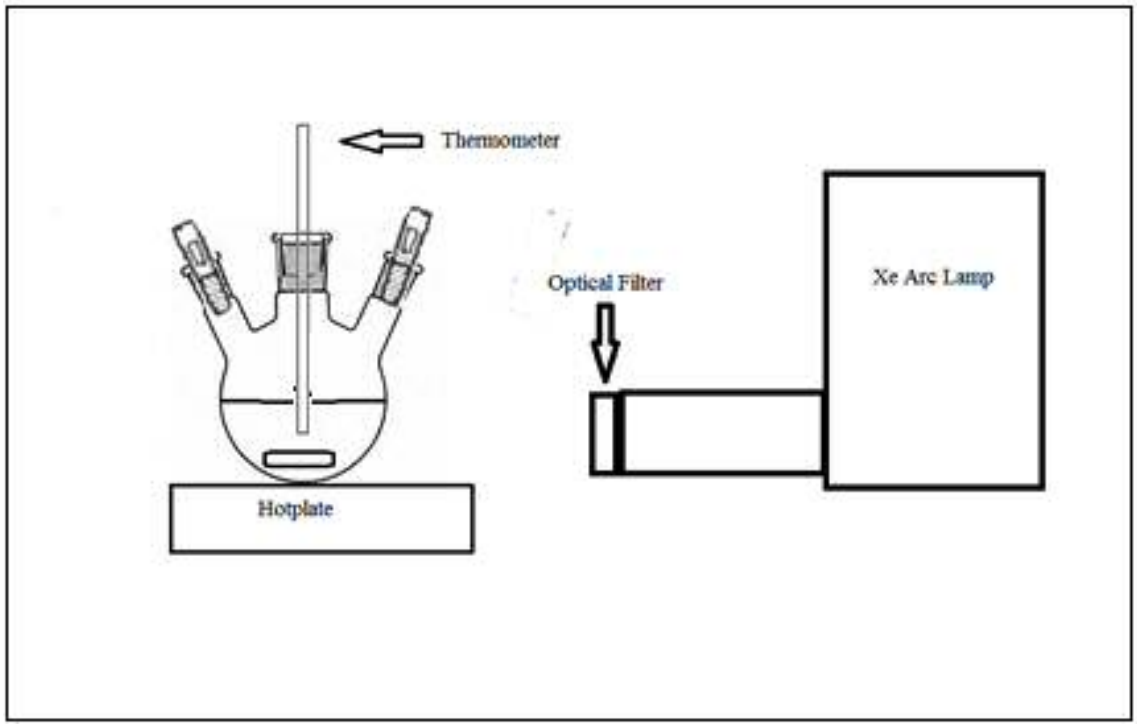

Figure 3.2: Experimental set-up of Visible-Only and UV-only reactions.

2.2.3 Ion Chromatography

Analysis of reactants and one reaction side product (NO_2^-) was carried out using a DionexICS-1100 using a DionexIonPac AS22 Fast column with polymeric packing material for use with a mixed solution of Na_2CO_3 and $NaHCO_3$ as eluent A conductivity detector was used to qualitatively analyse the analytes. A photograph of a DionexICS-1100 is shown in **figure 2.3**.

Figure 2.4: Picture of Ion Chromatography unit

Ion chromatography shares many of its fundamental principles with those of liquid chromatography. In both techniques a mixture of analytes is separated by the differing extents of interaction with a stationary phase material that either coats or is packed into a tube; typically called a column.

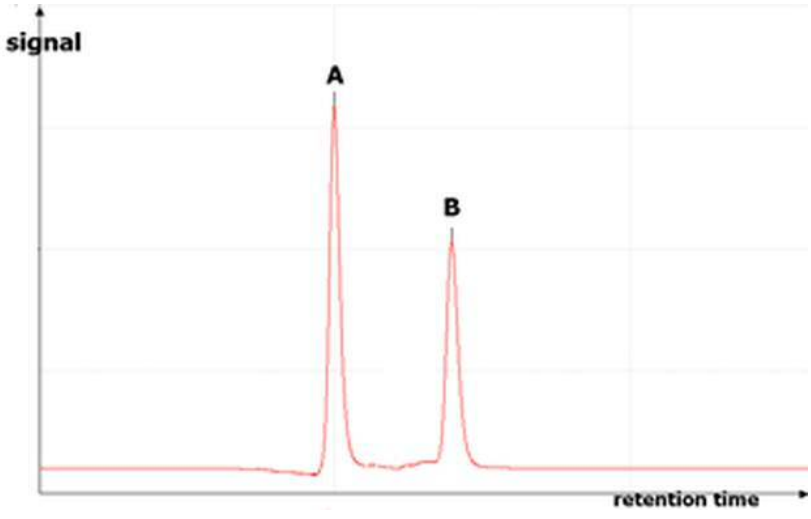

Figure 2.5: Typical chromatogram showing the separation and detection of analytes A and B (arbitrary axis units).

The analyte is carried through the column by a mobile phase and the differing strengths of interaction between the analyte and the stationary phase result in differing retention times and thus the analytes elute separately where they are quantatively analysed by some

sort of detection system. A large mixture of analytes can lead to the need for extremely slow flow rates so that each analyte has more contact time with the stationary phase and thus better separation is achieved. This can lead to very long retention times and if using an isocratic mobile phase (concentration of mobile phase stays constent). A solution to this is to increase the concentration of eluent over time or to use a mixture of eluents and changing the concentration of one or both over time; this is known as gradient elution. For our experiments an isocratic elution with sodium carbonate/bicarbonate as an eluent was sufficient for good peak separation. Consistent elution times are achieved often by the use of a column oven or column chiller that maintains a constant column temperature and thus a constant strength of interaction between the analytes and the stationary phase. **Figure 2.4** shows a typical chromatogram where analytes A and B have been separated by a column and quantitatively analysed, the peak area gives the concentration of the analytes by comparing against peak areas of standards with known concentration.

Ion Chromatography (referred to herein as IC) differs from HPLC largely in the type of stationary phase used as the column packing material. IC, as the name implies, is used only for the analysis of ionic species and thus an ion exchange column must be used. Ion exchange columns often employ functionalised polymers known as ion exchange resins in order to achieve ionic separation as is the case in the IC equipment used in this project. The type of resin employed is dictated by the charge on the analyte ion, anion exchange utilises polymer gels that are functionalised to be strongly or weakly basic. Unlike HPLC where a wide range of detector devices can be employed IC relies most often on conductivity detection to quantify the analyte. Conductivity detection works by measuring the changes in electrical conductivity of the eluent caused by the presence of the analytes as it reaches the detector. This change in conductivity is plotted against elution time and results in peaks corresponding to individual components of the analyte mixture such as is shown in **Figure 2.4.**

A unique component of IC that is often employed when using a conductivity detector for the analysis of anions is a unit called a suppressor that is located pre-detector in the system. This component is necessary when the mobile phase consists of sodium carbonate/bicarbonate components as is employed in the system used in this project. The purpose of this unit is to simply replace the cationic sodium from the sodium bicarbonate/carbonate eluent with hydronium ions before the mobile phase enters the detector. This achieves a lower background conductivity and lower level of background

noise in the system because of the comparatively higher conductivity of carbonate/bicarbonate ions that exist pre-suppression to that of carbonic acid that is present post-suppression (**Figure 2.5**).

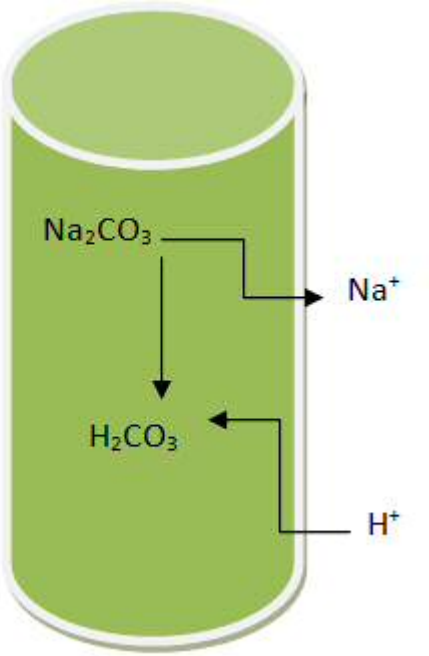

Figure 2.5: Schematic of a chemical suppression in an IC system designed to analyse anions.

The main parameters of the IC used throughout the project are as follows:

Flow rate: 0.3 ml/min

Column Temperature: 50°C

Mobile Phase composition: 0.0045M Na_2CO_3/0.0014M $NaHCO_3$

2.2.4 Ammonium Selective Ion Probe

Ammonia analysis was carried out using an ion selective electrode from Thermofisher. An ion selective probe uses a transducer to convert the activity of an analyte ion in solution into a voltage that can be compared against a reference electrode with a known potential and displayed on a meter. It is important to make the distinction between activity and concentration in this case since ions in solution do not behave ideally.To make the solution more ideal in nature an ionic strength adjuster (ISA) is added to both sample solution and calibration standards. The ISA served to increase the ionic strength of the solution.

The probe used in this project combines the indicator and reference electrodes into a single probe and achieved selectivity using an ion exchange resin at the tip of the probe which only allows the diffusion of ammonium ions into the probe. The probe was calibrated using a method built into the meter in which standards of 100, 50 and 25 ppm NH_4^+ were prepared by dilution from a 1000 ppm ammonium chloride solution.

2.3 Methodology

The reaction mixture was prepared by weighing 0.1371 g of sodium nitrate into a small glass vial which was transferred into a clean 1L volumetric flask, washing the contents of the vial thoroughly into the flask using deionised water. This process was then repeated using 0.3682 g of formic acid. The flask was then filled to the mark with deionised water and inverted several times, 500 ml of this solution was then measured out using a clean and dry measuring cylinder. From here the reaction solution is transferred to the clean and dry reaction vessel which can then be purged of dissolved gasses by bubbling nitrogen into the solution for 1 h through a tube fed through a small hole in a parafilm “lid” that is used to prevent oxygen re-dissolving into the system. In some experiments oxygen is bubbled into the vessel to increase the dissolved oxygen content, again for 1 h.

The filled reaction vessel is connected to the water pump and placed on the centre of the hot-plate and the stirrer bar is added and stirring applied. 120 mg of catalyst is added and the reaction is allowed to thermally equilibrate for 30 minutes before a t = 0 sample is taken and the lamp switched on.

Sampling is undertaken at 30 min, 1h, 2h and 3h elapsed time under illumination. Sampling is conducted with the light-source switched off which entirely stops the

reaction, this is confirmed by blank reactions shown in chapter 3. Sampling is done using a pipette to remove 2ml of reaction solution which is diluted in 2ml deionised water in a sample vial. Once shaken to homogenise the solution, 2 ml of reaction solution is pippetted into a 2ml centrifuge vial and centrifuged for 2 minutes to remove catalyst particles; this is done to protect the thin capillaries utilised by the IC system from blockage. 1ml of this solution is then transferred to a unique sampling vial made specifically for the IC auto sampler which automatically injects sample into the IC system at the start of each run.

2.4 Catalyst Preparation

The following is a list of all metal precursors used:

H_2AuCl_4, $HPtCl_6$, $PdCl_2$, $AgNO_3$, $CuCl_2$ (Sigma-Aldrich)

All of the catalysts mentioned in this report were prepared using the following methods unless otherwise stated using the precursors mentioned above.

2.4.1 Wet Impregnation

Wet impregnation catalysts (WI) were prepared in 0.5g batches by weighing X grams of TiO_2(P25 Degussa) into a glass vial. The value of X in grams is given by the equation below:

X = 1 - (target weight loading of metal)

A solution of metal precursor water was then added in excess to the vial and a small stirrer bar added. The vial is then placed on a hot plate set to around 80°C and watched closely as the water evaporates until a thick paste was formed. The paste as dried in an oven at (110°C, 16 h) and finally calcined (400°C, 3 h 20°C/min). The catalyst was then sieved using a 53 micron sieve.

2.4.2 Incipient Wetness

Incipient wetness catalysts were prepared in 1 g batches by pipetting 1ml of metal precursor at the required concentration to give the desired metal loading into a pestle containing (1 – (target metal loading weight)) g of titania. The material was ground with a mortar for 10 minutes at which point a thick paste had formed. The mortar was transferred to an oven and dried (110°C, 16 h) before the dry catalyst was calcined (400°C, 3 h, 20°C/min) or reduced (400°C, 3 h, 20°C/min under flowing H_2). The catalyst was then sieved using a 53 micron sieve. It must be noted that the formation of a paste indicates a slight excess of H_2O, this is different to a strict incipient wetness preparation where the amount of H_2O used is exactly equal to the pore volume of the support material. With this noted, the term Incipient Wetness (IW) will be used herein to describe the preparation method above when referencing catalysts made and tested in this study.

2.4.3 Sol Immobilisation

Sol immobilisation catalysts were prepared by preparing a beaker with 500ml water, an amount of metal precursor solution and differing amounts of polyvinyl alcohol (PVA). After 10 mins of stirring an excess of $NaBH_4$(>96% Aldrich, $NaBH_4$ /Au (mo/mol) 5) was added to the solution and a colour change from straw to dark brown was observed. The solution was stirred for a further 30 mins before the required amount of TiO_2 to make a 1 g batch of catalyst was added and the solution acidified (pH 2, 1 N H_2SO_4). After further vigorous stirring for 1 h the catalyst was filtered under vacuum, washed and dried in an oven (110°C, 16 h). Where stated the catalyst was sieved with a 53 micron sieve.

2.4.4 Modified Sol-Gel (N-TiO_2)

Taken from H.Sun *et al* [1]. To a beaker of 500 ml water 0.5 concentrated nitric acid was added to give Solution B. Solution B would also contain 7.75 g urea (99%, Aldrich) if N-doped material was desired. A separatory funnel was charged with 50ml ethanol, 10ml glacial acetic acid and 10 ml of titanium (IV) isopropoxide (Aldrich, 97%) to give Solution A. Solution A was added dropwise into Solution B and aged for 24 h before the solvent was removed by evaporation at 80°C. The resulting xerogel was calcined (400°C, 3 h, 20°C/min) to give the final catalyst. A considerable weight-loss was observed during calcinations. The catalyst was sieved using a 53 micron sieve.

2.4.5 N-TiO_2 and M/N-TiO_2 from TiN

N-TiO_2 was prepared by the incomplete oxidation of TiN and the preparation was taken from a 2001 paper by Huang *et al* [2]. TiN (99%, Aldrich) was calcined at various temperatures (3h, 30°C/min) and sieved using a 53 micron sieve.

2.5 Catalyst Characterisation

The equipment and methodologies used to characterise the catalysts used throughout this project, as well as a brief summary of the theory behind each technique are detailed in this section.

2.5.1 BET Surface Area Analysis

It is important to assess the surface area of the catalyst as the higher a catalysts surface area the more sites the reactants have available to them to adsorb and react, thus surface area has a huge bearing on activity. It is important to know the surface area of the catalysts after the various preparation/modification steps to determine whether any effect observed is due to changes in surface area or not.

The method used to asses surface area in this project is the BET method, first published in 1938 by Brunauer, Emmett and Teller from whom the technique receives its name [3].BET theory attempts to describe the physical adsorption of gases on a solid surface, it the existing Langmuir theory that deals only with mono-atomic adsorption and extends it to apply to multilayer hypothesis. To make this extension of Langmuir theory, the following assumptions are made:

- The surface is homogeneous
- There is no lateral interaction between adsorbed molecules
- The upmost layer of adsorbate is in equilibrium with the vapour phase
- Langmuir theory can be applied to individual layers
- At saturation pressure the number of layers becomes infinite.

Using these assumptions Brunauer, Emmett and Teller devised the following equation:

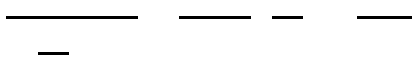

Equation 1: BET equation.

Where:

= The total volume of gas

= the volume of gas adsorbed in a monolayer

P = Pressure

P_0 = the saturation vapour pressure

C = BET constant derived from heat of adsorbtion of first layer and heat of liquefaction.

Equation 1 can be plotted as a straight line with — on the y-axis and on the x-axis P/P_0. This results in a BET plot (**Figure 2.6**) from which and C can be calculated using the slope (A) and intercept (I) (**Equations 2 and 3**).

Equation 2: Calculation of from A and I

Equation 3: Calculation of C from A and I

Finally the surface area is calculated using **Equation 4**.

Equation 4: Calculation of surface are (S) from where N is avagadros number and s is the adsorption cross-section of the adsorbing species.

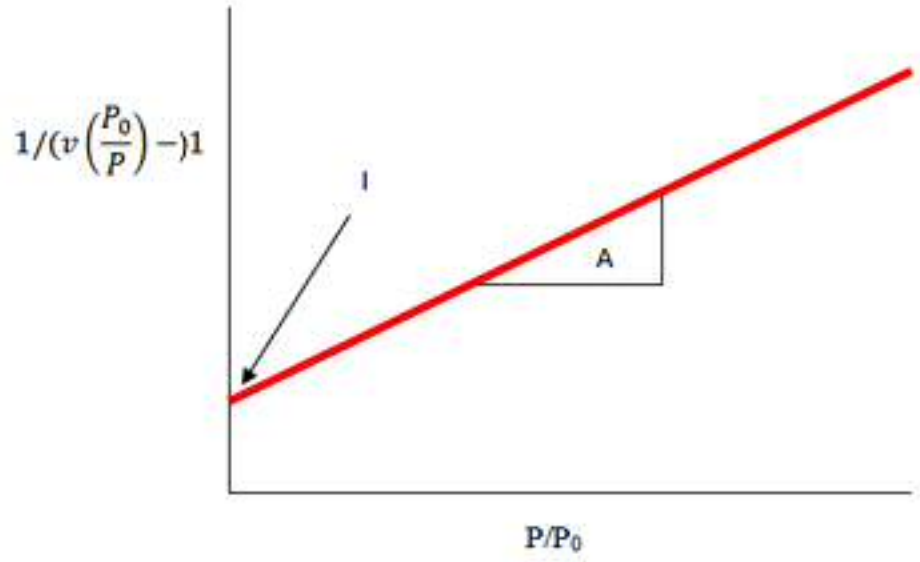

Figure 2.6: BET plot showing slope and intercept from which v_m and thus the surface area can be derived

The BET calculations carried out in this experiment were carried out using a Micrometrics Gemini Surface Area Analyser.

2.5.2 X-Ray Diffractometry

X-ray Diffraction (XRD) is an extremely useful non-destructive analytic technique that allows for the characterisation of crystalline materials and the discovery of their crystal structure. In an X-ray diffractometer electron are accelerated towards a target source in a cathode ray tube which produces X-rays. The X-rays are passed through monochromators which ensure an X-ray beam with a single wavelength which is then collimated and directed at the sample. The sample is mounted on a goniometer that allows the beam to hit the sample at different angles with respect to the detector (**Figure 2.7)**.

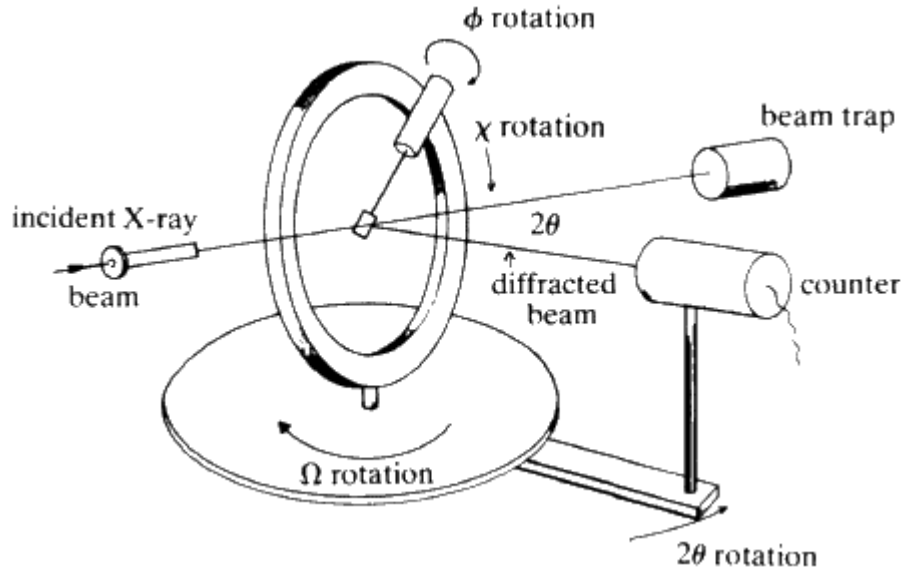

Figure 2.7: Schematic showing layout of typical XRD experiment

The X-ray beams can now undergo constructive or destructive interference as they are diffracted by the material and the intensity of rays that are not destroyed are quantified by the detector. Constructive interference is at its strongest when Bragg's Law is satisfied (**Equation 5**). A visualisation of this process is shown in **figure 2.8**.

Equation 5: Bragg's law where d = interplaner spacing in the sample, = scattering angle, n is a positive integer and = the wavelength of incident light.

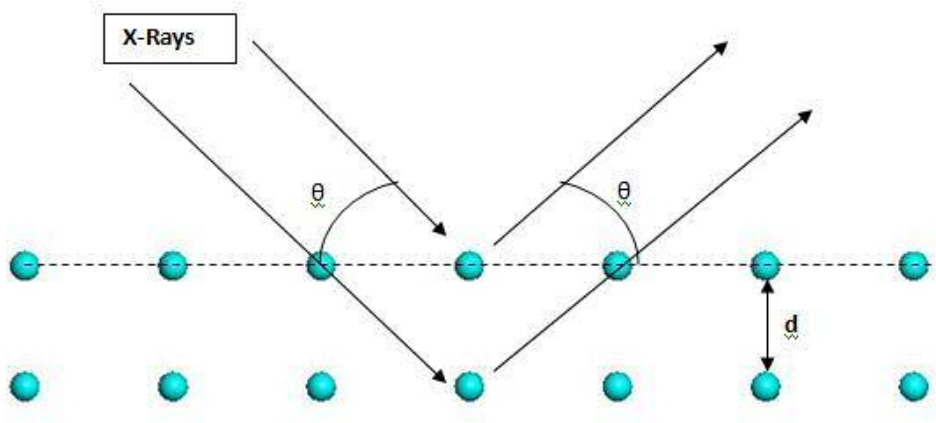

Figure 2.8: Schematic of irradiation of a sample with X-Ray beams showing scattering angle ( )and interplaner spacing d.

Bragg's Law was devised in 1912 by physicist William Lawrence Bragg and relates the scattering angle and interplaner spacing of a crystalline solid to the wavelength of light directed at it [4].

By changing the scattering angle all possible diffractions will be observed if a sufficiently powdered sample is used, this is due to the random orientations of individual crystallites in a powdered sample. The result of a diffractometry experiment is a series of peaks on a plot of X-ray intensity vs 2 which can be converted a set of d-spacings unique to the compound being analysed. Thus with the aid of a reference library of d-spacings it is possible to identify an unknown powdered crystalline solid using this technique.

The crystallite size of a crystalline solid can be assessed using another important equation in the field of X-ray crystallography; the Scherrer equation (**Equation 6**).

Equation 6: The Scherrer equation where = the mean size of the ordered crystalline domains, = the X-ray wavelength and = the Bragg angle. K here is a dimensionless shape factor close to the value of 1 which varies slightly with crystallite shape.

Devised in 1918 by Paul Hermann Scherrer, the Scherrer equation relates the peak width in an XRD pattern to the sample crystallite size [5].

The XRD analysis carried out in this project were carried out using Panalytical Pro XRD diffractometers using "Xpert data collector" software.

2.5.3 UV-Visible Spectroscopy

Electromagnetic radiation is a useful probe in characterising materials and each section of the electromagnetic spectrum sheds light on different properties of matter. Where X-rays were used previously to study the crystal structure of the catalysts here visible and UV light is used to induce electronic transitions in the material (**Figure 2.9**). Because of the quantisation of electronic states, the wavelength of light that induces such a transition can give us the energy of that transition and thus useful information can be derived such as the band-gap in our semiconductor-based catalysts.

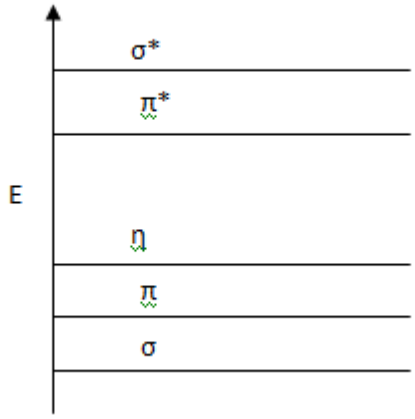

Figure 2.9: Schematic of the electronic transitions possible by illumination with UV/Visible light

The energy required for a particular electronic transition depends highly on the substances molecular structure. For example an electronic transition from a π orbital to a π^* orbital may occur in the UV region for one molecule, but in the visible region for another. An interesting phenomenon regarding this particular type of transition is that it generally gives rise to more intense absorption and shorter wavelengths when the π bonding is arranged in an alternating π σ pattern which is often exhibited by any organic molecules.

UV-visible spectroscopy quantifies the light absorbed at different wavelengths by a substance and thus is used as a means of monitoring the progression of chemical reaction where there is a clear difference in the absorption pattern between the reactant and the product. It cannot, however, be used as the sole means of identifying an unknown sample due to the many different factors that can influence the absorption pattern of a material. A key equation associated with the quantification of known material by UV-visible spectroscopy is the Beer-Lambert Equation (**Equation 7**).

Equation 7

Where:

A = measured absorbance of a material

= a wavelength specific absorptivity coefficient with units $M^{-1}cm^{-1}$.

b = is the path length the light travels through the sample solution

c = the concentration of the analyte solution

The type of UV-Vis spectroscopy utilised in this project is called UV-visible diffuse reflectance spectroscopy. The only difference between this and normal UV-visible spectroscopy is that normal UV-Vis measures the transmittance of light through a solution to determine how much a liquid analyte absorbs whereas diffuse reflectance spectroscopy measures the relative intensity of light reflected from a solid sample.

Practically, a UV-Visible experimental setup consists of typically two light sources, one that is responsible for the near IR through to violet light and one responsible for the UV portion of the spectrum. The machine will also consist of a sample holder and a tuneable monochromator to ensure a single wavelength of light illuminates the sample at any given time. When the measurement begins, the monochromator scans through the spectrum as the intensity of reflected light is recorded. The intensity is plotted as a function of wavelength to obtain a spectrum that consists of broad bands rather than discrete peaks (**Figure 2.10**). This is due to the fact that if a photon of energy slightly greater than the energy required for an electronic transition to occur strikes the sample the excess energy is taken up by the substance's much lower energy vibrational or rotational transitions. Likewise if a photon strikes the analyte with slightly less energy than required for an electronic transition, a transition in vibrational and rotational states will take place rather than no transition at all. Electronic states exist relatively far apart on an energy scale whereas vibrational states exist closer together and rotational states closer still.

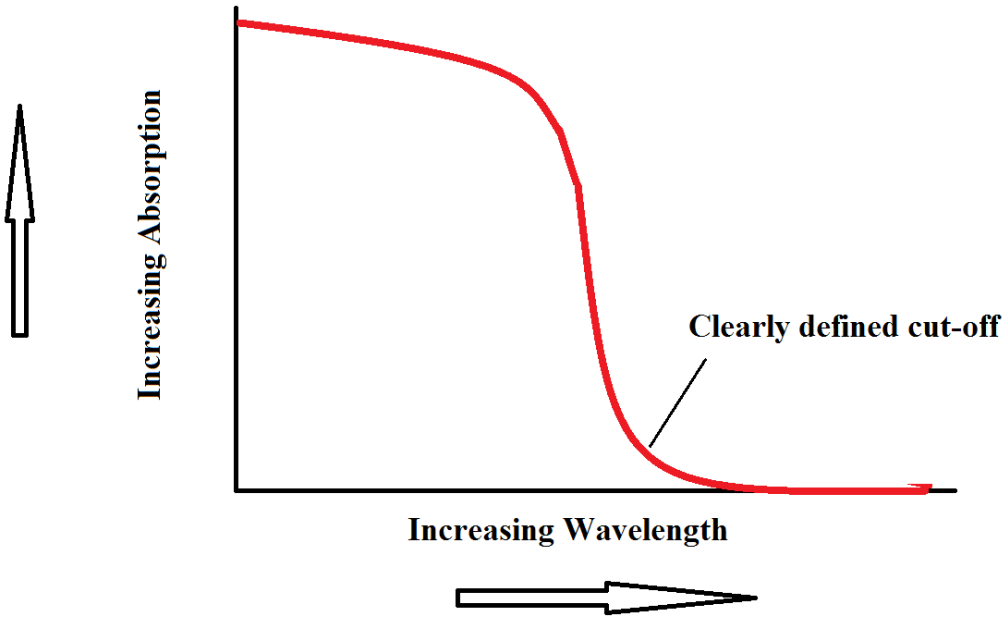

Figure 2.10: Typical UV-Vis diffuse reflectance spectra of semiconductor showing clear cut-off or absorption edge from which band-gap energy how may be calculated.

When analysing catalysts such as TiO_2 it is often useful to calculate the band-gap of the material. This can be done using a simple equation that relates the wavelength of the adsorption edge of a material to the band-gap (**Equation 8**).

$$\lambda$$

Equation 8: Where E is the band-gap energy, h is plank's constant, C is the speed of light and λ is the wavelength of the absorption edge.

A Cary 4000 UV-Visible Diffuse Reflectance spectrometer was used for determining adsorption edges, band gaps and the presence of surface-plasmon resonance bands in this project.

2.5.4 Electron Microscopy

Conventional optical microscopy is prohibited from achieving magnifications greater than 1000x that of the human eye. This is due not only to the difficulty in the manufacture of pristine lenses but due to limits in achieving a short enough wavelength of light to observe objects at magnifications higher than this. To observe an object the wavelength of light hitting it must be smaller than the object itself, this becomes impossible for optical microscopes when the goal is observing objects in the nano regime. To get around this problem, scientists since the 1920's have turned to electrons instead of photons due to their much shorter wavelengths, allowing for much higher magnifications. The two main types of electron microscopes available to scientists are the Scanning Electron Microscope (SEM) and the Transmission Electron Microscope (TEM). The two types share many characteristics, in both systems electrons are generated by an electron gun such as a heated tungsten cathode. The electrons are then accelerated towards an anode, the energy of the electron beam is closely controlled and can range from 0.2 keV to 40 keV. The electrons, much like the photons in an optical microscope, are directed and focused using lenses. Where optical microscopes use glass lenses, electron microscopes use magnetic condenser lenses to bend the beam of electrons. Unlike optical microscopes a hard vacuum is necessary to prevent ionisation of gas molecules along the beam path which would disrupt the beam. Here the two types of microscopy start to differ and it is best to discuss them separately. Schematics of the key components of a typical SEM and TEM setup are shown in **figure 2.11** and **figure 2.12** respectively.

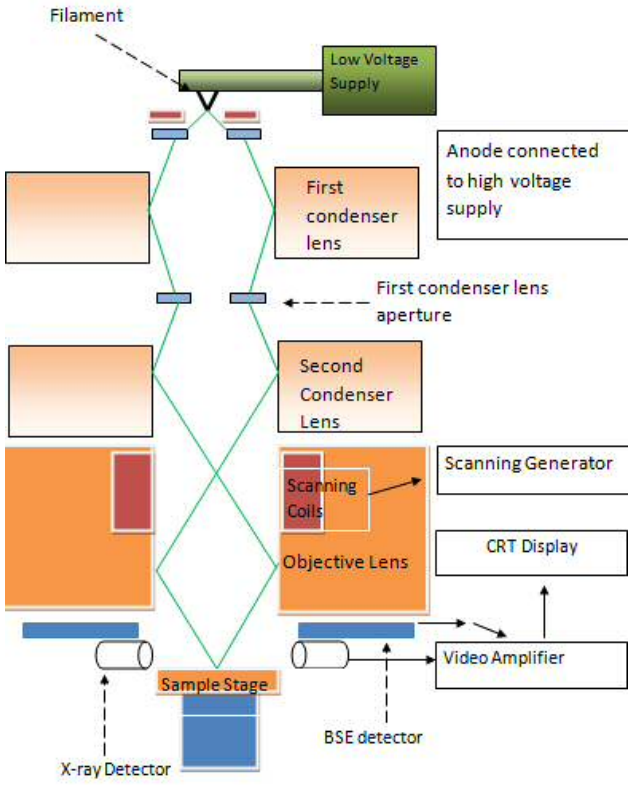

Figure 2.11: Schematic of a Scanning Electron Microscope (SEM)

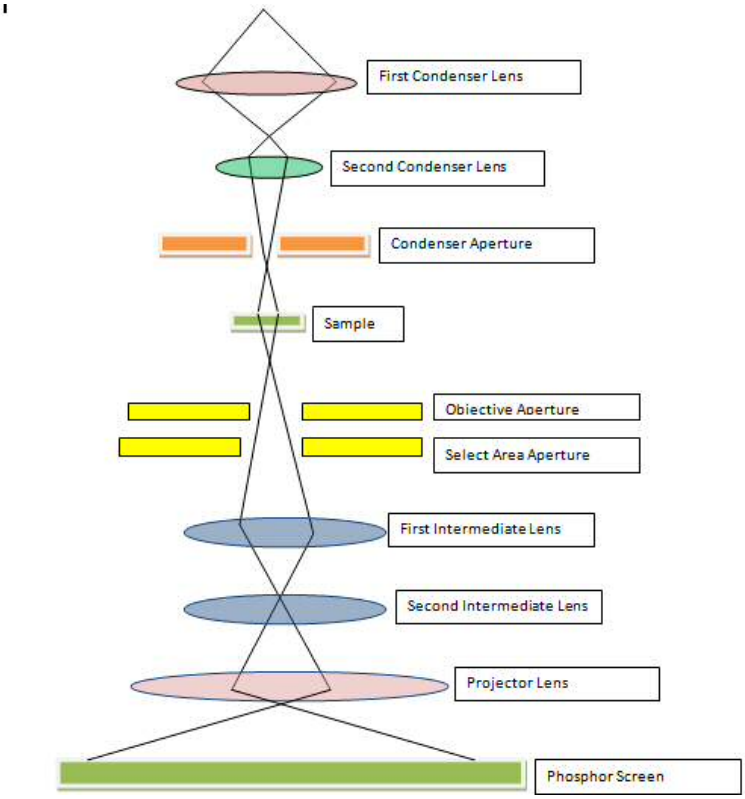

Figure 2.12: Schematic of a Transmission Electron Microscope (TEM)

SEM

In an SEM system, these condenser lenses curve the path of the electrons and focus them to a spot of around 3 nanometers in diameter. A set of scanning coils deflect the electron beam in the x or y axis to allow a square area of the target sample to be scanned and a raster image to be formed; hence the term "scanning" electron microscope. When electrons make contact with the sample several phenomena can occur, each providing a unique insight into the properties of the material being analysed.

A phenomenon all electron microscopes are equipped to measure is the generation of secondary electrons. As the electron beam strikes the sample electrons can be ejected from the innermost orbitals (k-shell) of atoms in the sample. These ejected electrons are referred to as secondary electrons and are generated by relatively low-energy electron beams (energy range 0-50 eV with the majority of secondary electrons generated at 3-5 eV). Due to the low energies associated with this process the generation of secondary electrons occurs relatively close to the sample surface (0-10 nm) and thus gives information on the topography of the surface of the material. Secondary electrons are detected using an Everhart-Thornley detector which uses an electrically biased metal grid to attract the secondary electrons towards the detector. The electrons are then accelerated further using higher voltage biases before they contact the phosphor screen which, upon contact with the accelerated electrons, emits very dim flashes of light. These flashes are the amplified using a photomultiplier and converted to the final digital image.

Another important phenomenon that many electron microscopes measure is the backscattering of electrons from the beam itself. Unlike secondary electrons, which are generated from the inelastic scattering of beam electrons (where energy from the beam electrons is lost upon collision with the sample) backscattered are generated from elastic scattering. These elastically scattered primary electrons are of a much higher energy than those that generate secondary electrons and thus data obtained from backscattering comes from deeper into the sample (close to 1 micron in depth). The amount of backscattering that occurs is proportional to the mean atomic number of the sample and thus images can be generated that show contrast according to atomic number; that is to say that areas of the sample containing atoms with higher atomic number will appear brighter than areas with lower atomic number. Due to the generally low ratio of primary electrons that undergo backscattering, the signal tends to be weaker and the resolution poorer than when

utilising secondary electrons. The relative depths of signal generation from secondary and backscattered electrons are shown in **figure 2.13**

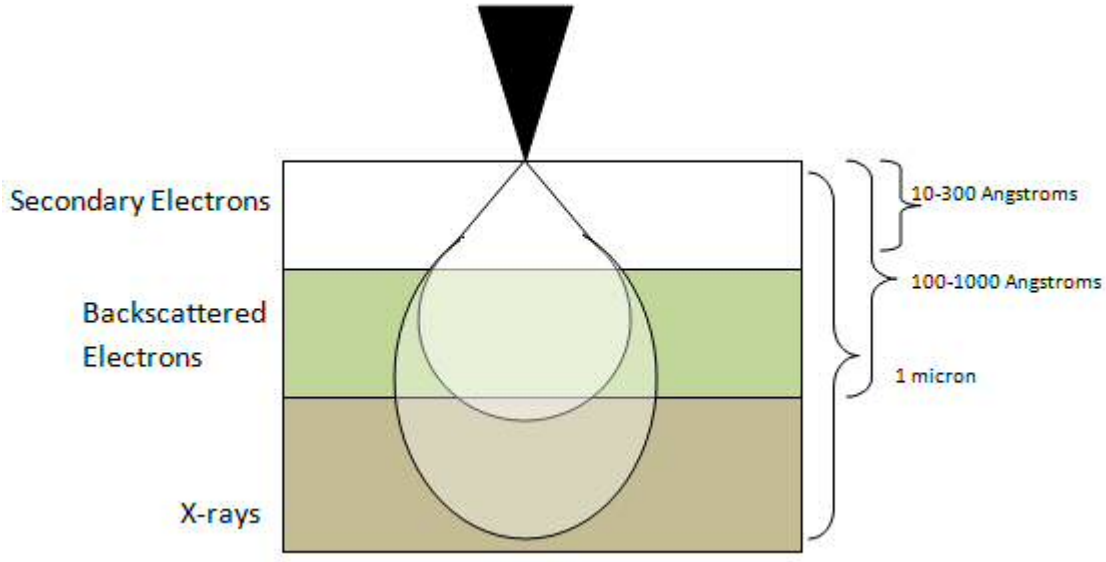

Figure 2.13: Diagram showing depth of signal generation when primary electrons strike a sample.

Although there are other phenomena that can be utilised in an SEM system such as Bremsstrahlung radiation, and photon emission from cathodoluminescence they are outside the scope of this project. The final process that shall be discussed here is Energy Dispersive X-ray Spectroscopy. This technique makes use of the X-rays generated when electrons in higher-energy orbitals relax to fill spaces caused by core-shell electrons being displaced by the electron beam (**Figure 2.14**). The wavelength of the X-rays emitted from this relaxation is dependent on the difference in energy between the electronic orbitals that the electron starts at and the energy of the orbital the energy moves to. These energies are indicative of the electronic structure of the sample and thus elemental analysis can be carried out using this phenomenon. A second scenario is possible when primary electrons collide with the core-shells of the sample and that is the emission of Auger electrons. Auger electrons are caused when the primary electrons displace a core-shell (k-shell) electron from a sample atom which again results in the relaxation of an electron from a higher-energy orbital which in turn results in X-ray emission (**Figure 2.14**). The difference here is that rather than escaping the atom and being detected the energy of the photon is transferred to another electron in the outer shells of sample atom which is then ejected from the sample.

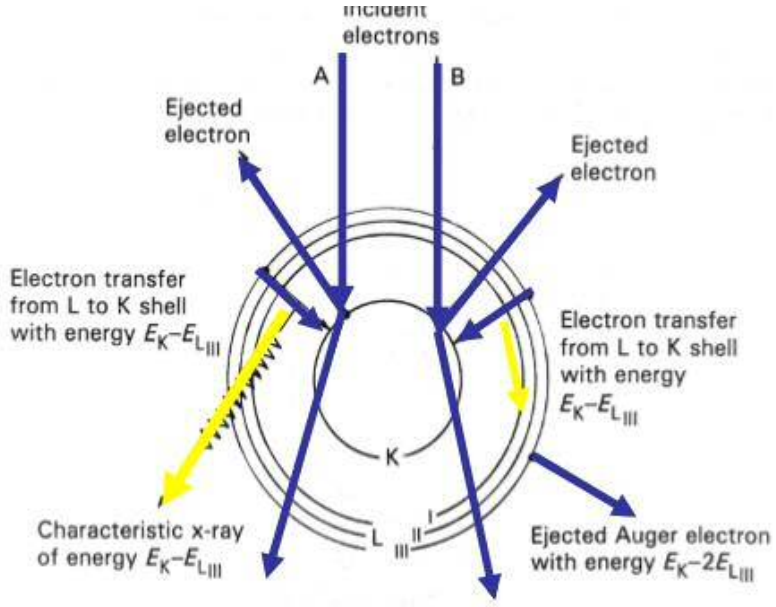

Figure 2.14: Schematic of possible outcomes when primary electrons strike the k-shell of a sample atom, A) gives rise to the emission of X-rays while B) gives rise to Auger emission

Analysis of the energies of Auger electrons can identify the elemental composition of the sample since that energy is dependent on the energies of the X-ray photon (which is known from the energies of the relaxation process that generated it) and the energy of the outer shell it was ejected from. Whether an atom undergoes x-ray emission or Auger electron emission when struck with the electron beam depends on the atomic mass of the sample atoms. Lower atomic masses give rise mainly to Auger electrons whereas heavier elements give rise mainly to X-rays.

The frequency of emitted X-ray radiation can be related to atomic number using Moseley's Law (**Equation 9**).

Equation 9: Mosley's Law relating frequency of generated X-rays to atomic number where v = frequency and Z = atomic number.

TEM

As mentioned previously, the initial portion of a TEM is comparable to an SEM, with electrons being generated and accelerated by an electron gun and then deflected using a magnetic condenser lens. In a TEM the sample is located much earlier in the beam-path and instead of the beam being focused to a tiny point it is spread out over the whole sample. The generation of an image in this case comes from the transmission of electrons through the sample which are the projected onto a phosphor viewing screen. This means an inherent requirement of TEM is that the sample must be sufficiently thin to allow electrons to pass through.

There are several imaging modes that can be used in TEM analysis, the most common by far is known as bright field mode. In this mode, contrast is formed by the difference in sample thickness in different areas and thus the difference in electron beam intensity when reaching the phosphor screen. This gives information on the topography of the sample. The beam intensity after passing through the sample will also be more greatly diminished if the atomic number is higher or the sample denser.

The TEM used in this project was a JOEL 2100 with a LaB_6 element.

2.5.5 Dynamic Light Scattering

Dynamic light scattering is a method by which properties of a suspension such as particle shape and size is determined by passing a monochromatic light source through the sample and analysing the resulting scattered light. The technique is used in a variety of application, particularly in the biological sciences in determining the hydrodynamic behaviour of proteins, nucleic acids and viruses. Dynamic light scattering works by measuring the Brownian motion of particles in a suspension and relating this motion to a particles' size via the Stoke-Einstein Equation (**equation 10**) [6].

Equation 10: The Stoke-Einstein Equation where D = Diffusion Speed, K = Boltzmann constant, T = absolute temperature, η = viscocity and D_h = hydrodynamic radius.

Though useful in determining the size of a macroparticle, dynamic light scattering has several notable weaknesses such as an extreme sensitivity to temperature and solvent viscosity.

2.6 References

[1] Hongqi Sun, Guanliang Zhou, Shizhen Liu, Ha Ming Ang, Moses O Tadé, Shaobin Wang, *Chemical Engineering Journal*, **2013,** 231, 18-25

[2] Huang JG, Zhao XG, Zheng MY, Li S, Wang Y, Liu XJ. *Water Sci Technol.* **2013**, 68(4), 934-9.

[3] S Brunauer, P H Emmett, E Teller, *J. Am. Chem. Soc*., **1938**, *60* (2), 309–319

[4] Friedrich, W.; Knipping, P.; von Laue, M. *Sitzungsber. Math.-Phys. ClasseKöniglich-BayerischenAkad. Wiss. München.* **1912**, 303–322

[5] P. Scherrer *Nachr. Ges. Wiss. Göttingen,* **1918**, 26, 98–100

[6] J Stetefeld, S.A McKenna, & Patel, T.R. *Biophys Rev.* **2016,** 8, 409

CHAPTER 3

3.1 Introduction

Of all the catalyst preparation methods used to yield photo-active gold catalysts perhaps the most simple is the impregnation method. The method consists of immersing a catalyst support in a solution of metal precursor commonly followed by a period of ageing, drying and subsequent heat-treatment. The impregnation method can be divided into two sub sets depending on the volume of solution used in relation to the total pore-volume of the catalyst; these methods are known as "Wet Impregnation" (WI) and "Incipient Wetness" (IW) with the former involving the use of an excess of solution with respect to the pore-volume and the latter using no more than the total pore-volume. During calcination, deposited gold chloride is typically oxidised to an oxide unless the temperature is sufficient to allow spontaneous decomposition of the oxide to metallic gold (achieved at calcination temperatures > 200°C). The nature of the adsorbed gold particles and thus the activity of catalysts made via impregnation methods are highly dependent on the nature of heat-treatment applied to them, with temperature, atmosphere, heating rate and heating time being the most important variables to consider.

The ease and speed of preparation has made this a popular method of making a variety of noble and non-noble-metal catalysts in spite of the fact that, as far as conventional catalysis is concerned, they have been shown to be inferior to gold catalysts made by deposition precipitation (DP) or co-precipitation (CP)[1]. This is largely due to the fact that these other preparation methods give rise to catalysts with a narrower particle-size distribution compare to impregnation methods, which often produce metal nanoparticles with sizes outside the useful range for a particular reaction. With regards to photo catalysis this trend no longer holds true; it has been shown in several cases that photo catalysts made by the impregnation method exhibit higher activities than comparative catalysts made via CP or DP [2]. Though this is true, the superiority of one preparation method over another will depend somewhat on the specifics of the reaction being carried out; it is for this reason that a comparison of preparation methods was used as a starting-point for the research reported in this thesis with IW being compared against WI, DP and sol-immobilisation.

3.2 Results and Discussion

3.2.1 Assessing the Effect of Metal-Modification on TiO_2

Before we can accurately assess the effect of depositing metal nanoparticles on titania it is important to understand what ways (if any) the preparation method changes the properties of the TiO_2. The incipient wetness method discussed here is the optimised IW method that gave the highest conversions, details of the optimisation are given in section **3.3**.

XRD

XRD analysis of the Degussa P25 and the incipient wetness –prepared 0.3% Au/TiO_2 show very little difference between the plain titania and the post-preparation samples. As expected the calcinations step did not result in any difference in phase composition between the pre and post –preparation samples with the anatase to rutile % ratio remaining at around 80:20. The presence of gold is not detected by XRD in even the higher Au loading catalysts which is indicated by the lack of any Au peaks. This is concurrent with analysis found in the literature for Au prepared by deposition precipitation [3]. A slight increase in crystallinity is observed by the very slight narrowing of anatase and rutile peaks post-calcination which is to be expected after heat treatment [4].

Table 3.1: Catalyst crystallite sizes calculated via XRD analysis

Catalyst	Crystallite size (nm)
P25 (Degussa)	6.8
1%Au/TiO_2	8.1

(Crystallite size estimated by measuring peak width which is inversely related to the crystallite size as described in the Scherrer Equation given in Chapter 2)

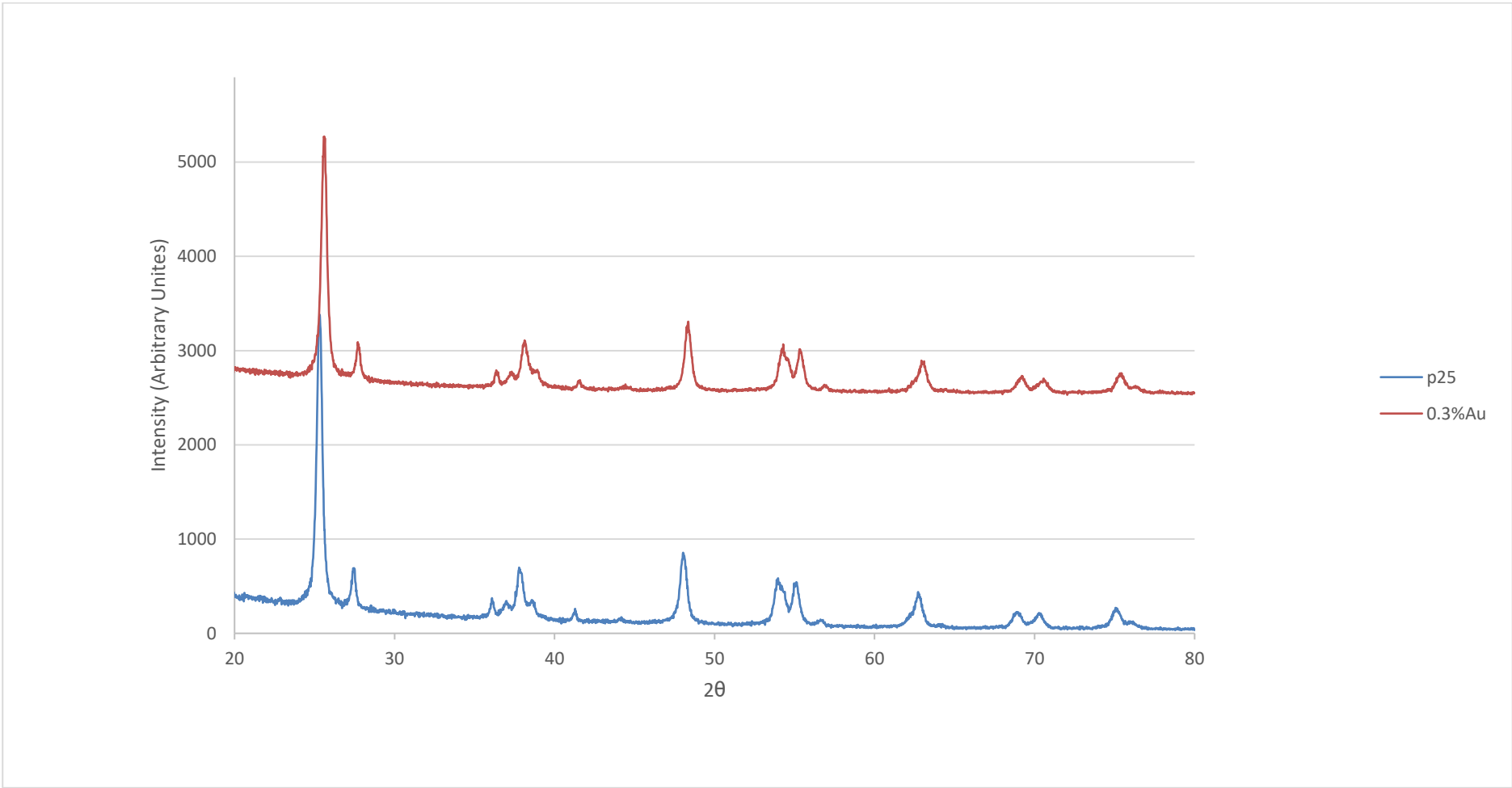

Figure 3.6: XRD analysis of P25 (blue line) and 0.3%Au/TiO_2 (orange line)

BET Surface Area Analysis

Likewise BET analysis shows very little difference between plain titania and the Au loaded sample with a slight decrease in surface are likely brought on by the calcination step [4].

Table 3.2: BET analysis of IW 1%Au/TiO_2 and plain P25

Catalyst	Surface Area (m^2/g)
1% Au/TiO_2	48.4
P25	51.1

SEM Microscopy

Scanning Electron Microscopy of plain P25 and the Au-modified catalysts indicated no clear change in terms of the TiO_2 support, although images of sufficient resolution could not be obtained to determine crystallite size. SEM imaging was found to be an unsuitable method in terms of metal nanoparticle analysis as no NMNP's could be detected in any of the Au/TiO_2 samples.

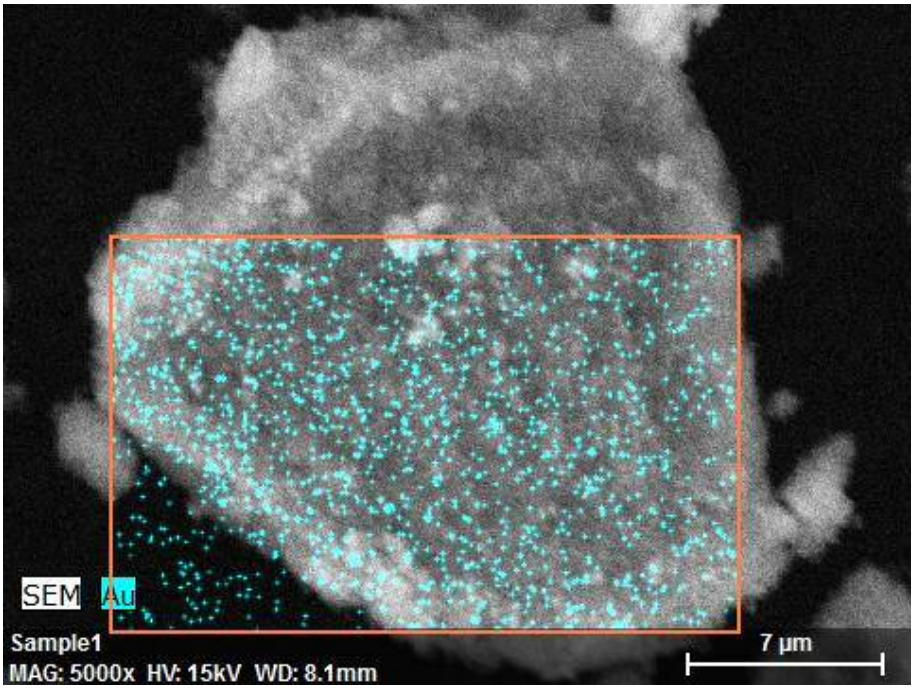

Figure 3.7: EDX mapping of an area of 1%Au/TiO_2 showing the detection of Au nanoparticles (blue spots) both on the TiO_2 support and carbon background in almost equal measure.

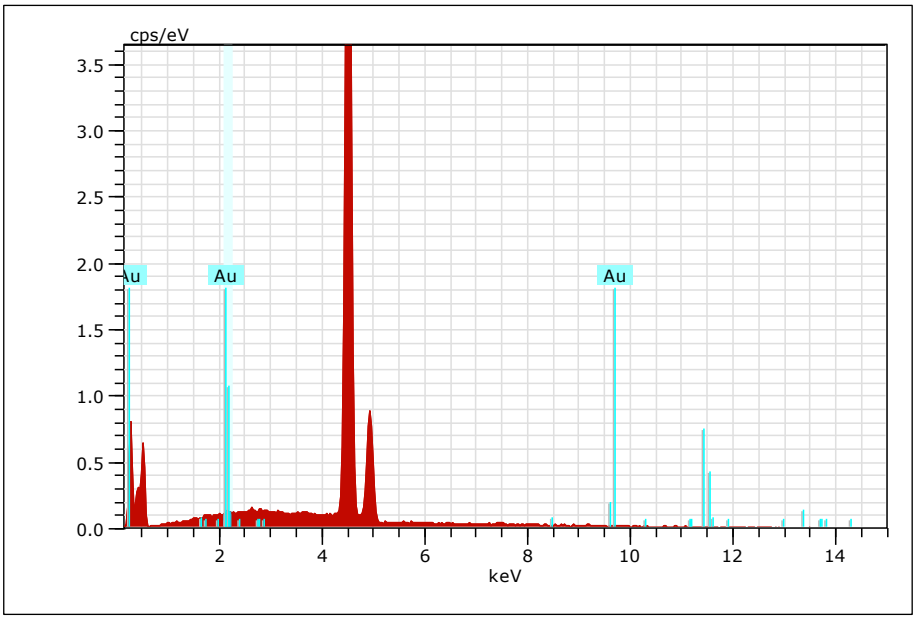

Figure 3.3: Elemental analysis of sample area shown in **Figure 3.2.**

EDX analysis of 1% Au/TiO_2 at 5K magnification showed no distinct Au peaks (**Figure 3.3**) although when set to detect Au the software gave the image (**Figure 3.2**). A problem arises when the software was set to also detect carbon which is the element that the catalyst is supported on during these analyses (**Figure 3.4**).

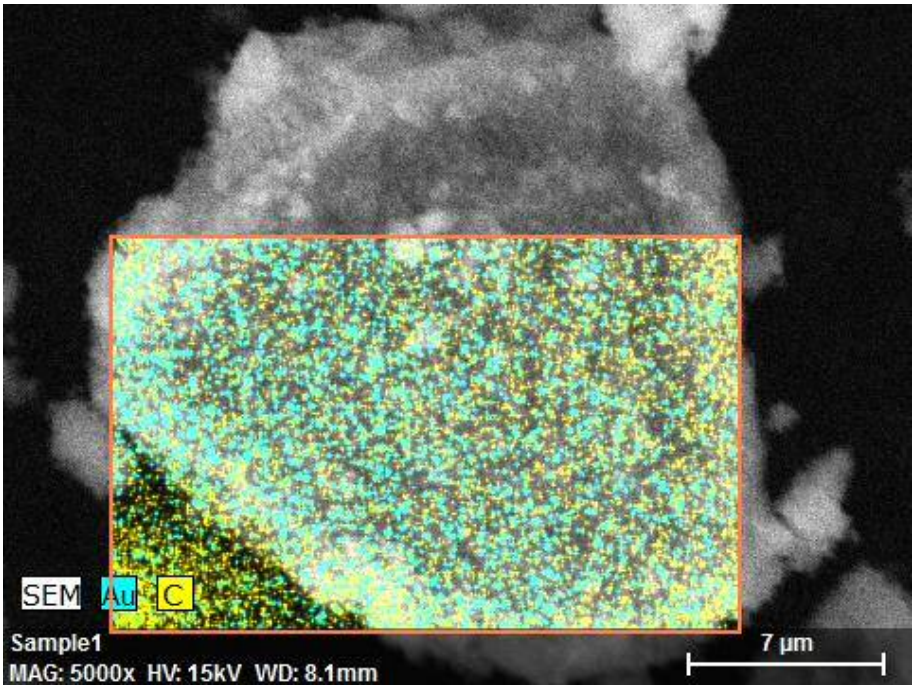

Figure 3.4: EDX mapping of an area of 1%Au/TiO_2 showing the detection of Au nanoparticles (blue spots) and C (yellow spots) both on the TiO_2 support and carbon background in almost equal measure.

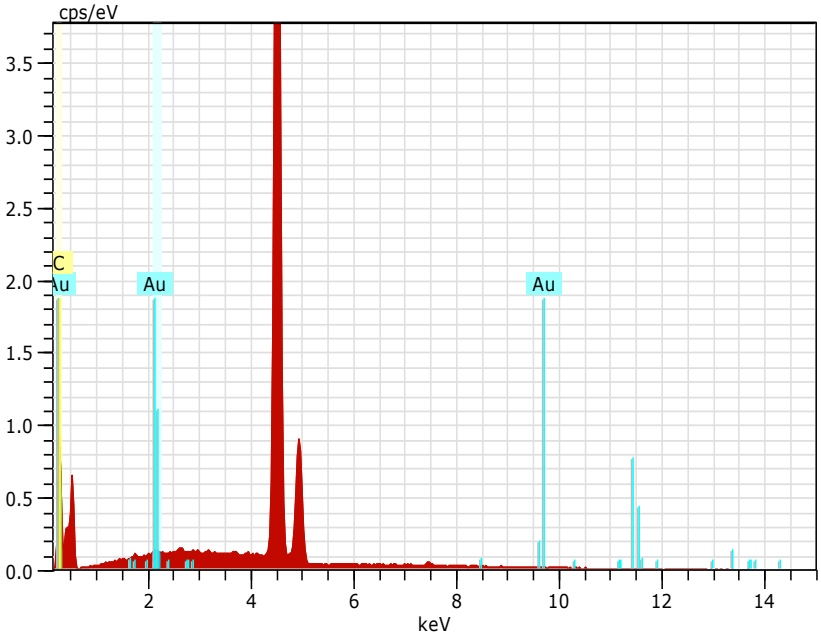

Figure 3.5: Elemental analysis of area shown in **Figure 3.4**

It can be seen from **figure 3.5** that the Kα transmission peak corresponding to elemental carbon sits atop the peak corresponding to the M transmission of Au in the EDX spectrum. Because of this, the software is unable to distinguish between Au and the carbon support material which explains the high amount of unsupported Au detected in the bottom left corner of the EDX scanning area in **figure 3.4**. That is to say that the Au detected in this region is not Au nanoparticles that have somehow separated from the TiO_2 but rather a misidentification of Au by the software with the signal actually being caused by the carbon support.

For this reason, the more valuable source of microscopy data was obtained from TEM techniques which will be discussed in **Section 3.4.**

In conclusion we can state that the incipient wetness preparation step has very little effect on the titania other than a small growth in crystallite size resulting in a small decrease in surface area (3.3 m^2/g).

3.2.2 Optimising Reaction Conditions

This section details experiments conducted in order to establish the effect of important reaction parameters such as catalyst mass, concentration of substrate, type of hole-scavenging species and more. The catalyst used for the majority of these experiments was 1%Au/TiO_2 made by the optimised incipient wetness method detailed in the experimental section and conducted under the standard reaction conditions unless otherwise stated.

Effect of Catalyst Mass:Nitrate Ratio

As in any catalytic process it is advantageous to establish in this photocatalytic reaction the minimum mass of catalyst required whilst maintaining sufficient rate and product selectivity. When catalyst mass was doubled from 120 mg to 240 mg a corresponding doubling of reaction rate was not observed both in terms of nitrate reduction and formic acid oxidation (**Figure 3.6).**

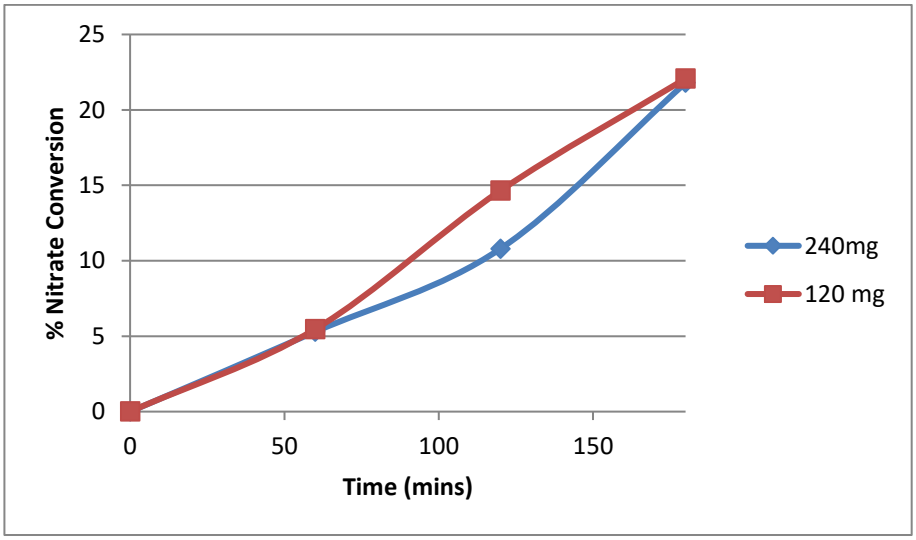

Figure 3.6: Effect of catalyst mass on photoactivity for nitrate reduction under solar simulated light using 1%Au/TiO_2 (400°C calcination temperature, 4°C/min ramp rate) showing 240 mg (blue diamonds) and 120 mg of catalyst (orange squares).

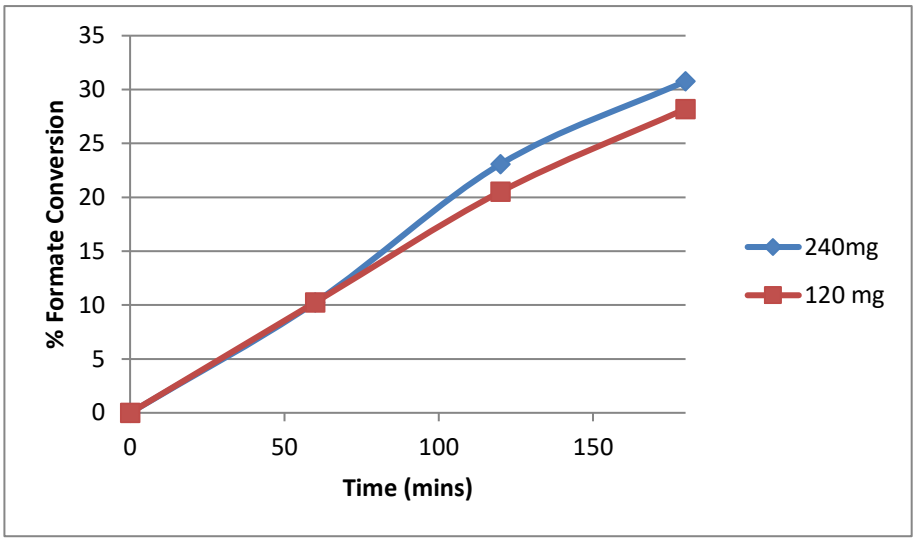

Figure 3.7: Effect of catalyst mass on photoactivity for formate oxidation under solar simulated light using 1%Au/TiO_2 (400°C calcination temperature, 4°C/min ramp rate) showing 240 mg (blue diamonds) and 120 mg of catalyst (orange squares)

In thermo-catalysis we would expect to see an increase in the reaction rate with increasing catalyst as more active sites would be available to interact with substrate. The reason this is not observed here is because of an optical effect and is partially due to the reactor design. As the concentration of the catalyst in suspension is increased the turbidity of the reaction solution increases and thus less of the solution is penetrated by incoming light from above; this counteracts the increase in active sites available for reaction. From the data (**Figures 3.6 and 3.7**) it can be seen that there is no benefit to increasing the catalyst mass above 120 mg due to the increase in the turbidity of the reaction medium.

Competition Between Nitrate and Oxygen

Literature has shown that dissolved oxygen can compete for photo-electrons with nitrate and slow the reaction [5]. An experiment was carried out in which nitrogen was bubbled through the reaction mixture for 30 minutes prior to illumination using a special apparatus that allowed N_2 to effectively diffuse efficiently (see Chapter 2). Nitrogen was continuously bubbled during the course of the reaction and a similar experiment was then done using oxygen for comparison. The purpose of this was to determine to what extent the oxygen affected the reaction; the results can be seen below (**Figure 3.8**).

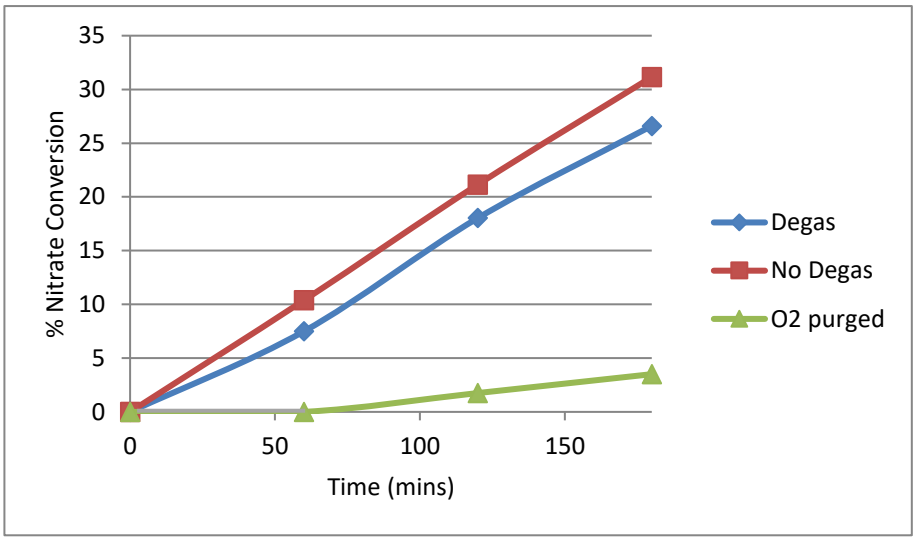

Figure 3.8: Effect of bubbling nitrogen (blue diamonds) and oxygen (grey triangles) into reaction solution for 1h prior to reaction and continuous bubbling throughout the reaction compared to no gas treatment (orange squares). Catalyst used here is 120 mg of 0.4%Au/TiO_2.

Surprisingly, and in contradiction to some literature, the removing of dissolved oxygen by nitrogen purging did not improve the rate of reaction, rather an unexpected decrease in conversion was observed; when oxygen was artificially introduced to the system however, the expected drop in activity was seen. It should be noted that the expected increase in formic acid oxidation was observed with O_2 purging. From this it can be concluded that while the presence of oxygen is indeed in competition with nitrate, although under normal conditions (using distilled/deionised water) it is not dissolved in sufficient concentration compared to nitrate as to cause a decrease in activity. As for the apparent superior activity of the non-degassed reaction there are the following possible explanations.

- The nitrogen adsorbs to the catalyst without reacting and blocks active sites.
- The nitrogen line was contaminated with some other substance detrimental to activity.

This result has strong implications in terms of the applicability of this catalyst in a real-world system as under atmospheric conditions the concentration of dissolved oxygen would not be high enough to cause any reduction in activity. This means an extra step of N_2 purging wouldn't need to be carried out and the process as a whole would be more viable.

Effect of Reaction Temperature

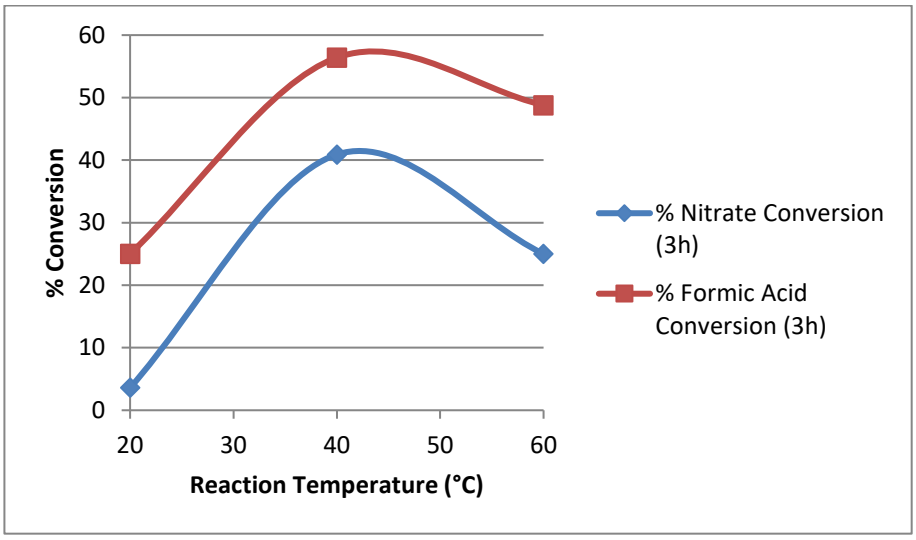

Figure 3.9: Effect of reaction temperature on nitrate conversion using 0.3%Au/TiO_2.

Photocatalytic activity is generally not affected by small changes in reaction temperature; this is because the true activation energy of a photocatalytic reaction is zero [6-8]. That is to say that the photo-generation of electron-hole pairs is fundamentally independent of temperature [9]. Though this is true, the apparent activation energy is often empirically measured at around 20 kJ mol^{-1} due to temperature having an effect on the adsorption and desorption isotherms of reactants and products and thus temperature dependence is observed in many reactions.

From **figure 3.9** we see that, as stated in the literature, photoactivity depends largely on the reaction temperature. Moreover, we see an initial increase in activity between 20°C and 40°C before observing a drop in activity between 40°C and 60°C. A positive and linear dependence on temperature has been noted for this reaction in the literature when using metal-modified TiO_2 catalysts over a 30-50°C temperature range [5]. The authors attribute this to either changes in adsorption/desorption equilibrium constants or some physical property of the system. Here we extend the temperature range and see a drop in activity between 40°C and 60°C. Though there is insufficient data to establish an activation energy via the Arrhenius equation we can state that within this temperature range the apparent activation energy would be negative. This too has been reported in the literature for photoreduction of NO with NH_3, here the authors rationalise the initial increase in activity by asserting an increase in the rate of the rate-determining step with

increasing temperature [10]. They go on to suggest that the subsequent decrease in activity with further temperature increase is due to a decreased rate of adsorption of NH_3.

This same increase and subsequent decrease in activity with increasing temperature has also been reported in many organic dye photodegredation reactions with an optimum temperature range cited as being between 40-50°C [11-13]. The shape of the activity curves shown in **figure 3.9** is likely caused by the same effect as mentioned in these papers which is as follows:

- At low temperatures the desorption of reaction products is disfavoured and this effect begins to dominate.
- At high reaction temperatures the adsorption of reactants is disfavoured and this effect begins to dominate.

This leads to the observed optimum temperature at 40°C.

Effect of Stirring

The effect of stirring was tested by running the reaction as normal under UV illumination and then stopping the stirrer bar and switching off the lamp at a certain point in the reaction, allowing time for the larger catalyst particles to settle, and finally switching on the lamp (**Figure 3.10**).

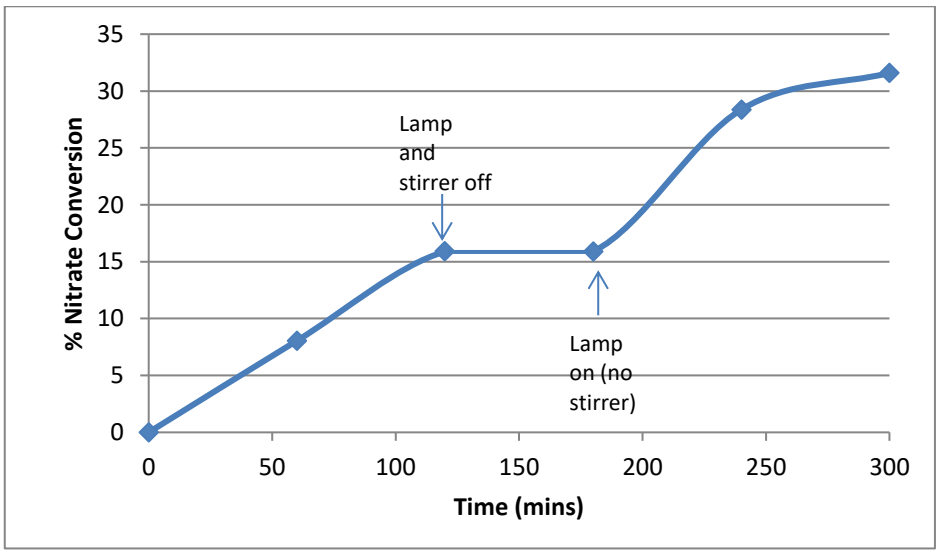

Figure 3.10: Nitrate conversion over time showing points at which illumination and stirrer was turned off as well as the point at which the illumination was resumed.

The first 180 minutes of the reaction proceed as expected with a steady rate of reaction being observed and activity falling to zero during the period in which the lamp was switched off. Upon observation of the reaction vessel during this period a great deal of sediment could be seen at the bottom of the reactor, the solution was noticeably less turbid. Upon re-illumination, activity not only resumes but resumes with a slight increase in rate compared to the stirred reaction. This is likely due to the fact that as the stirrer is stopped and catalyst allowed to settle, the turbidity of the solution is decreased allowing for better light penetration. This is analogous to reducing the catalyst mass in the system and indicates an optimum mass existing below the 120 mg mass used for the majority of the experiments conducted in this project.

Dynamic Light Scattering Experiments were also carried out in order to try and quantify the average size of the catalyst aggregates. To do this catalyst was shaken in water to form a suspension and this suspension allowed to settle for a measured time while contained in a cuvette inside the DLS machine. At regular intervals scans were conducted and the results recorded in the table below (**Table 3.3**).

Table 3.3: DLS analysis of a suspension of 10 mg catalyst in 10 ml H_2O

0.3%Au/TiO_2	
Time After Agitation (min)	**Average Particle Diameter (nm)**
0	3813
120	1021
P25	
0	6008
120	3451

From this we can see a marked decrease in average catalyst aggregate size as the heavier particles settle out, we can conclude from this that it is the smaller catalyst aggregates doing most of the work and that the average diameter of these particles is <1000 nm. We can also see from tables that there is a considerable difference in average aggregate size between plain P25 and the metal-modified catalyst.

Effect of Choice of Hole-Scavenger and Nitrate/Formic Acid Concentrations

When the catalyst mass is kept constant and nitrate concentration increases, we see an almost proportional increase in initial rate of the nitrate reduction reaction

Plotting the initial reaction rates at against initial nitrate concentration gives an almost straight line, indicating the reaction is 1st order with respect to nitrate. It must be the case then that the apparent linearity in the nitrate percent-conversion plots we have presented previously is not true, and a curve would become evident at higher conversions.

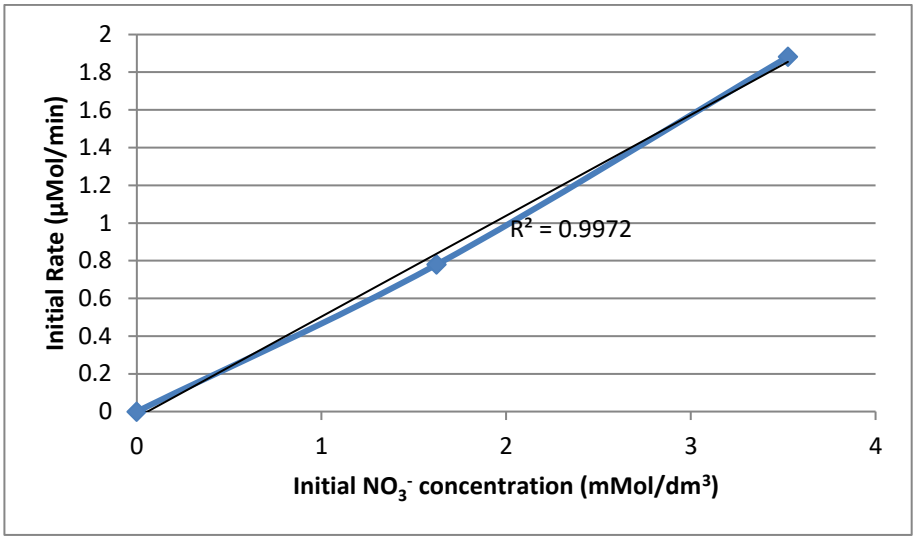

Figure 3.11: Initial rate of reaction vs initial nitrate concentration using a 1%Au/TiO_2 catalyst.

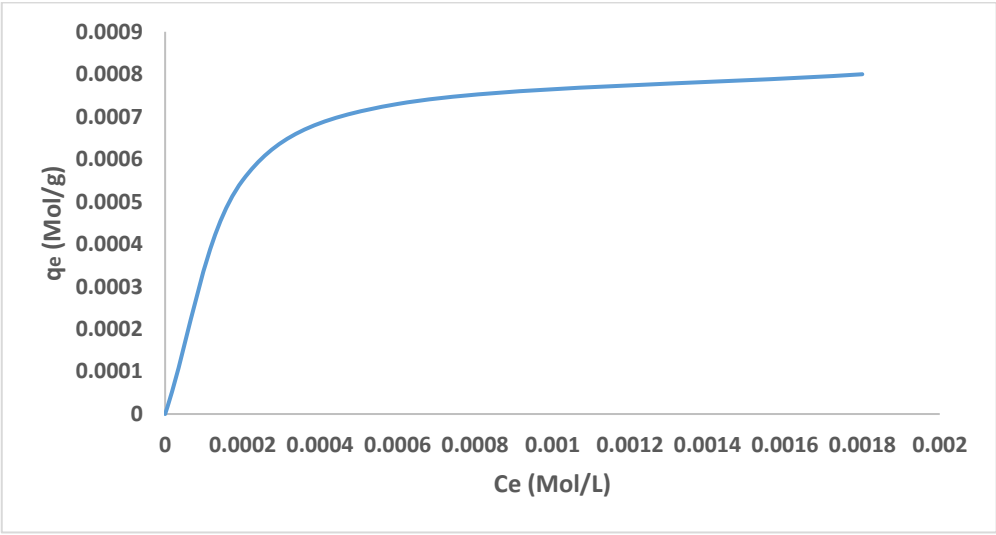

Figure 3.12: Langmuir isotherm of NO_3^- adsorption (reproduced) [16]

It has been reported in the literature however that the order of reaction with respect to nitrate is zero [14], therefore it could be that the nitrate to catalyst surface site ratio in experiments illustrated in **Figure 3.11** is < 1, that is to say that monolayer coverage is not achieved using the catalyst masses and nitrate concentrations used in these experiments. Strangely though, the order with respect to nitrate still seems to be 1st order even at

concentrations well into the plateau zones of the Langmuir isotherm for nitrate adsorption (**Figure 3.12**) [15].

When the starting concentration of nitrate was kept constant (100 ppm) and the initial formic acid concentration varied we see an initial increase in reaction rate between 0.004 and 0.008M and then no further effect upon increasing to 0.016M formic acid.

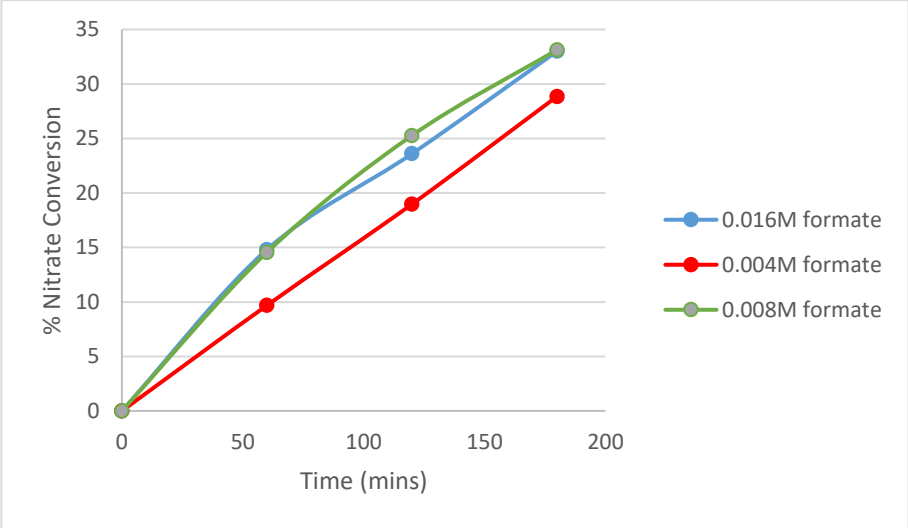

Figure 3.13: Percentage of nitrate converted vs time using several starting concentrations of formic acid (0.2%Au/TiO_2)

The linearity of the nitrate conversion vs time graphs of formic acid oxidation are indicative of a reaction order of zero with respect to formic acid (**Figure 3.13)**. Also indicative of zero order is the fact that as initial concentrations of formic acid increase a proportional increase in reaction rate is not observed. Concentrations of 0.004 M are well into the plateau area of the Langmuir isotherm for formic acid adsorption of P25 [16]. This implies that in a solution containing both adsorbates the formic acid dominates surface coverage since increasing the concentration of formic acid does not affect reaction rates nearly as much as the concentration of nitrate. It has been demonstrated that oxalic acid, while having a lower Langmuir isotherm coefficient than nitrate, heavily out-competes nitrate for surface sites in bi-component systems [15]. This is theorised to be due to the ability of the oxalate species to act as a bi-dentate ligand, or due to it having two modes of adsorption (two carbonyl bonds or one carbonyl and one hydroxyl). The data shown in **Figure 3.12** and **Figure 3.13** is good evidence for surface site domination by formic acid in a bi-component solution, perhaps due to the formate formed having an ability to bind both via its carbonyl and hydroxyl groups separately.

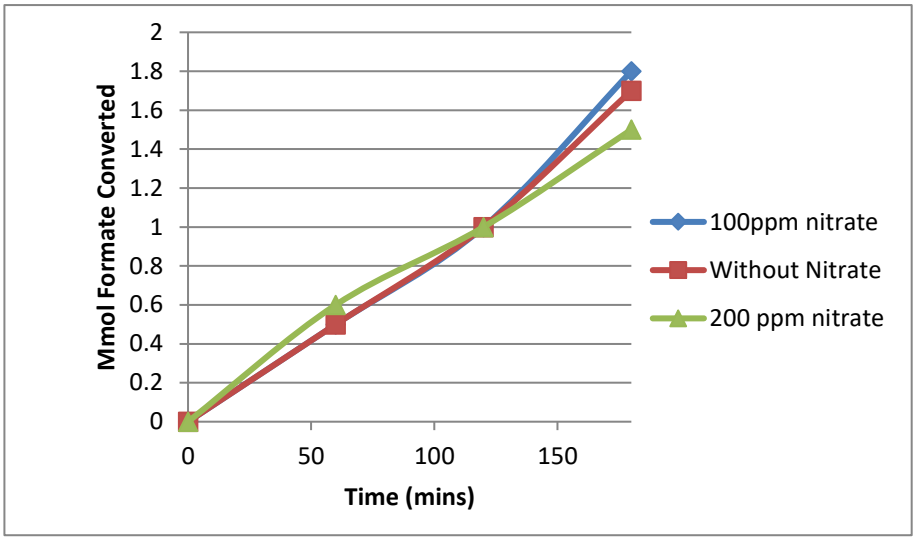

Figure 3.14: Mmol of formic acid converted vs time using different starting concentrations of NO_3^- (1%Au/TiO_2)

When considering the formic acid oxidation reaction, an apparent order of zero is observed with respect to nitrate due to linear plots of formic acid conversion against time and no significant effect on activity when changing initial concentrations of nitrate; even when nitrate concentration is zero (**Figure 3.14).**

This implies that in the absence of nitrate, the photogenerated electrons are able to react with other species in the reaction mixture (such as dissolved oxygen) and thus the catalytic cycle is not broken and oxidation of formic acid can continue. As the concentration of nitrate rises past a certain point the formic acid oxidation rate begins to fall, implying competition between formate and nitrate for catalyst surface.

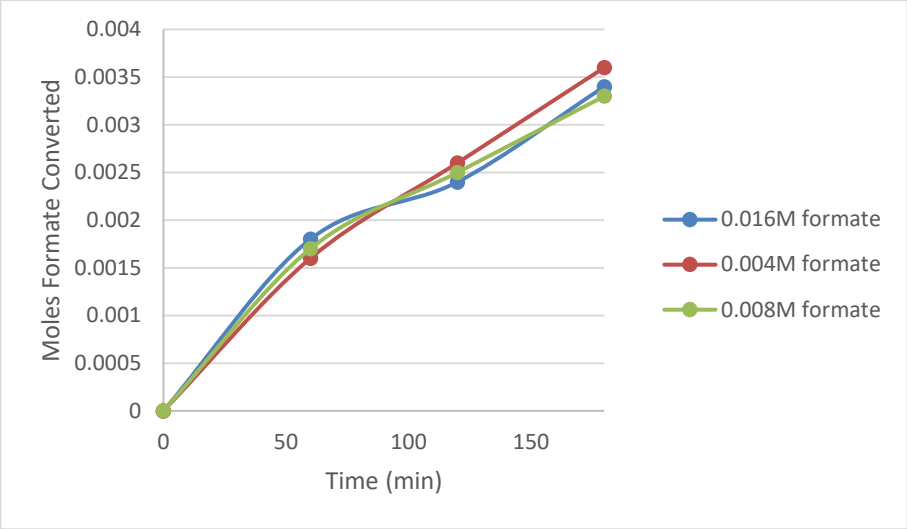

Figure 3.15: Mmol of formic acid converted vs time using different starting concentrations of formic acid (1%Au/TiO_2).

Figure 3.15 shows that, as expected from the concentrations used, the apparent order of reaction for formic acid oxidation with respect to formic acid is zero due to these concentrations occupying the plateau region of the Langmuir isotherm for formic acid adsorption on TiO_2.

Initially oxalic acid was used as a hole-scavenger to mimic the experimental conditions presented in Anderson's 2012 paper [3]. Several attempts were made to achieve activity using this hole-scavenger with sol immobilisation and IW catalysts being tested with different Au loadings. While oxalic acid decomposition was observed under illumination we could not achieve any activity for nitrate reduction using oxalic acid as a hole-scavenger. Formic acid was then tested as literature studies have shown it to yield better activities for several photocatalytic reactions over other organic acid scavengers.

Nitrate VS Nitrite Reduction

With regards the nitrate reduction reactions conducted using TiO_2 and Au/TiO_2 catalysts; no reaction products were detected using ion chromatography. From this it was suspected that nitrate is converted solely to N_2 since no ammonia was detected using an ion-selective probe in all but the highest conversions. To investigate this, NO_3^- ions were replaced with NO_2^- ions in the same concentrations and the experiment conducted again using a plain P25 TiO_2 catalyst.

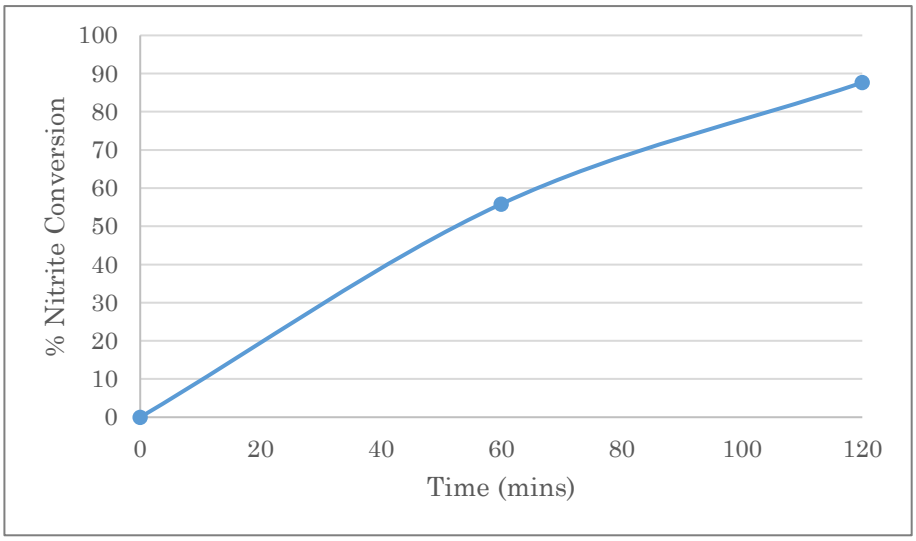

Figure 3.16: Nitrite conversion vs time using a 1%Au/TiO_2 Catalyst.

The result was a stark increase in conversion after 120 minutes of reaction time when compared to NO_3^-, showing NO_2^- to be preferentially reduced over NO_3^- (**Figure 3.16**). This drastic difference in rate of reduction rate is likely why no NO_2^- is observed as a side product of the nitrate photo reduction reaction, any of it that is formed is very quickly converted to N_2 and so no appreciable concentration of it remains in solution when sampled and analysed. This is supported by the standard reduction potentials of the reaction of nitrite to N_2 which is more positive than that of nitrate to nitrite [17].

E_0 (NO_3^- /NO_2^-) = 0.49 V

E_0 (NO_3^- /N_2) = 1.25 V

E_0 (NO_2^- /N_2) = 1.45 V

E_0 (O_2/H_2O) = 1.23 V

Our partial assumption of a selectivity of 100% with regards to N_2 when using TiO_2 catalysts is supported by literature that also notes a lack of reduction by-products when using plain TiO_2 with formic acid as a hole-scavenger [18]. Conversely, a decrease in selectivity in high pH environments has also been well documented [19-21].

Mikami *et al* in their 2003 paper attributed the accumulation of nitrite to OH^- ions retarding the adsorption of nitrite on the surface of Pd nanoparticles deposited on a TiO_2 support [22].

To summarise, the catalyst mass used in these experiments is sufficiently high that any increase in mass is offset by an increase in the turbidity of solution and in future works a

lower mass could be used to greater effect. Competition for adsorption sites exists between nitrate and O_2 but when using standard deionised water this competition is negligible. The order of the photo-reduction of nitrate reaction with respect to nitrate appears to be first order over the range of concentrations tested (100-200 ppm) while the reaction with respect to formic acid is zero order at higher formic acid concentrations (0.008-0.016 M). This is due to surface domination by formic acid at these concentrations. At a lower concentration of 0.008M formic acid concentration activity is affected, this is strange as the Langmuir isotherm for formic acid adsorption shows adsorption to have plateaued at even at this lower concentration. Formic acid oxidation is unaffected by nitrate concentration, dissolved O_2 likely acts as an electron scavenger here to complete the photo-catalytic cycle. Future experiments should be conducted in the absence of NO_3^- and O_2 to confirm. Finally, nitrite has been demonstrated to be photo-reduced by Au/TiO_2 at a much faster rate than nitrate which is reflected by the reduction potentials of these anions; explaining why no nitrite is observed when using these catalysts for nitrate photo-reduction.

3.2.3 Inactivity of Sol-Immobilisation Catalysts

Before initiating any catalytic testing, several different methods for nitrate, nitrite and ammonia analysis were explored before Ion Chromatography (IC) was eventually settled upon (Chapter 2).

The first preparation method to be explored was sol-immobilisation, this method chosen initially due to the ease of nanoparticle tuning through the use of various stabilising agents in varying concentrations [23]. A 1% Au/TiO_2 catalyst was made using aurochloric acid as the Au precursor and Poly Vinyl Alcohol as the stabiliser. The performance of this catalyst was tested against a 1%Au/TiO_2 catalyst of known activity using CO oxidation and later glycerol oxidation as the benchmark reaction. The reason glycerol oxidation was used in this case was due to the unavailability of equipment at the time to carry out photocatalytic nitrate reduction and because the results of this reaction may prove interesting as a side-project.

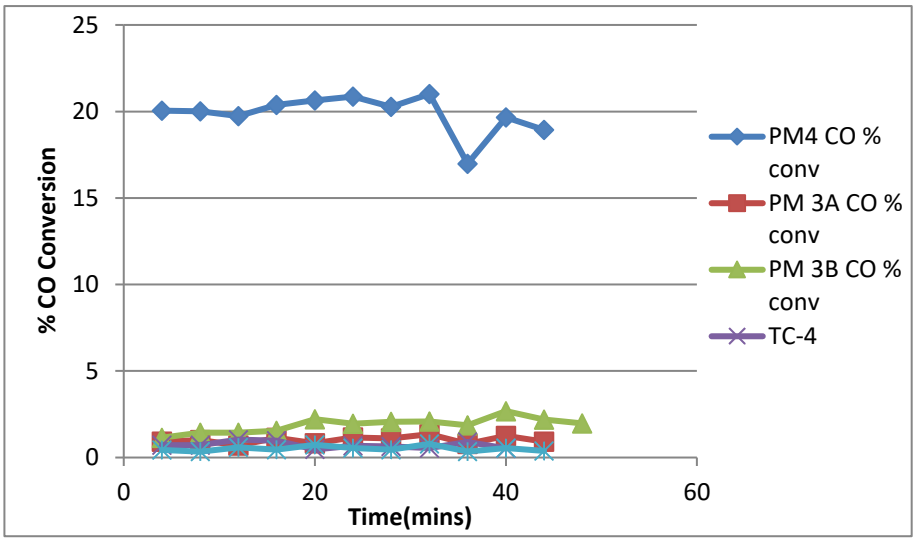

Figure 3.17: CO percent conversions using different batches of 1%Au/TiO_2 where PM denotes catalyst made by a supervisor and TC denotes catalysts made by the author. PM4 is a catalyst that has undergone a 1h reflux in water at 90°C to remove stabiliser.

Table 3.4: Activity comparison of Au/TiO_2 catalysts prepared using different methods.

Catalyst Used:					
P25	Time (mins)	Nitrate (ppm)	Formate (M)	Nitrate % Conversion	Formate % Conversion
	0	102.8	0.008	0.0	0.0
	60	99.2	0.0074	3.5	7.5
	120	91.2	0.0066	11.3	17.5
	180	86	0.006	16.3	25.0
Catayst Used: 1%Au/TiO_2 (DP)					
	0	101.2	0.007	0.0	0.0
	60	94.8	0.0066	0.0	5.7
	120	87	0.006	4.2	14.3
	180	80.8	0.0054	9.7	22.9
Catalyst Used: 1%Au/TiO_2 (IW)					
	0	102.6	0.008	0.0	0.0
	60	94.8	0.007	6.5	11.1
	120	87	0.006	14.7	17.8
	180	80.8	0.0048	21.8	26.7
Catalyst Used: 1%Au/TiO_2 (wet impreg)					
	0	114	0.009	0.0	0.0
	60	106.6	0.008	6.5	11.1
	120	97.2	0.0074	14.7	17.8
	180	89.2	0.0066	21.8	26.7

The activity of the sol-immobilised catalyst was found to match that of catalysts prepared by a supervisor (**Figure 3.17**) and eventually photo-catalytic nitrate reduction was carried out using a fresh batch. Very little or no activity was observed for photo-catalytic nitrate reduction using solar-simulated, UV-only or visible-only conditions; this result was repeated using several reaction temperatures. This inactivity seems to be unique to the sol-immobilisation method as the activities of 1%Au/TiO_2 catalysts made via other methods yield activities of up to 21 % nitrate conversion after 3h illumination (**Table 3.4**).

It was proposed that the sol-immobilised catalyst may not be active due to a blocking of incoming light by PVA on the surface of the Au nanoparticles, and perhaps the surface of the titania as well. This theory was supported by CO oxidation experiments performed using a 1%Au/TiO_2 catalyst that had been refluxed in water for an hour at 90°C and showed a significant increase in activity over the equivalent non-treated catalysts (**Figure 3.17**). The same phenomenon was not observed in photocatalytic nitrate reduction however with no activity being observed even after water reflux. It is possible that the PVA is removed during the reaction condition of nitrate reduction and that the refluxing step is unnecessary. Further experiments were carried out including the preparation of a sol-immobilisation catalyst using a different stabilising agent (citric acid) and with no stabiliser at all (**Figure 3.18).**

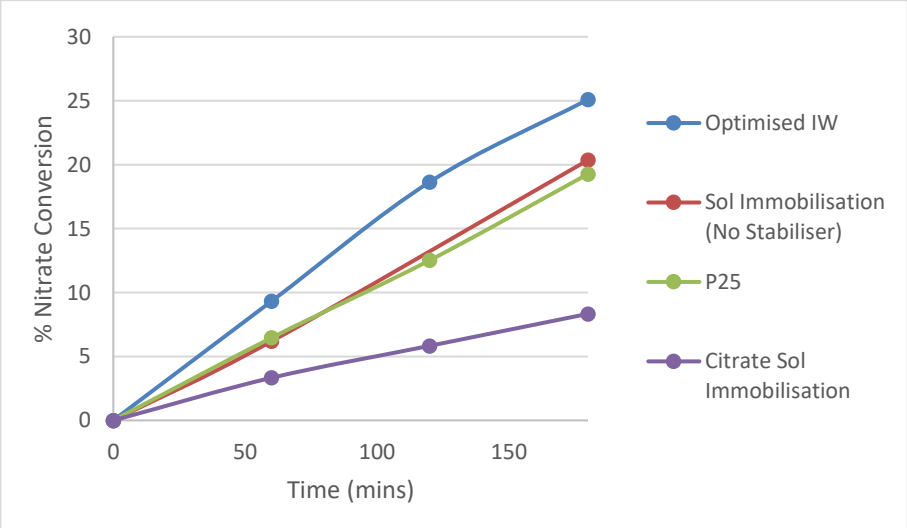

Figure 3.18: Comparison of activities of plain titania and 1%Au/TiO_2 prepared via IW and sol immobilisation methods.

From these experiments can be seen that the stabiliser-free catalyst showed similar activity to that of plain P25 whereas the citric acid-prepared catalyst was showed to be

inferior to plain P25. The evidence from these tests suggested that the presence of PVA stabiliser in particular was responsible for the inactivity of the original sol-immobilised catalysts. The apparent detrimental effect of PVA was further tested by treating P25 with PVA as per the sol-immobilisation method but in the absence of any Au precursor; this catalyst was then tested under the same conditions and compared against plain P25 (**Figure 3.19**).

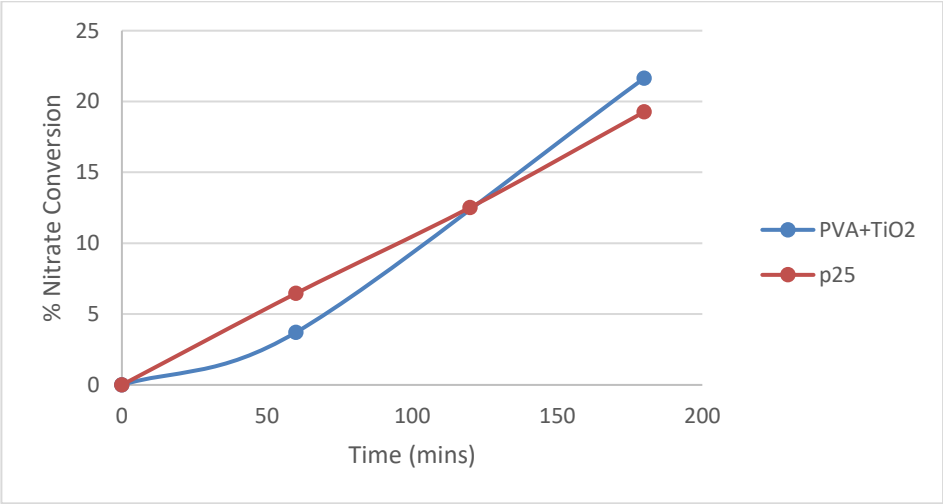

Figure 3:19: Effect of treating P25 with PVA as part of sol-immobilisation preparation.

The results of this experiment showed that the PVA itself is not responsible for the lack of activity in sol-immobilisation catalysts that make use of it as a stabiliser. A slight drop in activity is seen initially compared to the pure TiO_2 catalyst which might indicate that the PVA is decreasing activity, but this effect is slight and cannot account for the total lack of activity observed in the PVA-made sol-immobilisation catalysts. The PVA-treated titania actually slightly outperforms the plain P25 when the reaction is finished, indicating the PVA might have been removed from the surface of the catalyst under reaction conditions and thus the activity improves over time. Alternatively, and perhaps more likely, this slight drop in activity may be rationalised by the slight decrease in surface area of sol-immobilised catalysts with increasing PVA concentration as shown in **Figure 3:20.**

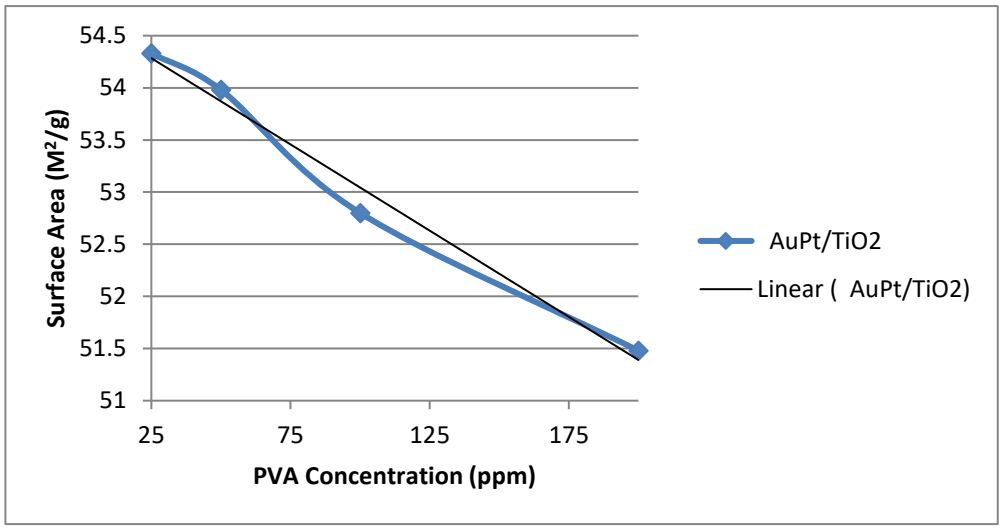

Figure 3:20: BET surface area of resulting catalyst vs PVA concentration in sol-immobilisation prep.

With PVA somewhat exonerated by these experiments as not being the direct cause of the inactivity it is logical that the effect that the stabiliser has on the Au nanoparticles must be important. TEM analysis of these sol-immobilisation catalysts show a relatively narrow particle-size distribution, with particles being on average around 5 nm in diameter. A comparable particle-size distribution could not be obtained for the IW catalysts as very few nanoparticles could be found by TEM, despite ICP confirming the presence of gold in the correct percentages. The particles that were found tended to be much larger than the average particle-size of the sol-immobilisation catalysts. Analysis of citrate-made sol-immobilisation catalysts resulted in no clear Au particles being found.

It could be hypothesised at this point that:

1. Very large Au particles are important for photo-activity as suggested in some of the literature [24] [25].
2. The nanoparticles in the IW and citrate sol-immobilised catalyst actually exist as extremely small clusters of Au atoms that could not be detected by TEM and that these small Au nanoparticles are key achieving to active photo catalysts.

Some evidence was obtained that supports the former when nitrate photo-reduction reactions were carried out using PVA-made sol-immobilisation catalysts that had been calcined for 3h at 400°C. After this heat-treatment the catalysts showed some activity (5% after 3 h illumination) where the untreated catalysts did not, suggesting that perhaps the sintering of small Au clusters during heating in some way facilitated activity.

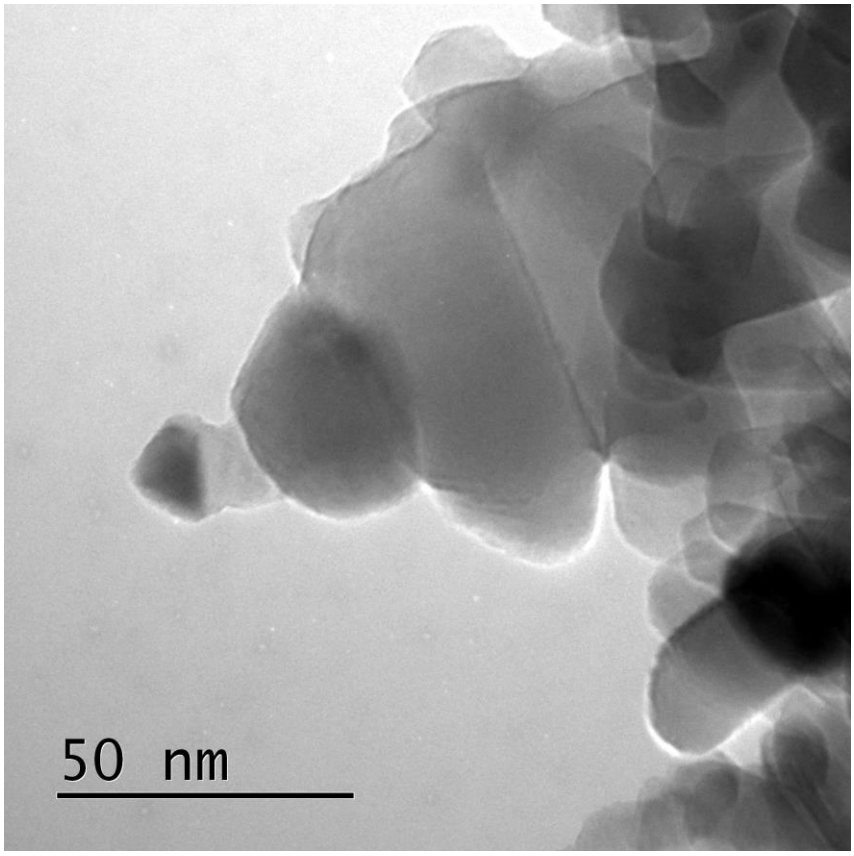

Figure 3:21: TEM analysis of sol-immobilised TiO_2 using citrate as a stabiliser and reducing agent.

The problem with these suggestions is that there is no reason why a catalyst prepared with unfavourably-sized Au nanoparticle should not still have some activity inherent to the plain P25, which is not observed in the PVA-made sol immobilisation catalysts. This issue is addressed in section **3.3.4.**

3.2.4 Blank, Dark and Visible-Light Reactions

In order to confirm the observed reduction of nitrate was photocatalytically accomplished, and to rule out thermochemical and non-catalytic reactions, the reaction was carried out under the following different conditions:

- Under illumination in the absence of catalyst.
- Without illumination in the presence of catalyst.

Table 3.5: Blank and dark reactions of 1%Au/TiO_2

No catalyst, Illumination				
Time (mins)	**NO_3^- (ppm)**	**Formate (M)**	**NO_3^- % conversion**	**Formate % conversion**
0	87.6	0.0082	0.0	0.0
180	88.4	0.008	-0.9	2.4
Catalyst No Illumination				
Time (min)	**NO_3^- (ppm)**	**Formate (M)**	**NO_3^- % conversion**	**Formate % conversion**
0.0	96.0	0.0082	0.0	0.0
180.0	100.0	0.0084	-4.2	-2.4

It is clear from the table that the breakdown of nitrate is indeed catalytically driven as there is no activity observed in the absence of catalyst. Further, from the lack of reaction in the absence of light we can determine that the reaction is indeed a photocatalytic reduction.

Next to be determined was the portion of the solar-simulated light that was responsible for activity; though the absorption edge of plain titania occurs in the UV-region it is possible that Au may serve to extend the portion of the spectrum available for photo catalysis.

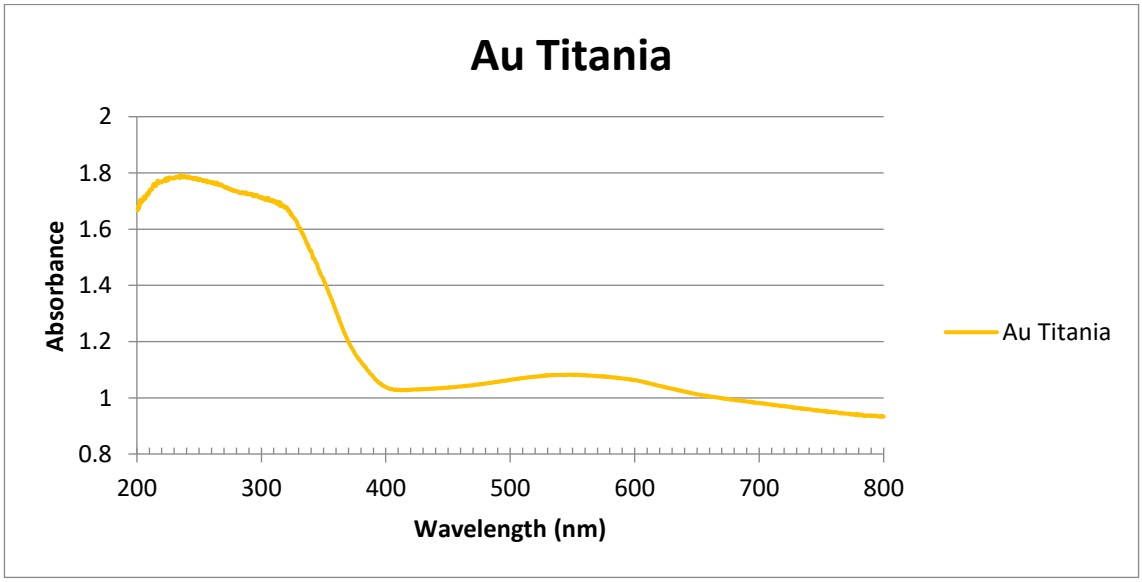

Figure 3:22: Diffuse reflectance UV-Visible Spectrogram of 0.3% Au/TiO_2 showing an SPR band at ca 550 nm.

It has been suggested in the literature that metal nanoparticles such as Au can extend the range of light that is available for catalysis by semiconductors such as TiO_2. As described in Chapter One, the general mechanism for this is the excitation of gold surface electrons by visible light, resulting in oscillations known as Surface Plasmon Resonance which can result in the injection of an electron from Au into the TiO_2 conduction band.

When a UV-blocking (> 420 nm) filter was applied to the reaction apparatus we observe a decline in activity to nil whether using plain TiO_2 or any metal-modified catalyst.

Table 3.4*:* Example of loss of activity when applying UV-filter to reaction setup using M-TiO_2 catalysts

0.4%Ag IW (Filter)				
Time (mins)	**NO_3^- (ppm)**	**Formate (M)**	**NO_3^- % conversion**	**Formate % conversion**
0	99	0.0082	0.0	0.0
180	100	0.008	-1.0	2.4
0.4% Ag IW (No Filter)				
Time (mins)	**NO_3^- (ppm)**	**Formate (M)**	**NO_3^- % conversion**	**Formate % conversion**
0	99.6	0.0082	0.0	0.0
180	78.6	0.0004	21.1	95.1

It is clear then that although there is an SPR band present when observing the catalyst under UV-DRS this band does not facilitate the transfer of electron into the conduction band of the semiconductor as is proposed in the charge-transfer theory of SPR.

Although many reports exist of visible-light photodegredation of organic dyes, there are very few literary examples that are available which report nitrate reduction under exclusively visible light; there are fewer still that involve the use of titania. Successful outcomes for the degradation of dyes and also of phenol have been reported by using catalysts which have been treated with inorganic compounds such as N, F or S which are substituted into the titania lattice, replacing oxygen [26] [27]. One of the few examples of successful nitrate reduction reported in the literature utilises the co-doping of N and Nb into the TiO_2 lattice [28] . Efforts to induce visible-light activity via this non-metal doping method combined with the deposition of NMNP's is discussed in the next chapter (Chapter 4).

Nevertheless these results show that, for the photo-reduction of nitrate ions under solar-simulated light using NMNP-TiO_2, catalytic activity is improved by increased charge-carrier separation only.

3.3 Optimising Incipient Wetness

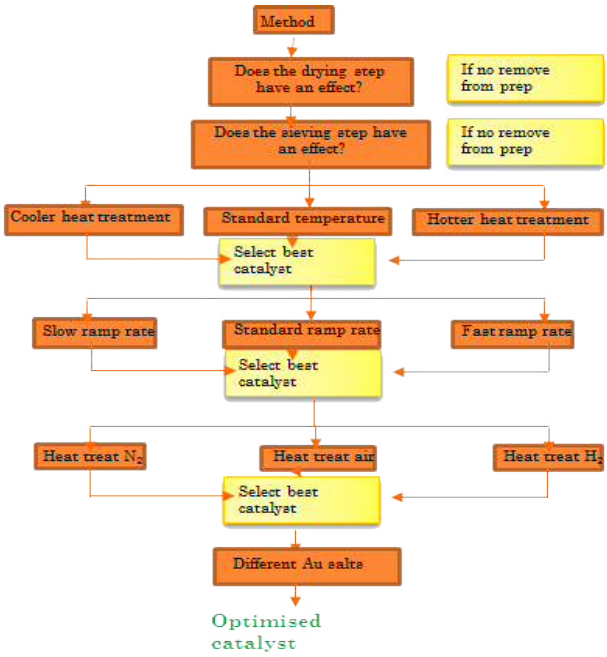

Figure 3:23: Schematic of Incipient Wetness Optimisation Method

From here it was decided that the IW method should be looked at in more detail and efforts were made to optimise this preparation in the hope of finding out why it makes for such highly active photo catalysts. 1%Au/TiO_2 is the catalyst in question during the next section unless specifically stated otherwise. A general plan was laid out which makes clear the process by which this optimisation would occur (**Figure 3.23**).

In this section we will look at each step in the schematic shown in **Figure 3.23**

3.3.1 Effect of Drying Step and Order of Heat-Treatment

The heat-treatment of NMNP-TiO_2 catalysts plays an important role in determining factors such as how strongly the Au binds with the semiconductor as well as the size of the Au nanoparticles. It is important that the temperature of the heat treatment is high enough to bind the Au to the semiconductor as poor binding will cause the metal to leach into the reaction medium. Too high a temperature introduces its own unique effects as the

agglomeration and thus increase in size of the NMNP's is promoted by heat. A series of experiments was carried out in which the catalysts were prepared with the removal of one or both of heat treatment steps, and with their orders reversed. This was done in order to investigate the effect of the drying step and the importance of its particular place in the catalyst preparation.

As can be seen from **Figure 3.24** the order of the heat-treatment has a small effect on the activity of the catalyst. The order that yields the best catalyst is a drying step followed by a calcination step; with the removal of either step resulting in a similarly inferior catalyst.

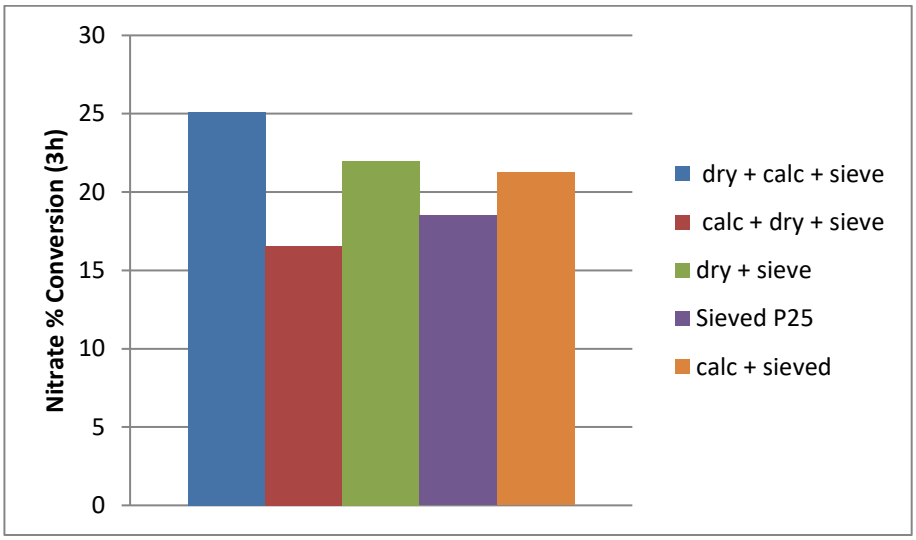

Figure 3.24: Nitrate conversions after 3h using 1%Au/TiO_2 catalysts prepared using differing combinations of heat-treatments.

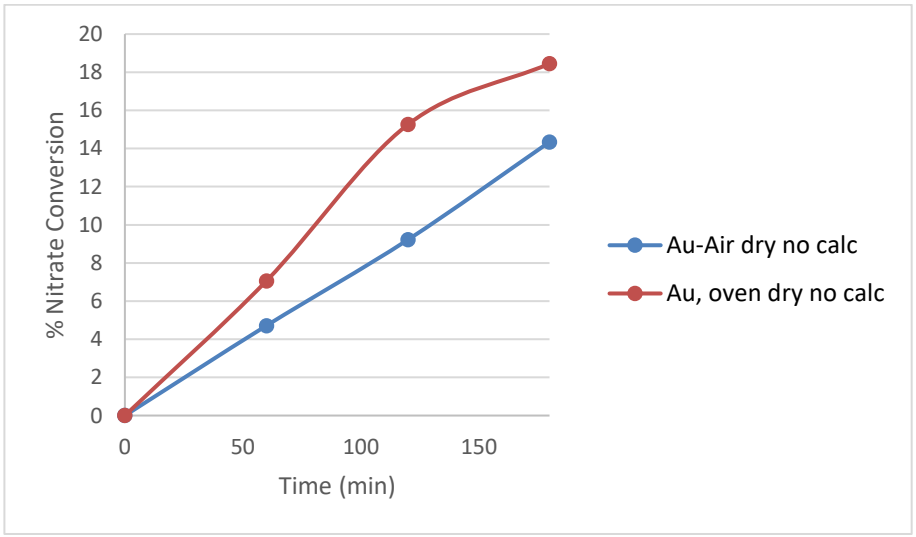

Figure 3.25: Nitrate conversions of 1%Au/TiO_2 made with different drying steps.

The reasoning behind this is likely due to each step's effect on the size of Au nanoparticles, with the drying step followed by calcinations providing optimum conditions in terms of temperature, heating time and heating rate to yield nanoparticles of a more favourable size compared to the other heat treatment combinations. The effect of the heat treatment steps will be looked at in more detail in section 3.3.3.

Figure 3.25 compares the performance of two Au/TiO_2 catalysts made via incipient wetness without the calcinations step; they differ in that one was dried at ambient temperature in air while the other was dried in an oven at 110°C. It is well known that high temperatures cause sintering of supported noble metal nanoparticles, resulting in larger particles. It has also been shown that for some photocatalytic reactions, a larger Au particle can yield higher activities than smaller ones. One such paper is a 2017 paper by She *et al* which report an increase in photocatalytic activity for the destruction of rhodamine B with the increase in Au particle size [29].

A

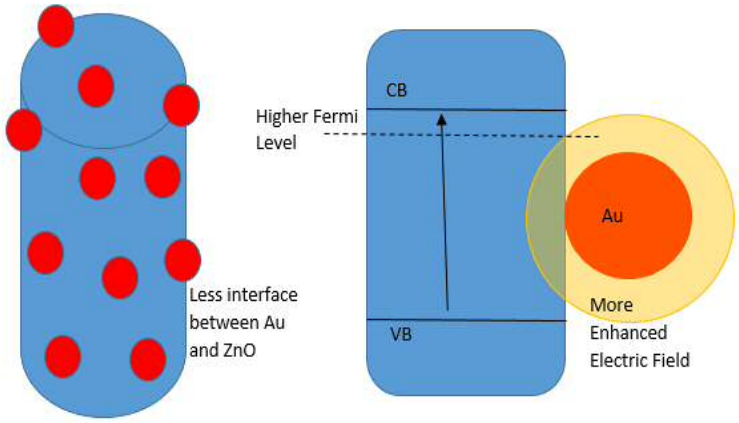

B

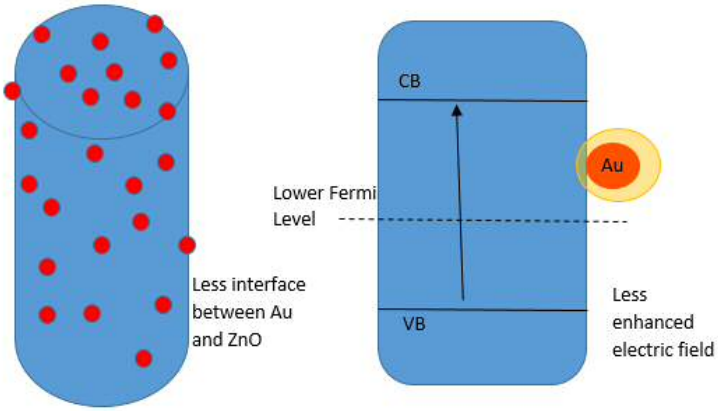

C

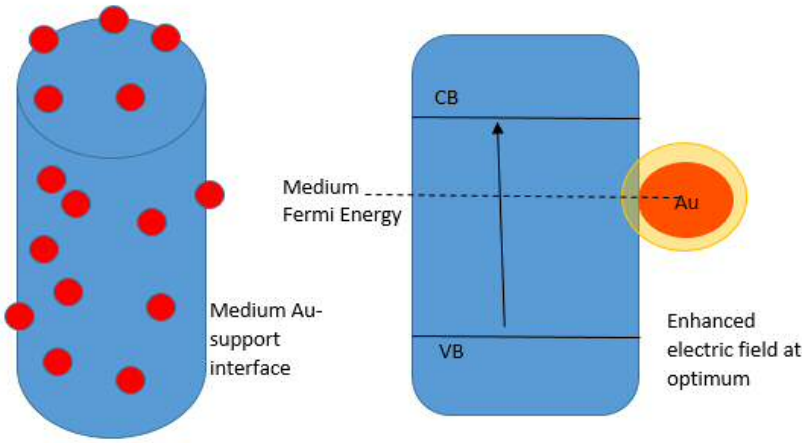

Figure 3.26: Diagram explaining the occurrence of an optimum Au particle size on a ZnO support: A) large Au particles B) Small Au particles C) Medium Au particles

(reproduced [29]).

The authors note an optimum nanoparticle size (*ca* 40 nm), with any increase in size past this point causing losses in activity. The authors also offer an explanation as to why this effect is observed, postulating that as nanoparticles increase in size they increase the range of light available for utilisation which is counteracted by a decrease in the Au/support interfacial area which leads to inefficient charge transfer between Au and TiO_2 (**Figure 3.26**).

Conversely, low temperature drying in the absence of a high-temperature calcination step should promote the formation of smaller Au nanoparticles; the lower activity of the catalyst dried in this way may be further evidence that larger Au nanoparticles are favoured in the photoreduction of nitrate.

It is interesting to note that drying temperature has been reported in past literature to have an effect on the photo-activity of plain titania thin-film catalysts. In their 2011 paper, Cybula *et al* demonstrated that activity for the photo-conversion of CO_2 to methane was increased with increasing drying temperature up to an optimum of 120°C. The authors of the paper provide no rationalisation of this phenomenon and since the temperature differences are not likely to cause any change in phase composition, pore structure or surface area it remains hard to explain [30].

In addition to nanoparticle size effects, the drying step can have a major influence on the distribution of metal deposited on a catalyst [30] [31]. It has been shown using experimentation and computer simulation that high drying temperatures (>80°C) can cause strong convection currents to move metal towards the surface of the catalyst. This is known as an egg-shell metal profile and the effective increase in surface concentration of the metal might contribute to the increase in activity observed when catalysts are dried in an oven compared to ambient drying.

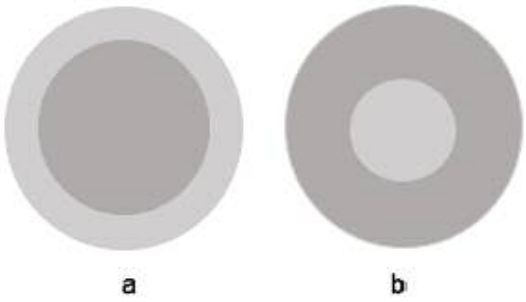

Figure 3.27: Diagram showing different configurations of active material (light grey) and inactive support (dark grey) where; a) egg-shell, b) reverse egg-shell.

It is important to note that in the absence of a high-temperature calcination step the catalysts would likely be unstable and leach metal into the reaction solution. The activity of colloidal Au for this reaction is shown to be zero later in the chapter.

3.3.2 Effect of Sieving

The effect of passing the catalyst through a metal sieve with a 53 micron mesh size was tested by comparing sieved and un-sieved samples of P25 and 1%Au/TiO_2.

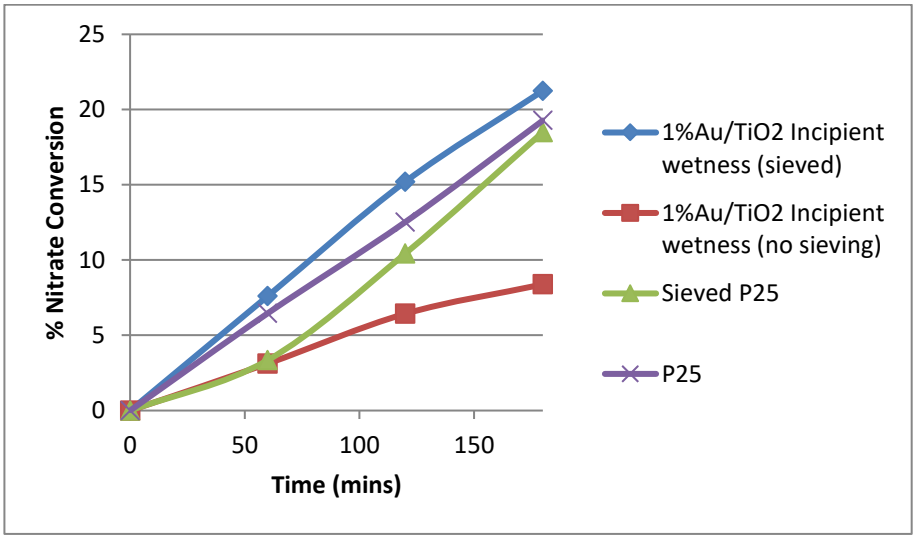

Figure 3.28: Effect of sieving step on nitrate conversions.

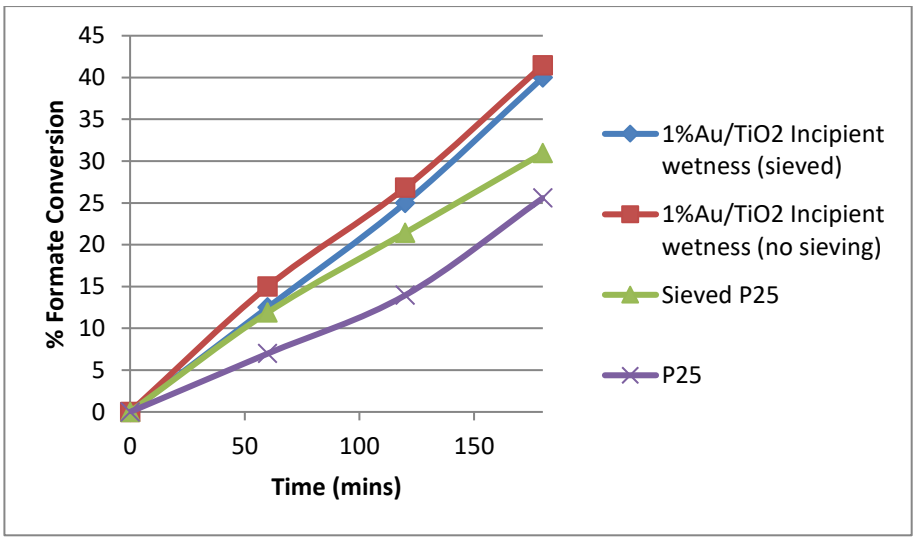

Figure 3.29 Effect of sieving step on formic acid conversions.

The intention behind the sieving step was to prevent the agglomeration of catalyst during the various steps involved in the preparation method and so was only intended to prevent large catalyst particles from entering the reactor (>53 micron). It can be seen from **Figures 3.28 and 3.29** that there is a marked improvement in catalytic activity between sieved Au/TiO_2 and the non-sieved equivalent. DLS analysis shows this to be due to the sieving step countering the agglomeration of catalyst during the preparation step because the average particle size is smaller post-sieving compared to pre-sieving.

Table 3.5: DLS analysis of 1%Au/TiO_2 and P25 pre-sieving and post-sieving.

1%Au/TiO_2	**Average Particle Diameter (nm)**
Pre-sieve	6218
Post Sieve	4101
P25	
Pre-sieve	8954
Post-sieve	7355

The most obvious explanation for this increase in activity is the increase in the available surface area for photons to interact with that is inherent with removing larger catalyst aggregate particles with sieving. It is strange then how sieving of P25 causes such a large increase in activity when the crystallite size of the P25 is claimed by Degussa to be 25 nm, much smaller than the mesh size of the sieve. It may be that the P25 has agglomerated somewhat over time due to the storage conditions and that the sieving step removes the particles larger than 53 microns. This is supported by DLS analysis which shows a decrease in average particle size post-sieving. It must be noted that the DLS data can only be used comparatively as the estimation of particle size is likely to be poor.

3.3.3 Effect of Calcination Conditions

Figure 3.24 showed that removing the calcination step completely only has a slight effect on the activity of the catalyst. Therefore you might expect that changing the temperature of the calcination would have very little effect on the activity of the catalyst. Nonetheless in the interest of optimising each variable in the incipient wetness process three batches of catalyst were made using differing calcination temperatures while keeping all other steps in the preparation identical. The temperatures chosen were 250°C, 400°C and 550°C for the following reasons;

- 250°C – a temperature significantly lower than 400°C but significantly higher than the drying temperature.
- 400°C – a temperature commonly reported in the literature as for several different preparation methods due to the fact that organics and anions such as Cl^- are generally lost at this temperature [32].
- 550°C – a temperature significantly higher than the middle temperature while being safely below the lowest temperature at which temperature-induced phase change (anatase to rutile) is reported [33].

XRD analysis was not conducted on these catalysts but XRD analysis of commercial anatase heated at 250-600°C showed no change in phase and thus none should be expected to have taken place here. This is supported by BET analysis data which shows very little change in surface area between 250°C and 550°C (**Table 3.7**).

Table 3.6: BET Surface areas and corresponding calcination temperatures of 1%Au/TiO_2

Calcination Temperature (°C)	Surface Area (new) (m^2/g)
250	49.9
400	48.4
550	47.5

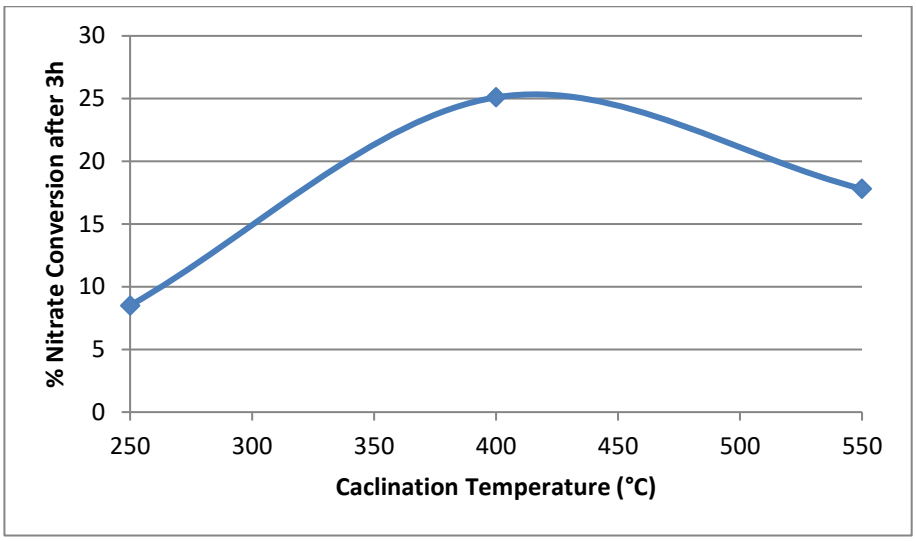

Figure 3.30: Activities after 3h vs calcination temperature using 1%Au/TiO_2 catalyst.

The results of running photo-reactions with these catalysts yielded a "volcano plot" (**Figure 3.30**) with the catalyst calcined at 400℃ being the most active. With TiO_2 phase and surface area contributions considered minimal, the differences in activity must be attributed to differences in Au nanoparticle size or morphology.

Once again this leads us to the trade-off between the Au surface area coverage and particle size as discussed in section 3.3.1 as a likely explanation for the volcano plot observed in **Figure 3.30**. Following this line of enquiry, it seems strange then that the catalyst calcined at 250°C would have achieved a conversion of around 9% after 3 hours whereas in **figure 3.24** we demonstrated an equivalent uncalcined catalyst that yielded a conversion of around 22% after the same reaction time. If the difference in the activities of the catalysts in **figure 3.30** are due to Au particles sintering to an optimum size at an optimum temperature (400℃) then why does a catalyst exposed to only the 120℃ drying temperature have a higher activity than one calcined at 250℃?

The answer to this could be due to the lack of adhesion of the Au nanoparticles to the TiO_2 support when used uncalcined [34]. If the Au particles break away from the TiO_2 during the reaction then there are two possible scenarios that may explain the higher activity of the uncalcined catalyst:

- The free Au nanoparticles are active for nitrate photoreduction and contribute to the conversion alongside TiO_2.

- The Au particles are small (due to low temp) and inactive and their removal from the TiO_2 surface frees the TiO_2 for reactants to adsorb (i.e the reactivity is due to plain TiO_2).

Table 3.7: Activity of colloidal Au for the photoreduction of NO_3^-.

1.2 mg Au (colloidal)				
Time	Nitrate conversion	Formate	NO_3^- % conversion	Formate % conversion
0	101.2	0.0082	0.0	0.0
60	101.8	0.008	-0.6	2.4
120	100	0.0079	1.2	3.7
180	102	0.0079	-0.8	3.7

In order to investigate the first case a colloidal Au solution was prepared by reduction of H_2AuCl_4 in H_2O with $NaBH_4$. No stabiliser was used in order to rule out any deactivation due to stabiliser coating the nanoparticles; 1.2 mg of Au metal was used which is equivalent to a 120 mg of a 1%Au/TiO_2 catalyst. $NaNO_3$ and formic acid was then added and the vessel subjected to illumination under our standard conditions.

It is clear from this experiment that we can rule out the scenario mentioned previously where colloidal Au is responsible for an increase in activity as there is no nitrate conversion when using an Au colloid in the absence of TiO_2. This leaves us the explanation that the activity of this catalyst must be coming from the plain TiO_2, however a conversion of 22% after 3 hours is anomalously high compared to the average conversion of plain P25 in that time (18.7%). This is, however, only slightly outside the average error of a reaction (± 2%). Future reactions should be conducted to confirm the activity of uncalcined catalyst and a reaction could be carried out using a mixture of colloidal gold and plain titania to see if some interaction between the free Au nanoparticles and titania is causing the slight increase in activity over plain P25.

Other variations of the calcination step were investigated but were found to only have a slight bearing on photo-activity. These variables included the atmosphere of calcination (**Figure 3.31**) and the calcination ramp rate (**Figure 3.32**).

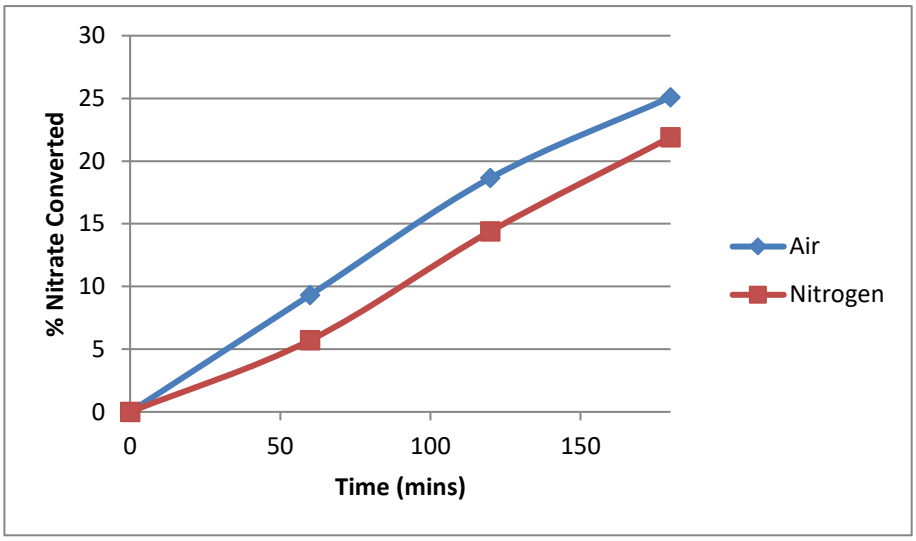

Figure 3.31: Effect of heat-treatment atmosphere on photo-activity for nitrate reduction using 1%Au/TiO_2

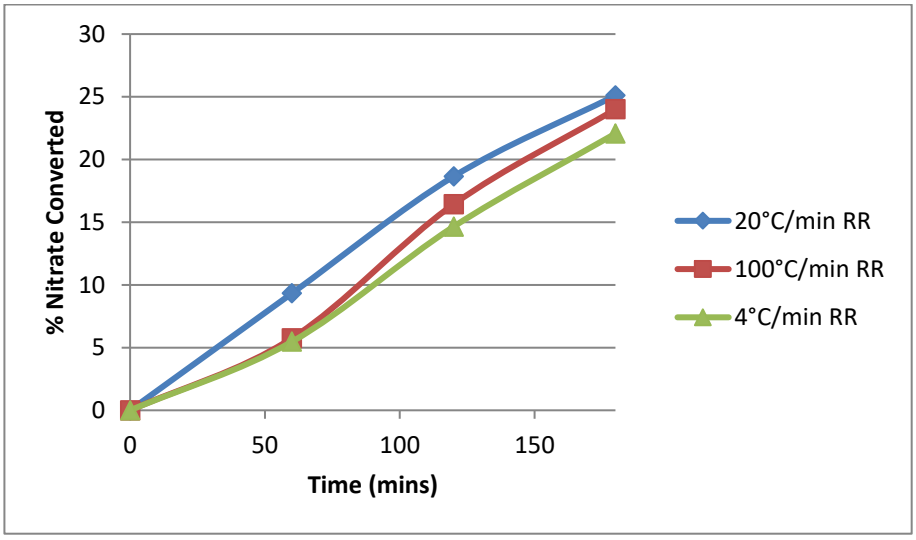

Figure 3.32: Nitrate conversions after 3h using different heating ramp rates during the calcination step (1%Au/TiO_2)

From **figure 3.31** It was found that there was a very slight advantage to heating under static air than near-static (slow flowing) N_2. This slight superiority of an O_2 atmosphere over an N_2 atmosphere has been noted in a paper by N.-L. Wu *et al* as well reporting a large increase in photo-activity for water splitting when using an Ar atmosphere (**Table 3.9**) [35].

Table 3.8: Rates of H_2 production from photocatalytic water splitting using sol-gel titania calcined under different calcination atmospheres.

Calcination Atmosphere	Maximum H_2 Production Rate (µMol/min)
Ar	30.2
N2	5
Air	7.1
Vacuum	2.9
H2	3

Wu *et al* propose that the difference in activities is due to differing concentrations of the surface TiOH or "titanol" groups as evidenced by XPS analysis, this effect is likely responsible for the difference in activities noted in the photo-reduction of nitrate reaction. **Figure 3.32** shows the effect on calcination heating rates on photoactivities of a 1%Au/TiO_2 catalyst. From the data it can be seen that the calcination rate only has a small effect on catalyst activity, with faster heating rates generally being favoured over slower ones and an optimum heating rate of 20℃/min. The 100℃/min and 20℃/min conversions after 3h are so close that the effect of heating faster than a rate of 20°C/min seems to be almost negligible. This is hard to explain as the heating rate effects the total time the catalyst exposed to heat and so catalysts calcined at 4°C/min, while experiencing the same peak temperature time, are exposed to heat for longer as they reach maximum temperature compared to the faster heating rates. An attempt at explaining this effect would be that the higher calcination temperatures facilitate faster nanoparticle crystallisation and thus smaller nanoparticles which are then allowed to sinter to an optimum size during the remainder of the calcination step. It may be that the very slow heating rates result in nanoparticles that are larger than the optimum size and so a reduction in photoactivity is observed.

In conclusion, the most active catalysts prepared by the IW method were achieved by drying at 110°C for 16 h followed by calcination at 400°C at a heating rate of 20°C/min before sieving the catalyst using a 53 micron sieve. It was found that oven drying yielded a better catalyst likely due to convection moving Au from inner-channels in the catalyst to the surface with larger nanoparticles likely being formed over ambient drying. The calcination temperature was found to be optimal at 400 °C due most likely to nanoparticles sintering to optimal sizes at this temperature. Catalysts were found to perform better with faster heating rates, likely this time due to the slower rates forming

undesirably large nanoparticles. Finally sieving was found to have a large influence on activity due to the lowering of the average catalyst particle size.

3.3.4 Effect of Gold Loading

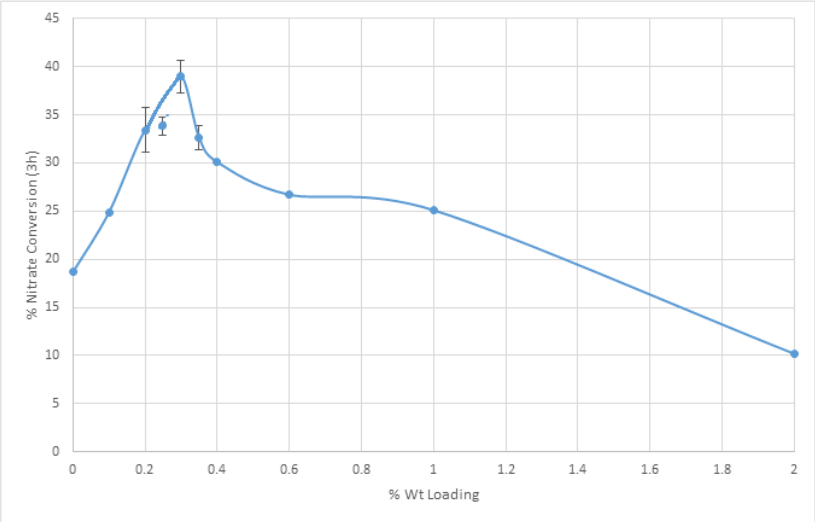

Figure 3.33: Effect of Au % loading by weight on nitrate conversions after 3h reaction time. Error bars are included where experiments were carried out multiple times and give the standard deviation from the mean. Data points with error bars are averages of three experiments at that weight loading.

From this point on in this chapter, all Au catalysts mentioned are made using the optimised method described thus far, that is to say drying at 110°C followed by calcination at 400°C in static air and finally sieving using a 53 micron sieve.

By far the most influential variable in the optimisation of the catalyst however was the Au loading (**Figure 3.33**). From this data we see a clear decrease in photo-activity as we move away from the value of 0.3% wt Au in either direction. This can possibly be rationalised by the trade-off between the increasing photoactivity with increased gold loading and the decreasing activity with a higher surface coverage of titania by gold; leading to an observed optimum at around 0.3% wt Au. An optimum metal loading of around 0.5% has been reported in the literature for other photocatalytic reactions and has been documented using both Au and Pd [36] [37]. This was explained by evidence that the reactions described in these papers took place at the nanoparticle perimeter and that maximum perimeter length must be achieved at weight loadings of around 0.5% wt before overlap occurs.

If we assume atomic dispersion of Au this hypothesis seems plausible, it has been shown however that Au nanoparticle size has been shown to increase with Au loading which makes the two effects hard to decouple [38].

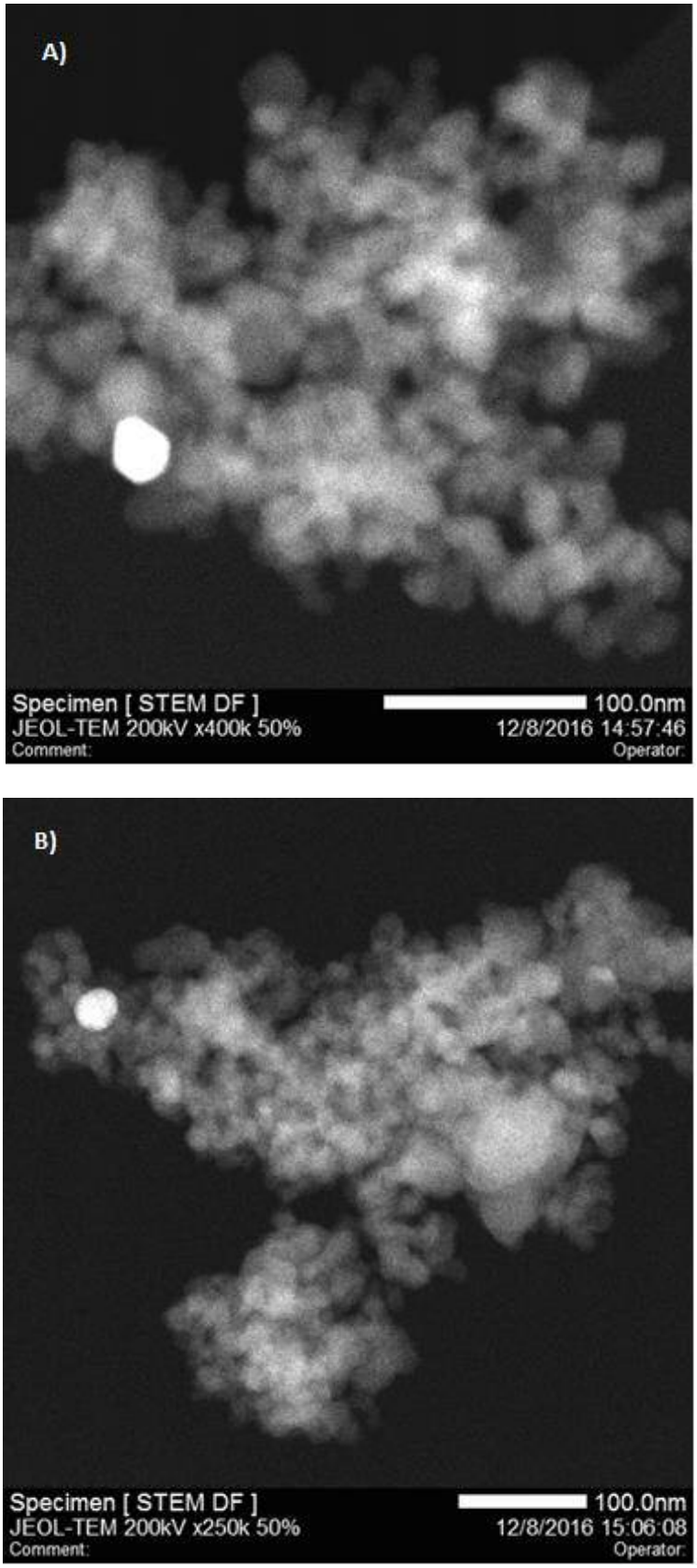

Figure 3.84: TEM analysis of two different areas of 0.3%Au/TiO_2 showing presence of large Au nanoparticles (*ca* 40 nm) which appear as bright circular shapes.

TEM analysis of catalysts in this loading range initially supported the theory of atomically dispersed Au or extremely small clusters as finding any Au nanoparticles at all proved difficult. Initially no Au nanoparticles could be observed even in catalysts with higher loadings as shown by ICP analysis (**Table 3.10**). Further TEM analysis however yielded images of large nanoparticles of between 20- 50 nm or so (**Figure 3.34**). Images at higher magnifications yielded no evidence of very small Au nanoclusters although it is possible that near-atomically-sized particles are present on the surface but are not being detected due to resolution and magnification limitations.

Here then there are two possible scenarios regarding the metal nanoparticle sizes:

1. The active nanoparticles are extremely small and the drop in activity with increased loading is due to increased surface coverage of the TiO_2, if true this could also imply that the active sites are the metal nanoparticle perimeter and nanoparticle overlap is playing a part in reducing activity with increased metal loading. This would also imply the effects of heat treatment variables are due to altering the size and distribution of these small nanoparticles rather than the formation of large nanoparticles as previously postulated.
2. The metal nanoparticles exist only as large (> 20 nm) particles and there is some, as yet unknown reason as to why at higher weight loadings the catalyst activities drop below that of plain titania.

It is possible that the presence of Cl^- in the Au precursor material has a detrimental effect on the activity of the catalyst via a poisoning effect, in fact that is demonstrated to be true in the Chapter 4. Thus the logic here is that with increasing metallic content there is a larger increase in Cl^- ions with respect to the catalyst surface area which remains constant and thus after an optimum is reached we see a decline in catalytic activity. We shall see however, that in Chapter 4 we observe the same volcano plot when using Ag/TiO_2 made using $AgNO_3$ as a precursor meaning that, while Cl^- does act as a poison, it is not solely responsible for the drop in activity when using weight percentages higher than the optimum.

Table 3.9: ICP analysis of several weight loadings of IW-prepared Au/TiO_2

ICP Analysis	
Desired %Wt Au	Measured % Wt
0.2	0.18
0.25	0.2
0.3	0.25
0.35	0.29

3.4 Catalyst Reusibility

An important attribute of any viable photocatalyst is how slowly it deactivates and how well it perfoms upon reuse. There are many examples in the literature of catalytic activity decreasing upon reuse, especially in conventional catalysis. This can be caused by several phenomenon such as coking and metal-particle sintering.

There is far less literature with regards to the resue of Au/TiO_2 photocatalysts however, and the literature that is available suggests excelent resiliance to reaction conditions and sustained activity even over several uses. One such study is a study conducted by Padikkaparambil *et al* which demonstrates negligible loss of activity for the degradation of various dyes even after 10 uses.

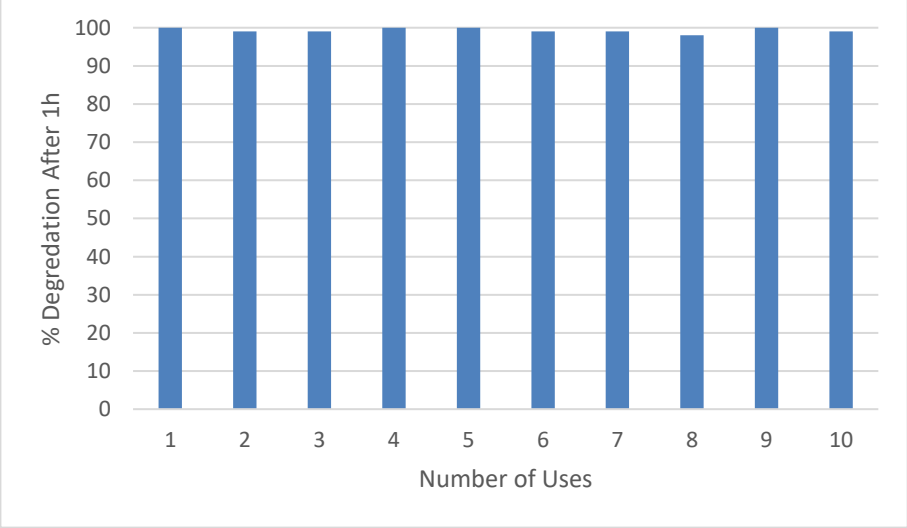

Figure 3.35: Reusability study of 2%Au/TiO_2 for the degradation of methylene blue (reproduced [39])

It has been determined in a previous section that the concentration of hole-scavenger species does play a role in determining the activity of the catalyst. What was not determined, however, is whether the reaction would continue to completion if given more time and sufficient concentrations of hole-scavenger.

To test this, a longer experiment was carried out with a total illumination time of 300 minutes (**Figure 3.36**). It was found that the rate slowed at the reaction progressed with activity dropping off as formate levels approach *ca* 0.004 M. To determine whether this drop in activity was indeed due to low formic acid levels, or by another factor such as catalyst poisoning, another experiment followed in which the same process was carried out with the addition of 0.0092M formic acid after sampling at t = 240 min.

The results showed a massive increase in activity upon the addition of formic acid, showing that the formic acid was the limiting factor in achieving a higher conversion.

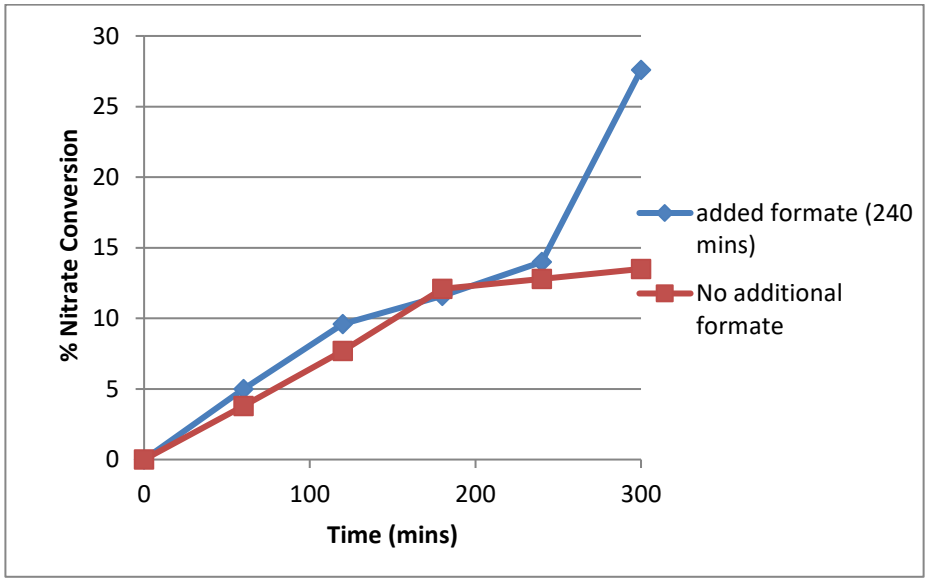

Figure 3.36: Effect off adding additional formic acid as Nitrate conversion tapers off using 1%Au/TiO_2

It must be noted that an anomolously low activity is observed here for this 1%Au/TiO_2 (made via optmimised IW) catalyst that was used for both the formate-addition and non-addition experiments. In these experiments the catalyst yielded only around 11% conversion after 3 hours reaction time whereas previous experiments have shown that the catalyst is capable of converting around double that quantity in the same time frame. This may be down to the age of the catalyst used in these reactions as they had been stored for several months by the time the experiment was conducted, unlike other results reported

in this chapter which were all tested while relatively fresh (> 1 week from preparation to testing).

The reasoning behind catalyst deactivation with prolonged storage has been discussed in the literature. Wu *et al* compared fresh Au/TiO_2 prepared by deposition precipitation with those stored under various conditions including in a deicator and in a freezer [40]. It was found that minimal changes in Au oxidation state, nanoparticle size and nanoparticle distribution occured when the sample was kept frozen even after 300 days storage. Samples strored at room temperature in a dessicator however were found by TEM analysis to have almst doubled in Au particle size (from 3.4 to 5.9 nm) after 15 days storage time. It was also noted that the Au in the dessicator-stored sample became unevenly distributed in comparison to the relatively uniform distribution observed in the fresh sample. This uneven distribution and growth in nanoparticles to an unfavourable size is the likely cause of the lower than expected activity observed when using this particular batch of catalyst.

Table 3.10: Table showing the nitrate and formate concentrations with formate being added at t=240 mins.

1%Au/TiO_2 (added formate)				
Time (mins)	**Nitrate (ppm)**	**Format (M)**	**Nitrate % Conversion**	**Formate % Conversion**
0	100	0.0084	0	0
60	95	0.0072	5	14.3
120	90.4	0.006	9.6	28.6
180	88.4	0.0044	11.6	47.6
240	86	0.003	14	64.3
300	72.4	0.0176	27.6	-109.5

The reason we see an increase in activity when formic acid is added here and not when initial concentrations of formate were increased is because now the formate is being added after the concentration has fallen such that it lies on the rising portion of the Langmuir isotherm for formic acid adsorption.

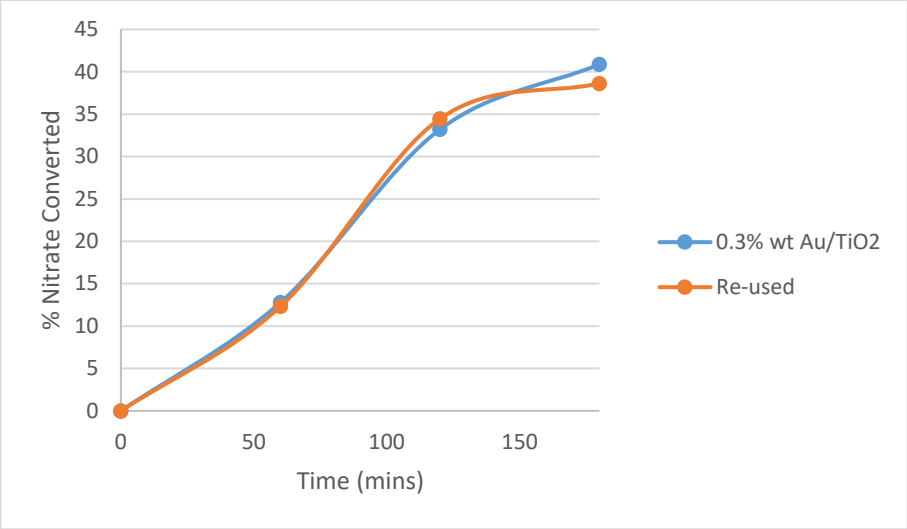

Figure 3.37: Reusability of a batch of 0.3% Au/TiO_2 for photocatalytic reduction of nitrate.

True reusibility experiements were carried out on fresh 0.3%Au/TiO_2 catalysts prepared using the optimised IW method. To achieve this a batch of 0.3%Au/TiO_2 was made and then tested using the standard conditions described in the experimental section. The results of this reaction run are shown in blue circles in the graphs (**Figure 3.3.7**). Next a reaction was run using double the ammount of catalytst (240 mg), with all other variables remaining the same. Samples were not taken during this run. Once the reaction time reached 3h the catalyst was filtered off and washed before being dried in an oven at 110˚C; the catalyst was then re-sieved.

120 mg of the received catalyst was then used in another reaction under the standard conditions defined in the experimental chapter, the results of this experiment are shown using orange circles in the graphs (**Figure 3.37 and 3.38**).

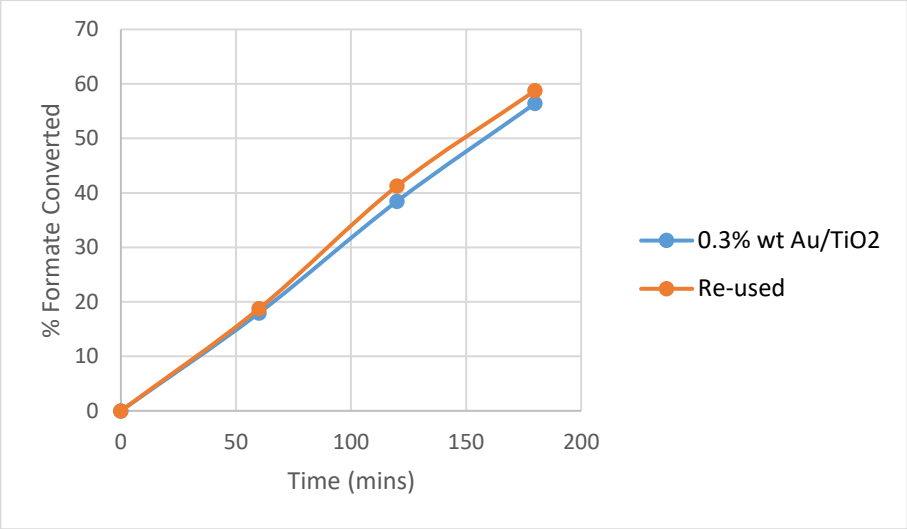

Figure 3.38: Reusability of a batch of 0.3% Au/TiO_2 for photocatalytic oxidation of formic acid

This data shows that the catalyst activity remains largely unchanged with regards to both formic acid oxidation and nitrate reduction after one previous use; this is complimentary to the data found in the literature.

Further experiments could be conducted in which the re-used catalyst is dried at ambient temperatures and tested without the re-sieving step to see how these factors contribute to the activity of the catalyst upon reuse. From the evidence shown so far a prediction can be made that ambient drying would not negatively affect the activity of the catalyst since the NMNP's have already formed and sintered to an optimum size during the previous (and much hotter) heat treatment steps included in the preparation method. I believe the removal of the re-sieving step prior to reuse however will have a detrimental effect on activity due to the agglomeration of catalyst particles during drying.

3.5 IW Treatment on Plain Titania

An experiment was devised in order to ensure that the increase in activity observed when adding Au to P25 using the optimised method is due to the presence of metal and not some effect on the structure of P25 itself. In this experiment, plain p25 was treated using the optimised IW method with the single difference being the use of distilled water in place of aurochloric acid solution. The resulting catalyst converted around 4% less nitrate that the untreated catalyst under the same conditions, confirming that the presence of metal is indeed responsible for the increase in activity.

This result compliments XRD and BET data that suggest no change in catalyst particle size nor any significant change in surface area with the additon of Au.

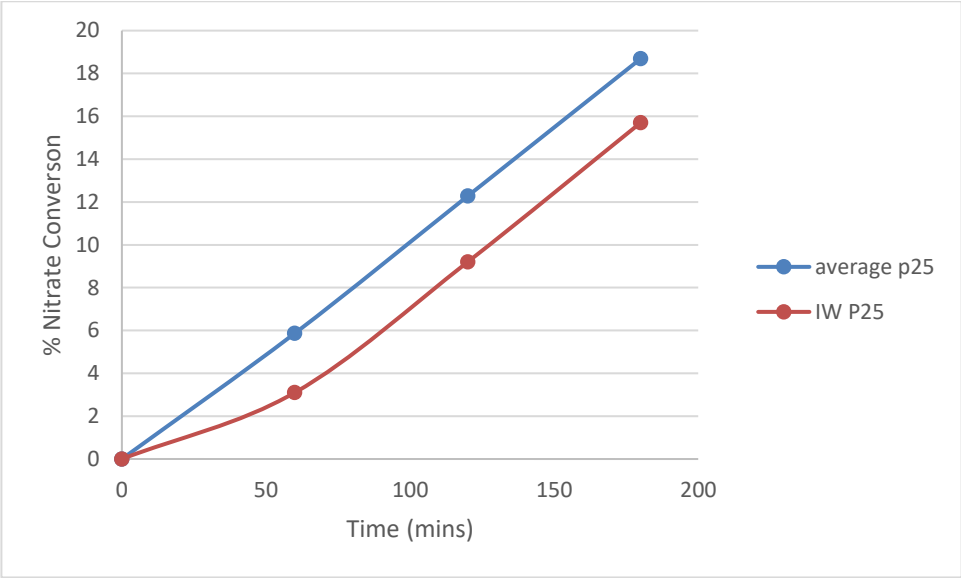

Figure 3.39: Nitrate conversion of P25 pre-IW treatment and post-IW treatment.

3.6 Selectivity to N_2

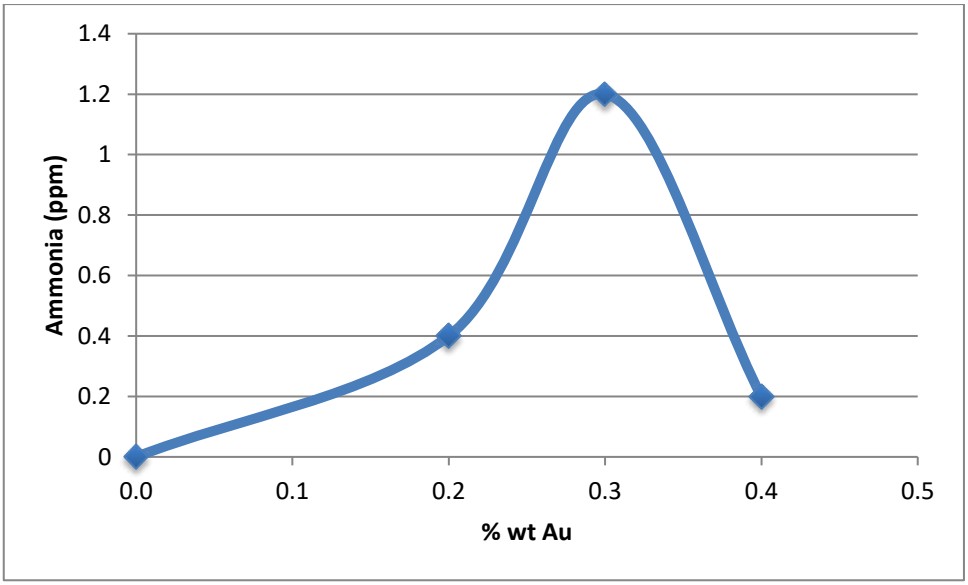

Figure 3.40: Plot of ammonia concentration vs gold loading showing peak ammonia concentration at 0.3%Au/TiO_2

Ammonia was only detected at high conversions of nitrate using Au/TiO_2 catalysts with the highest amount of ammonia being detected at 0.3%Au/TiO_2. No nitrite was detected in any experiment using Au/TiO_2. At this weight loading the selectivity to N_2 was calculated to be 97.1%.

While generation of ammonia is clearly not a big problem with regards to Au/TiO_2 it is still prompts the investigation of other noble-metals to see if 100% selectivity to N_2 can be achieved

3.7 Conclusions

In conclusion, the deposition of Au nanoparticles on TiO_2 by optimised incipient wetness has been shown to improve activity over plain titania by almost 20% with 97.1% selectivity to N_2 and ammonia being the sole by-product. Due to the lack of activity using visible-only light it can be concluded that Au improves the photo-activity of titania by improving charge-carrier separation only and not by extending the range of light available to the catalyst. The activity of these catalysts were found to be dependent on temperature, explained by the changing rates of adsorption and desorption of reactants and products at different temperatures. The catalysts were found to be re-usable with minmal loss of activity upon filtering, washing, drying and subsequent re-use.

One of the biggest factors in determining catalyst activity is catalyst loading, with an optimum loading being found to be at $0.3\%Au/TiO_2$ and weight loadings either higher or lower than this being less active. TEM analysis of these catalysts show only very large Au nanoparticles which have been shown in the literature to improve photo-activities of TiO_2 . However the mechanism by which large nanoparticles are thought to improve the activity of titania is by enhancing the SPR effect and extending the utilisable light into the visible range. It has also been theorised in the literature that a drop in activity with increased metal loading is due to the formation of very small nanoparticles which overlap at high weight loadings, reducing the metal nanoparticle boundry at which reactions such as water-splitting are thought to occur.

It is reasonable to conclude that these very large nanoparticles observed by TEM are not responsible for the increase in activity of Au/TiO_2 for the nitrate reduction reaction and that there must be a presence of small Au nanoclusters which overlap with increasing concentration, diminishing activity either by reducing the perimeter of Au boundry sites or simply by blocking the surface of the titania, preventing the photo-generation of electrons. This explains how some Au/TiO_2 catalysts, such as ones dried in air or subjected to low-temperature heat-treatments, are less active than plain titania, an observation that cannot be accounted for by the presence of only very large Au particles.

Calcination temperature was also found to play a large role in determining catalyst activity. The observed optimum calcination temperature at 400℃ then is explained not by the optimal formation of very large Au particles but perhaps by preventing the overlap of very small Au nanoclusters through sintering, exposing more TiO_2 surface with increasing temperature. This explains why we see a drop in activity below that of plain P25 only in low temperature calcinations, where surface coverage/particle overlap is high enough to be detrimental to the inherent activity of P25.

3.7 References

[1] Ayati A, Ahmadpour A, BaharehTanhaei F, Mänttäri M, Sillanpaa M, *Chemosphere* **2014**, 107, 163-174

[2] 2nd International Conference on Environmental Science and Technology IPCBEE , 6 , **2011**

[3] J.A. Anderson, *Catalysis Today,* **2012** 181**,** 171– 176

[4] Yung-Fang C, Chi-Young L, Ming-Yu Y, Hsin-Tien C, *Journal of Crystal Growth* , 247, **2003**, 363-370

[5] Danielle de Bem L, Silvia A, Carolina B, Humberto J, deRegina F, Peralta M, *Journal of Photochemistry and Photobiology A: Chemistry*, **2012**, 246, 36-44

[6] S. Malato, P. Ferna´ndez-Iba´n˜ez, M. I. Maldonado, J. Blanco and W. Gernjak*, Catal. Today,* **2009**, 147, 1–59.

[7] D. Li and J. Qu, J. *Environ. Sc*i., **2009**, 21, 713–719.

[8] J.-M. Herrmann, *Appl. Catal., B*, **2010**, 99, 461–468.

[9] M.A. Fox, M.T. Dulay, *Chem. Rev*, **1993**, 93, 341

[10] AYamamoto, Y Mizuno, K Teramura, T Shishidoab, T Tanaka, Catal. *Sci. Technol.,***2013**, 3, 1771

[11] K Mehrotra, GS Yablonsky, AK Ray, **2005**, Chemosphere, 60, 1427–1436

[12] ET Soares, MA Lansarin, CC Moro, **2007,** *Braz J Chem Eng*, 24, 29–36

[13] S Zhou, AK Ray, **2003**, *Eng Chem Res*, 42, 6020–6033

[14] J Anderson, *Catalysis Today* **2011**, 175, 316-321

[15] J Anderson, H Adamu, *Proceedings of the World Congress on New Technologies Barcelona, Spain* , **2015**, Paper Number 162

[16] A. Turki, C Guillardb, F Dappozzeb, G Berhaultb, Z Ksibia, H Kochkara, *Journal of Photochemistry and Photobiology A: Chemistry***, 2014**, 279, 8–16

[17] M Shand, JA. Anderson *Catal. Sci. Technol.,* **2013**, 3, 879—899

[18] F Zhang, R Jin, J Chen, C Shao, W Gao, L Li, N Guan, *Journal of Catalysis*, **2005,** 232, 424–431

[19] M Kima, S Chunga, C Yooa, M Suk Leea, H Choc, D Leea, K Leea, *Applied Catalysis B: Environmental,* **2013,** 142– 143, 354– 361

[20] G Strukul, R Gavagnin, F Pinna, E Modaferri, S Perathoner, G Centi, M Marella, M Tomaselli *Catalysis Today,* **2000** 55, 139–149.

[21] D Yang, W Feng, G Wu, L Li, N Guan, *Catalysis Today*, **2011**, 175, 356–361

[22] I Mikami, Y Sakamoto, Y Yoshinaga, T Okuhara, *Applied Catalysis B: Environmental,* 2003, 44, 79–86

[23] Villa, Alberto, Wang, D Veith, M Veith, Gabriel, Vindigni, Floriana, L Prati. *Catalysis Science & Technology* **2013**, 3, 30-36.

[24] A. Zielińska-Jurek, E. Kowalska, J. W. Sobczak, W. Lisowski, B. Ohtani, and A. Zaleska. *Applied Catalysis B,* **2011**, 101, 504–514,

[25] A. Ayati, A. Ahmadpour, F. F. Bamoharram, B. Tanhaei, M. Manttari, and M. Sillanpaa, *Chemosphere*, **2014**, 107, 163-74

[26] R. Asahi, T. Morikawa, T. Ohwaki, K. Aoki, and Y. Taga, *Science*, **2001**, 293, 269

[27] X. Zhang, K. Udagawa, Z. Liu, S. Nishimoto, C. Xu, Y. Liu,H. Sakai, M. Abe, T. Murakami, and A. Fujishima, *J. Photochem.Photobiol. A: Chem.* **2009**, 202, 39

[28] J Yang, J Dai, J, Li *Science of Advanced Materials*, **2013**, 5(8), 1013-1023

[29] P She, K Xu, S Zeng, Q He, H Sun, Z Liu, *Journal of Colloid and Interface Science,* **2017**, 499, 76–82

[30] A cybula, M klein, A zielinska-jurek, M janczarek, A zaleska *Physicochem. Probl. Miner. Process,* **2012**, 48(1), 159–167

[31] X Liu, J G. Khinast, B J. Glasser, *Ind. Eng. Chem. Res*. **2014**, 53, 5792−5800

[32] K Yanagisawa, J Ovenstone, *J. Phys. Chem. B, 1999*, 103 (37), 7781–7787

[33] N Wetchakun, Burapat Incessungvorn, Khatcharin Wetchakun, S Phanichphant *Materials Letters,* **2012**, 82 195–198

[34] N Bowering, G S. Walker, P G. Harrison, *Applied Catalysis B: Environmental*, **2006***,* 62, 208–216

[35] N LWu, M S Lee, Z J Pon, J Z Hsu, *Journal of Photochemistry and Photobiology A:Chemistry*, **2004** 163 277–280

[36] L Millard, M Bowker *Journal of Photochemistry and Photobiology A: Chemistry,* **2002** 148 91–95

[37] D James, M Bowker, L Millard, J Greaves, J Soares, *Gold Bulletin*, **2004**, 37, 3–4

[38] M. Murdoch, G I N Waterhouse, M A Nadeem, J B Metson, M A Keane, R F Howe, J. Llorca, H. Idriss, *Nat Chem, 2011, 3(6), 489-492.*

[39] I Padikkaparambil, B Narayanan, Z Yaakob, S Viswanathan, S Tasirin*, International Journal of Photoenergy,* **2013***,* 2013, 10

[40] Y Wu ,K-Q Sun, J Yu, B-Q Xu, *Phys. Chem. Chem. Phys., 2008, 10, 6399-6404*

CHAPTER 4

4.1 Introduction

It is clear that Au is an excellent element with which to modify a number of supports in heterogeneous catalysis as a whole. This is reflected in the vast number of journal entries detailing an increase in a particular reaction's activity and as we have seen from the previous chapter, the photoreduction of nitrate is no exception. Although this is true there are very good reasons to expand the list of possible metal candidates from simply gold to the rest of the noble metals and beyond.

One of the reasons a replacement for Au is welcomed in many catalytic scenarios is an obvious one, cost. There are many examples in the literature of activities and selectivities rivalling that of Au but by instead using cheaper, more readily available metals such as Ag, Cu, Pd, Rh and Ru. That being said Pt is also a good candidate for this application due to its ability to produce the strongest Schottky barrier and extend charge-carrier lifetimes by more effective electron trapping [1] [2]. In this chapter we will see how a variety of other metals perform when made via the same optimised incipient wetness method detailed in the previous chapter.

So far the focus has been largely on the effect of monometallic addition of Au to titania, which has yielded good results. Though this is true it has been shown in many other areas of catalysis that synergies can exist between elements such as Ag and Au which give rise to increased activities, selectivities or stability over their monometallic counterparts. The reasoning behind the improvement in activity of bimetallic catalysts over monometallics is varied and individual to the particular reaction being investigated. It is thought that in the case of photocatalysis the addition of a second metal can improve activities in two ways. Firstly, the second metal can extend the range of visible light that can induce surface Plasmon resonance which is thought to improve the visible light activity of photocatalysts for some reactions. We have seen from the data in the previous chapters that the SPR effect does not increase the range of useful light available to the catalyst for the photoreduction. Perhaps more important in the context of the photoreduction of nitrate reaction is the lifetime extension of charge-carrying species with the addition of a second metal, more so than the use of either individual metal. For example, Pt may be used for its strong charge-separating effects but in conjunction with another metal like Au to offset

platinum's tendency to be easily poisoned by species like Cl^- [3]. In this chapter we will detail some investigations into the potential benefits of bimetallic AuAg, AuPt, and AuPd catalysts.

The previous chapters have so far only dealt with the improvement of titania via the increase of charge-carrier lifetimes and not by increasing the portion of light available to the catalyst. In this chapter we will report on a number of experiments using N-modified titania with the aim of shifting the band-gap of the material into the visible region and achieving a visible-active catalyst for the photoreduction of aqueous nitrate. Furthermore, a combination of N-doping and metal-modification was explored with the aim of improving the efficiency of the catalyst by both routes and synthesising a more efficient solar-light catalyst than via metal-modification or non-metal-doping method alone.

4.2 Results and Discussion

4.2.1 Alternatives to Au

A series of silver-modified TiO_2 catalysts of different metal loadings were prepared once again using the optimised incipient wetness preparation method detailed in Chapter 3 (**Figure 4.1**).

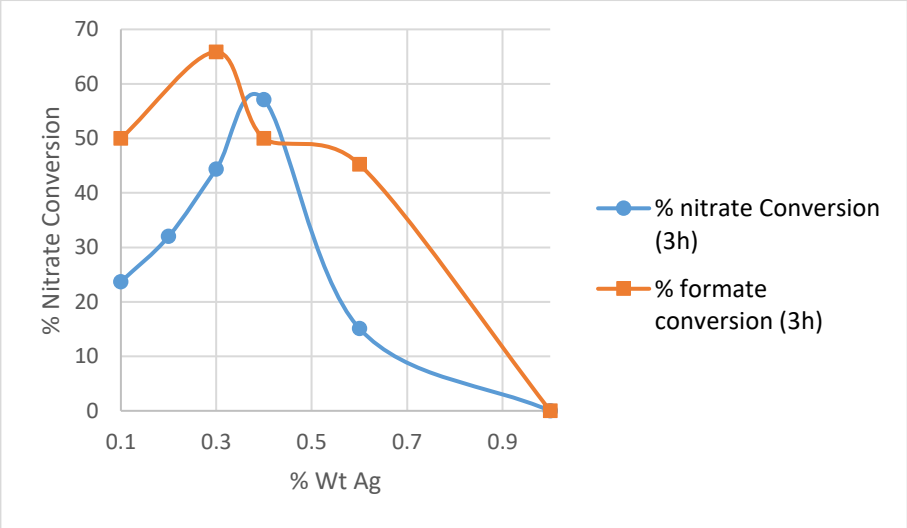

Figure 4.9: Percent conversion of formate and nitrate after 3h reaction time vs Ag % wt of catalyst used.

From the data above we can see that the relationship between Ag loading and activity is that of a volcano plot with an optimum loading occurring at 0.4% wt Ag; this is very similar to the plot seen in the Au/TiO_2 weight % experiments presented in Chapter 3

which showed an optimum Au loading of 0.3% wt. What is different in this case is that when moving to higher wt % we see a complete drop-off in activity at 1% wt Ag. As with the Au experiment, this phenomenon is down to two possible scenarios:

1. Very small metal nanoparticles - A result of a trade-off between increasing charge-carrier separation with increasing Ag loading and a decrease in activity due to the blocking of TiO_2 surface sites and/or overlapping nanoparticles.
2. Large metal nanoparticles – A result of nanoparticles sintering to an optimal size with increasing metal loading followed by a decrease in activity with further increases in loading. The large particles improving activity via enhanced SPR effects.

Here the drop in activity to zero at 1%Ag/TiO_2 gives further credence to theory that very small metal nanoparticles are indeed present on the catalyst surface which result in detrimentally high surface coverage or nanoparticle overlap at high loadings. The presence of large particles alone could not account for the "switching off" of the inherent activity of plain titania.

The plot of formate conversion after 3h reaction time vs Ag loading also roughly follows a volcano plot trend; in general activity for formate oxidation increases up to a point and then decreases but the peak of the formate conversion line does not synchronise with the nitrate conversion plot. The peak nitrate conversion when using IW-prepared Ag/TiO_2 catalysts was 57%, a 17% increase over the best-performing Au catalyst.

Since the Ag catalysts are made using $AgNO_3$ it dispels the notion that the volcano plot observed when using Au catalysts was somehow cause by a poisoning effect Cl^-. We can also rule out the possibility that these Ag catalysts are being poisoned by the NO_3^- counter ion as this would be destroyed by photoreduction during the reaction and is likely removed during the calcinations step via thermal decomposition.

By plotting the moles of nitrate converted against the moles of formate converted we can use a simple linear regression model to estimate the stoichiometry (**Figure 4.2**).

From the linear regression trend-line we can see that the molar ratio of formate : nitrate measured empirically for this reaction is 4:1. The theoretical stoichiometry for the reduction of NO_3^- to NO_2^- reaction assuming 100% selectivity to N_2 (as is observed) is 2.8:1. This means the Ag catalyst here is using almost twice as much formate as it needs

to per unit of nitrate being converted, this however is still better than the measured formate:nitrate conversion ratio of the best-performing Au-based catalysts, which was found via the same linear regression analysis, to be 5.5. However, to draw an accurate comparison between the different metals equivalent metal loadings must be prepared. Time-on-line data is not available for the 0.4%Au catalyst but data is available for the 0.3% Ag. When the catalysts of equal metal loading are compared (0.3% wt M/TiO_2) we see that the apparent superiority of the Ag based system is not due to more efficient use of formic acid as the ratio of formate:nitrate conversion in this system is 14:1.

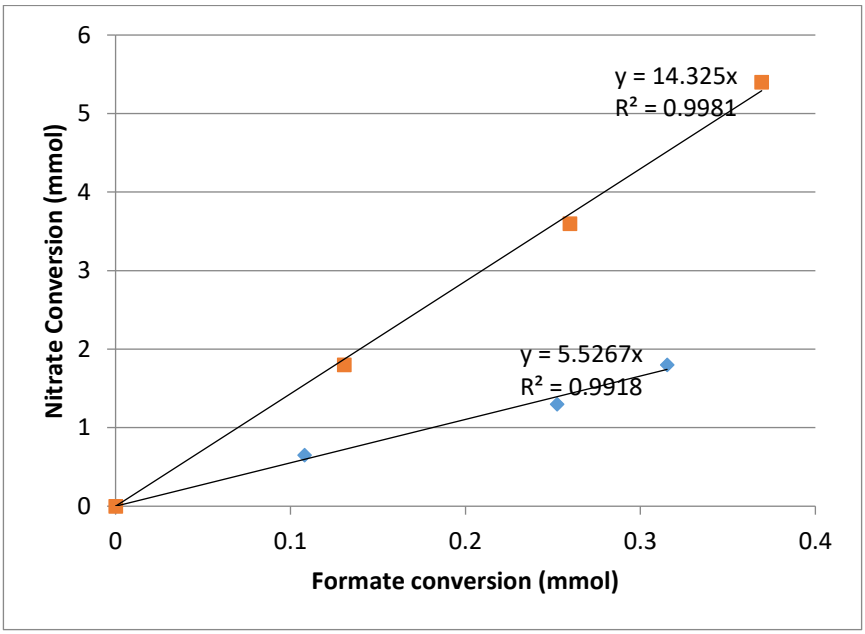

Figure 4.2: mMol of nitrate converted vs mMol formate converted after 3h illumination using 0.3%Ag/TiO_2 (red squares) and 0.3%Au/TiO_2 (blue diamonds)

It is likely then that the superiority of Ag over Au catalysts is due to better charge-carrier trapping. Ion chromatography analysis showed the presence of nitrite forming during the reaction but interestingly, this was only observed in the lower loading (0.1-0.3%Ag) (**Table 4.1**). The highest concentrations of nitrite were recorded during the initial stages of the reaction with the selectivity gradually improving with respect to N_2 as the reaction goes on (**Table 4.2**). The initial formation of nitrite followed by its subsequent destruction here shows the sequential reduction of NO_3^- to NO_2^- followed by NO_2^- to N_2.

It is interesting that no nitrite is observed when carrying out this reaction with an Au/TiO_2 catalyst although ammonia is (at high conversions) whereas the opposite is true when using Ag/TiO_2, which is to say nitrite is present but ammonia is not. The lack of ammonia is due to a combination of an acidic reaction medium (OH^- ions are known to promote

ammonia formation) and the weaker hydrogen overpotential of Ag compared to Au, leading to less over-reduction and thus less ammonia formation. The latter point is also why we see nitrite present when using these catalysts but not when using Au/TiO_2 systems.

Table 4.11: Selectivity to N_2 of different percent-weight Ag/TiO_2 catalysts

Catalyst Ag wt %	Selectivity to N_2 (3 h)
0.1	77.7
0.3	94.5
0.4	100.0
0.6	100.0

Table 4.12: Time online selectivity data for $0.3\%Ag/TiO_2$

0.3% Ag	
Time (mins)	Selectivity to N_2
0	100.0
60	71.6
120	88.3
180	94.5

It must be noted that the tendency for Ag catalysts to form considerable amounts of nitrite at lower weight loadings and at the initial stages of reaction is more detrimental than the tendency for Au catalysts to form small amounts of ammonia at very high conversions. The EU has suggested a limit for nitrate ions in groundwater at 50, nitrite at 0.1 and ammonia at 0.5 ppm. This means we can consider each ppm of nitrite to be as dangerous as 500 ppm of nitrate and thus it is clear that the formation of NO_2^-, even in small amounts, must be avoided. Later in this chapter the use of bimetallic $AuAg/TiO_2$ will be presented as a means of tuning the selectivity of the catalyst in a way that eliminated the generation of harmful nitrite while still using Ag to substitute the more expensive Au.

1% M/TiO_2 catalysts were prepared using H_2PtCl_4 and acidified $PdCl_2$ solutions as precursors and tested under the standard conditions given in Chapter 2 (**Figure 4.3**). From this we can see that the addition of 1 wt % Pd to titania has no effect on the overall conversion after 3 h and the addition of 1% wt % Pt reduces the activity to zero in the same manner as $1\%Ag/TiO_2$. Due to the trends that were observed by varying the wt %

of Au and Ag a new set of catalysts was prepared using the same method but at 0.3% wt metal.

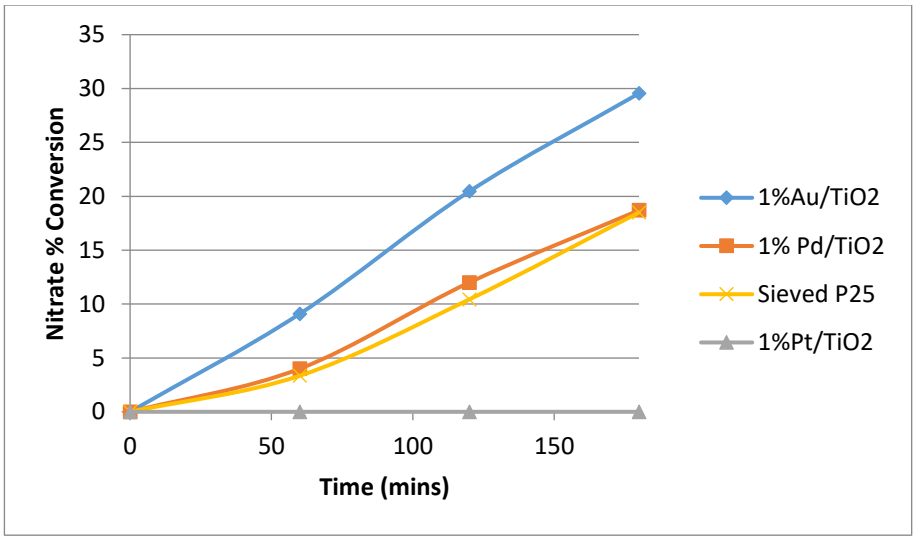

Figure 4.3: Comparison of activities of IW 1%M/TiO_2 for photo-reduction of nitrate

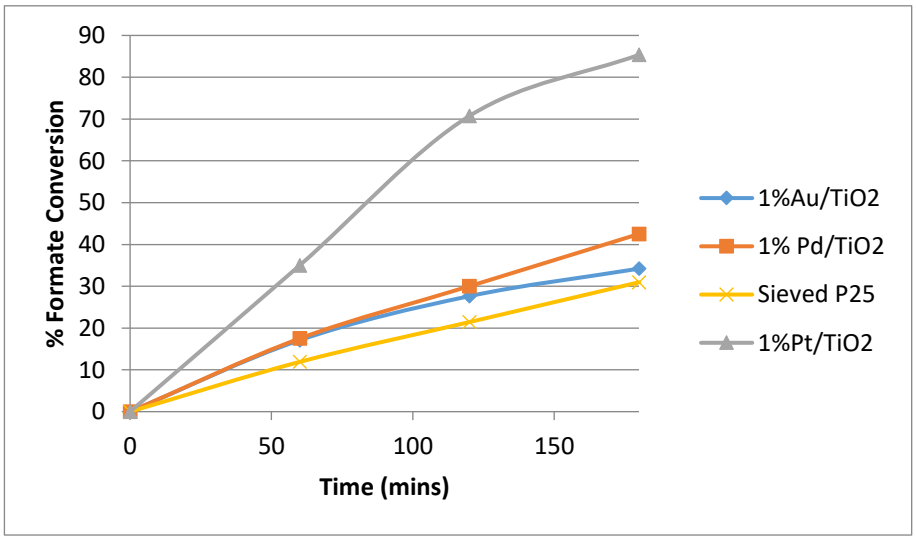

Figure 4.4: Comparison of activities of IW 1%M/TiO_2 for photo-oxidation of formic acid

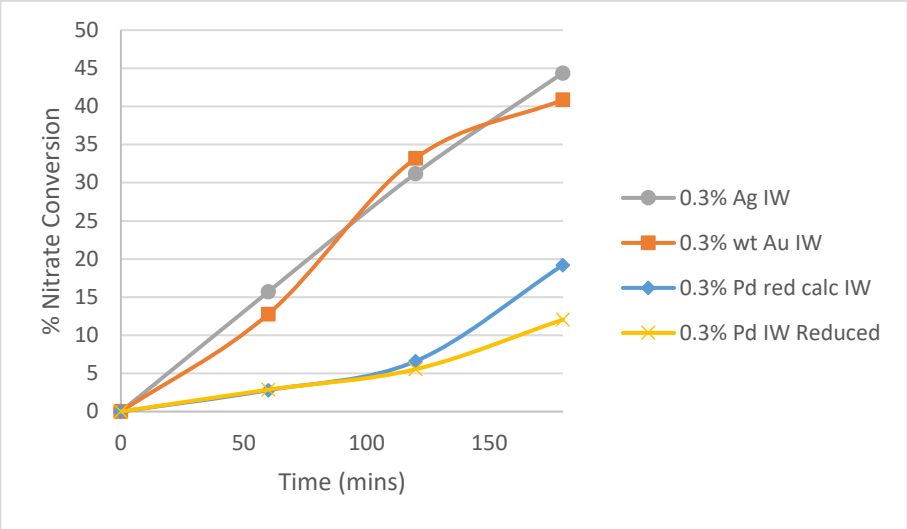

Figure 4.5: Comparison of activities of IW 0.3%M/TiO_2 for photo-reduction of nitrate

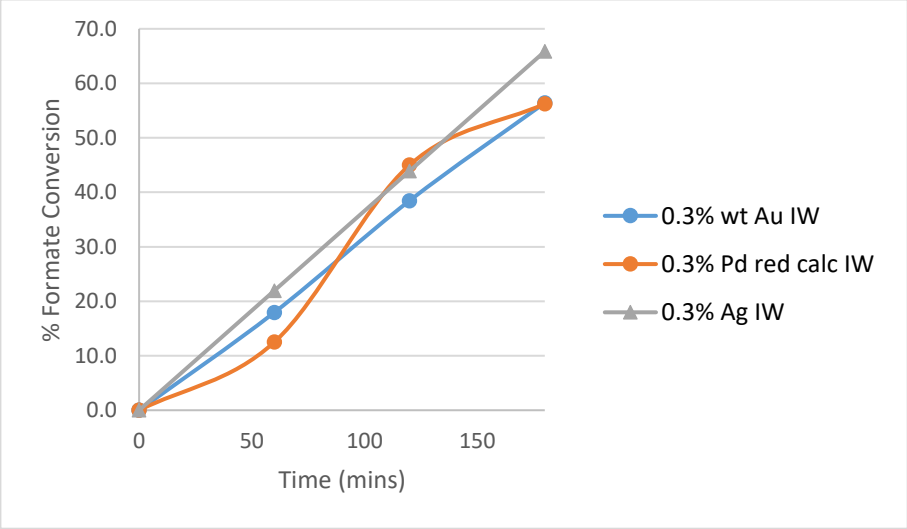

Figure 4.6: Comparison of activities of IW 0.3%M/TiO_2 for photo-oxidation of formic acid.

Unfortunately Pt could not be included in this series due to time constraints and issues accessing the required platinum precursor for this preparation. Regardless the data shows that indeed the 0.3% Pd-based catalyst is active whereas the 1% Pd catalyst is not, once again demonstrating that metal loading has a very large effect on photoactivity. The activity observed for the Pd catalyst however is only marginally better than that of plain titania and in fact, a heat treatment procedure of sequential reduction under H_2 followed by standard calcinations has to take place to produce the activities seen in **Figure 4.5**.

Initially a 0.3% Pd/TiO_2 catalyst was produced using the standard IW preparation detailed in Chapter 2. This preparation led to a catalyst that was inactive for both nitrate reduction and formic acid oxidation under solar simulation. A similar preparation in the literature using the same precursor and similar calcinations temperatures reported the presence of Pd and PdO as discovered by XRD analysis [4]. To remedy this two more batches of 0.3%Pd/TiO_2 were prepared, one in which a reduction step at 400°C (**Table 4.3**) was carried out under flowing H_2 and one in which a the same reduction step was carried out followed by a further calcinations in static air at 400°C (**Figure 4.5).** From **Table 4.3** it can be seen that activity is induced when the reduction step is added due to the reduction of cationic Pd. At this point, the activity is still below that of plain TiO_2, indicating that high surface coverage by small metal nanoparticles is hindering activity. Upon re-calcining, some sintering occurs and TiO_2 surface sites are freed, improving activity to levels beyond that of P25. Pd/TiO_2 prepared by reduction and subsequent calcination have been shown to be somewhat oxidic in nature, indicating that the metal-oxide is also capable of enhancing photocatalyis [5].

Also worth considering are Cu/TiO_2 catalysts that were made via the incipient wetness method detailed in Chapter 2 using $Cu(NO_3)_2$ as a precursor. Cu has been shown to increase the photoactivity of TiO_2-based catalysts for reaction such as CO_2 reduction and there are few papers that explore its usefulness for photocatalytic nitrate reduction [6].

Table 4.13: Performance of 0.3%Pd/TiO_2 after reduction at 400˚C under flowing H_2 (no calcination step).

0.3% Pd IW Reduced				
Time (mins)	NO_3 (ppm)	Formate (M)	NO_3 % conversion	Formate % conversion
0	104.6	0.0082	0.0	0.0
60	101.6	0.007	2.9	14.6
120	98.8	0.0058	5.5	29.3
180	92	0.005	12.0	39.0

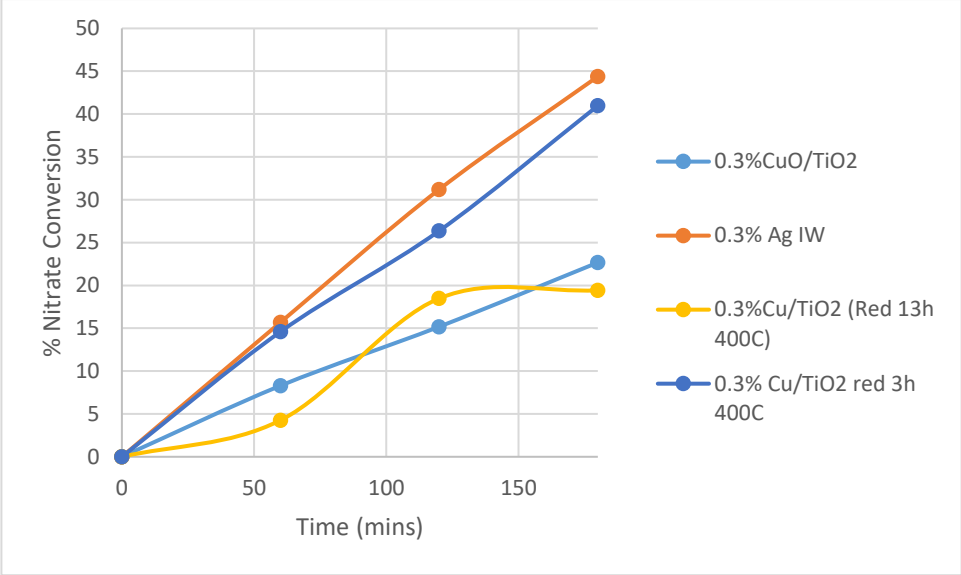

Figure 4.7: Photo-activities for nitrate reduction of several variations of 0.3%Cu/TiO_2 catalysts compared against best-performing Ag/TiO_2

Figure 4.7 shows how several variations of 0.3%Cu/TiO_2 perform against the equivalent Ag catalyst. One again the wt % of 0.3% was chosen based on the Au and Ag weight % series shown previously. These Cu-based catalysts showed activity when prepared via the standard IW method which includes a drying step and calcinations without a reduction step (0.3% CuO/TiO_2). This can be explained by looking at previous studies on IW-prepared Cu/TiO_2 catalysts which show that for the photocatalytic production of H_2 it is the Cu_2O species that is most active. One such paper is the 2013 paper by Behnajady *et al* which shows that in-situ oxidation of the reduced Cu^0/TiO_2 led to the most active catalyst, the authors also showed that calcinations in air at 400°C yielded copper in a +2 oxidation state (CuO). Also important is literature which shows that Cu/TiO_2 catalysts made via wet impregnation methods and calcined at 773K produce large nanoparticles up to 17 nm in size [17]

From **Figure 4.7** we can see that the calcined catalyst (presumably CuO) is active for nitrate reduction at levels greater than that of plain P25. This gives indicates that, while not as active at their metallic counterparts, metal oxides can be used in improving the activity of plain titania for this reaction

4.2.2 Microscopy of IW Ag/TiO_2 Catalysts

As with Au-based catalysts SEM and TEM analysis was carried out on the 0.4%Ag/TiO_2 catalyst. SEM data once again yielded no useful insight into the catalyst with the support

staying unchanged from plain P25 and metal nanoparticles being undetected at SEM-levels of magnification. TEM microscopy with EDX analysis however was successful in identifying a few areas of the catalyst containing Ag nanoparticles (**Figure 4.8b**).

As with the Au TEM images the Ag nanoparticles are detected as a few large nanoparticles (*ca* 50 nm) that were difficult to find.

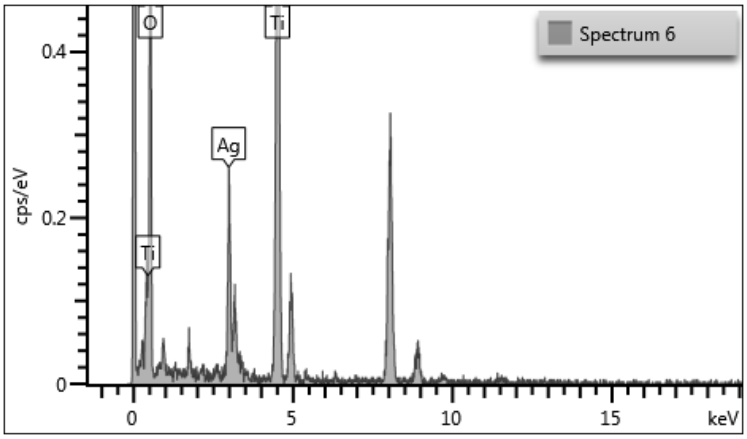

Figure 4.8a: EDX spectra of an area of 0.4%Ag/TiO_2 shown in figure 8b

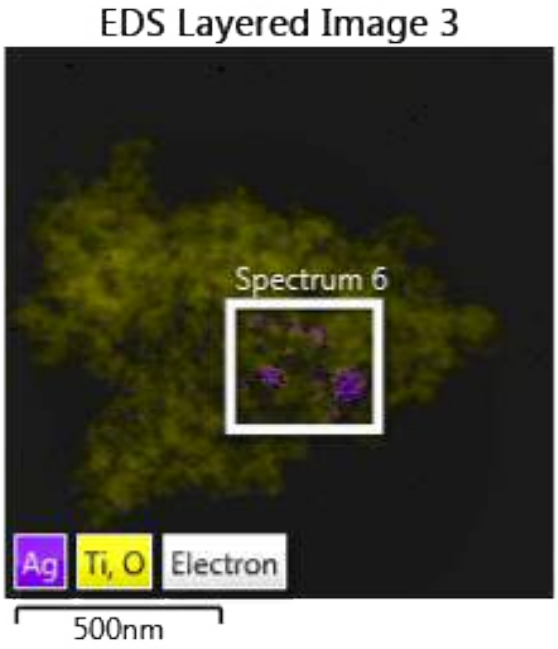

Figure 4.8b: Elemental mapping by EDX of an area of 0.3%Ag/TiO_2 suspected of containing Ag nanoparticles

Table 4.14: Measured weight-percentage of Ag from elemental mapping in **figure 4.8a** and **figure 4.8b**

Element	Line Type	k factor	Absorption Correction	Wt%	Wt% Sigma
O	K series	2.05018	2.21	49.53	1.34
Ti	K series	1.08940	0.90	33.17	0.98
Ag	L series	1.84974	0.91	17.30	0.95
Total:				100.00	

.

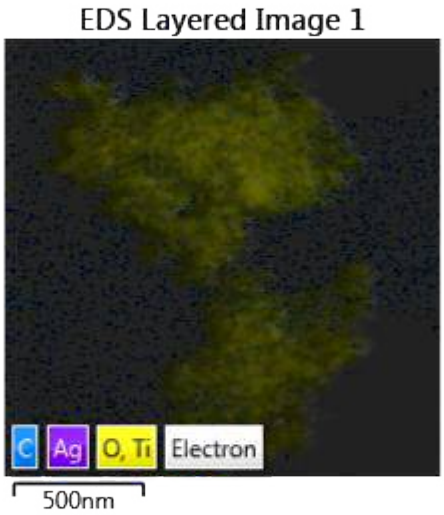

Figure 4.9a: Elemental mapping by EDX of an area of 0.3%Ag/TiO_2 suspected of containing no Ag nanoparticles

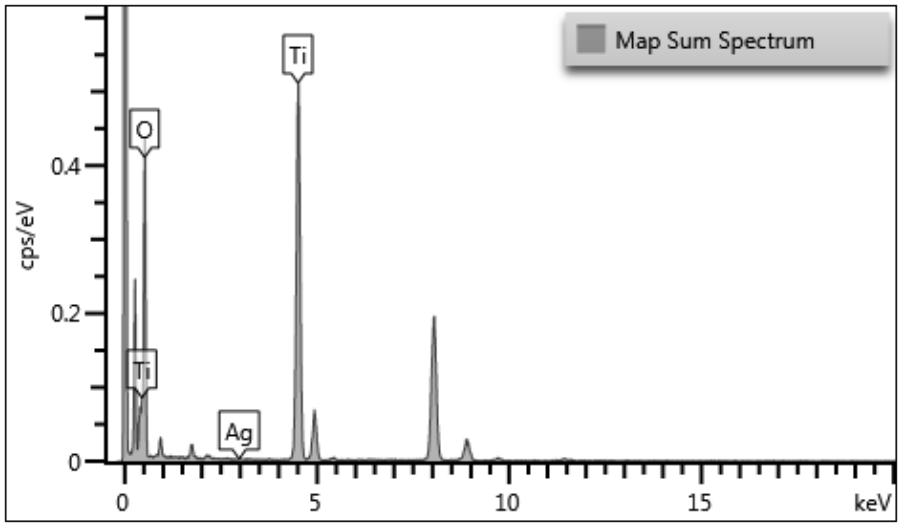

Figure 4.9b: EDX spectra of an area of 0.4%Ag/TiO_2 shown in **figure 4.9b**

Table 4.15: Measured weight-percentage of Ag from elemental mapping in **figure 4.9a** and **figure 4.9b**

Element	Wt%	Wt% Sigma
O	60.94	0.43
Ti	38.97	0.42
Ag	0.09	0.11
Total:	100.00	

Elemental analysis with the EDX software shows that for a random area of catalyst not containing large nanoparticles there is around a 0.1 weight percentage of Ag. This indicates that although not visible, very small nanoclusters of Ag do exist on the surface of the catalyst. The low Ag signal is explained by the fact that the majority of X-rays generated for EDX comes from the sub-surface of the catalyst. If Ag is distributed near-atomically on the surface the EDX analysis would still show a very low signal.

4.2.3 Visible-Light Reactions

As with Au/TiO_2 catalysts the Ag catalysts mentioned in this chapter showed no activity for nitrate reduction when illuminated with visible-only light, once again demonstrating that deposition of noble metal nanoparticles onto TiO_2 increases catalytic efficiency by reducing charge-carrier recombination rates only and does not extend the range of light available to the catalyst into the visible regime. The lack of visible light activity is likely due to the fact that the small nanoparticles present have weak electrical field enhancement via the SPR effect.

Table 4.16: Activities of 0.4%Ag/TiO_2 when using optical filters

0.4%Ag IW (UV-blocking Filter)				
Time (mins)	**NO_3 (ppm)**	**Formate (M)**	**NO_3 % conversion**	**Formate % conversion**
0	99	0.0082	0.0	0.0
180	101.6	0.008	-2.6	2.4
0.4% Ag IW (No Filter)				
Time (mins)	**NO_3 (ppm)**	**Formate (M)**	**NO_3 % conversion**	**Formate % conversion**
0	99.6	0.0082	0.0	0.0
180	78.6	0.0004	21.1	95.1
0.4%Ag IW (visible-blocking Filter)				
Time (mins)	**NO_3 (ppm)**	**Formate (M)**	**NO_3 % conversion**	**Formate % conversion**
0	101.2	0.008	0.0	0.0
180	83.5	0	17.5	100.0

When a visible light-blocking filter was applied the activity appears to drop somewhat, it is likely that this small decrease in activity is due to the slight drop in transmission as light is passed through the filter.

4.2.4 Investigations into Bimetallic Photocatalysts

In this section we examine the potential synergism that may occur when using a combination of two metals in the preparation of these catalysts.

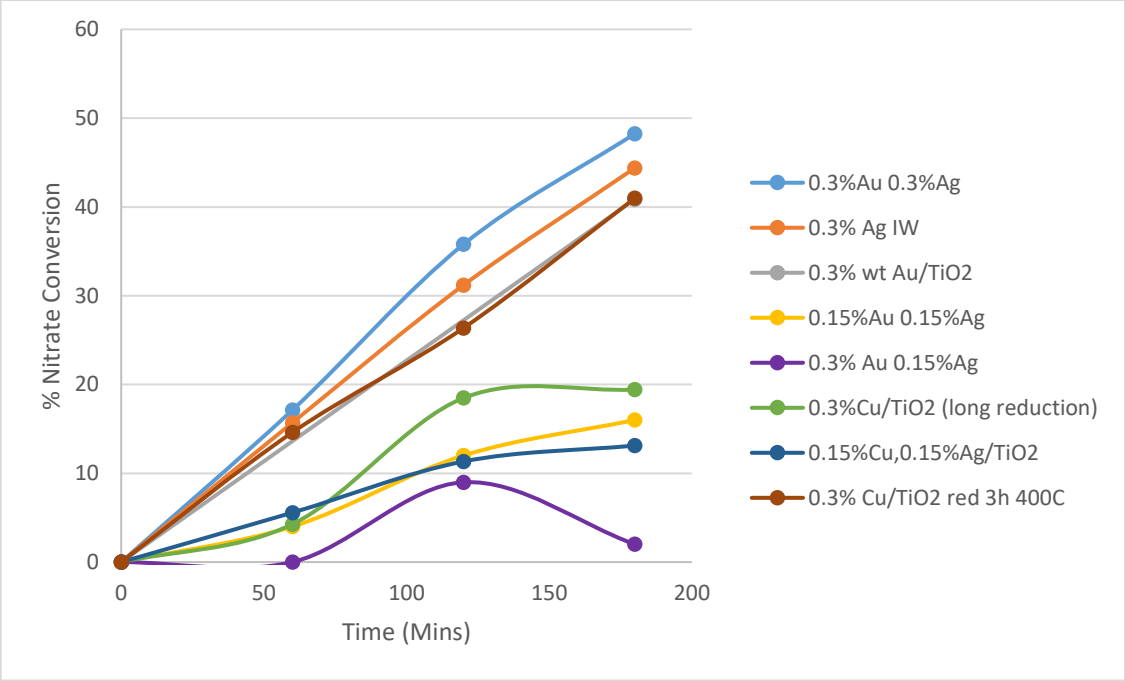

Figure 4.10: Conversions of several 0.3%M/TiO_2 Bimetallic catalysts made via IW for the photoreduction of nitrate

A variety of catalysts were prepared in order to investigate the effect of the addition of a second metal to the catalyst. For the most part the catalysts were prepared to have a collective metal weight percentage of 0.3%, to match the total metal weight percentage of the monometallic catalysts. Several iterations of the AuAg/TiO_2 catalyst was made with metal loadings of 0.15%Au0.15%Ag, 0.3%Au0.15%Ag, and 0.3%Au0.3%Ag, this was done because of how promising the metals were as monometallic catalysts. Catalysts were made via sequential deposition, for convenience the order by which the metals were deposited on the metal is indicate by the order they appear in the name. 0.15%Cu0.5%Ag/TiO_2 for instance implies that Cu was deposited first, followed by drying, deposition of Ag, drying again and finally heat treatment (reduction in this case).

Figure 4.10, shows the nitrate conversions of each bimetallic catalyst tested after 3 hours illumination time. Starting with the Cu-containing catalysts we see that the addition of Ag yields no increase in conversion after 3h illumination. On the contrary, the addition of Ag to the Cu catalyst results in a decrease in photoactivity compared to that of either

of the equivalent monometallic catalysts. In order to obtain an active Cu catalyst a reduction step had to be conducted, no further calcinations step was performed. This reduction, rather than calcination may have in some way resulted in a loss of activity of the Ag portion of the catalyst, although due to time constraints no tests have been carried out on a monometallic Ag catalysts prepared in this way. It is more likely, however that the addition of Ag to a Cu/TiO_2 catalyst is anti-synergistic.

The preparation of $AuAg/TiO_2$ catalysts is more straightforward due to the fact that the same heat treatment is required for both metals and so that is no longer a factor that may influence the results. From **Figure 4.10** we can see that the bimetallic AuAg catalysts that have a collective metal % weight of 0.3% are far less active than their monometallic counterparts and thus we observe an anti-synergy between Au and Ag at these weight loadings. Anti-synergistic effects of noble-metal bimetallic catalysts have been noted in the literature but few examples of this are noted with respect to photocatalysis and none with respect to the photoreduction of nitrate reaction [10]. As the Au content is increased the photoactivity improves, unfortunately an equivalent Ag-dominant catalysts was not made to compare due to time constraints.

At this point it could be concluded that the mixing of metals in this way leads to anti-synergistic effects and that bimetallic catalysts are likely not suitable for this particular reaction. Interestingly though as the combined metal content is increased to 0.6% wt at a 1:1 Au:Ag ratio synergy between the Au and Ag is observed and the resulting catalysts is not only more active than the equivalent monometallic catalyst but is in fact the most active catalyst prepared out of any tested. What's more is that analysis of the reaction solution by ion chromatography and a selective-ion ammonia probe show 100% selectivity to N_2 and unlike their monometallic catalysts show no over-reduction to NH_3 (as observed with Au at high conversions) or under-reduction to the highly undesirable NO_2^- (as observed with Ag). It must be noted that the presence of NO_2^- was not detected at any stage of the reaction, unlike with monometallic Ag catalysts which, while exhibiting no NO_2 after 3h reaction time, did produce NO_2^- mid reaction.

It is strange then that these catalysts would exhibit anti-synergism at low metal loadings and 1:1 metal ratios but show strong synergism at higher total metal loadings and the same metal ratios. To investigate this further the nature of the bimetallic catalyst must be better probed to elucidate the Au and Ag speciation as well as the extent of alloying which

could be achieved through XPS and electron microscopy techniques. It seems possible that the preparation method used here favours the formation of unalloyed nanoparticles due to the sequential deposition of metals although it is entirely possible that at higher weight loadings alloying of Ag and Au increases during the heat-treatment step because of the closer proximity of metal particles. **Figure 4.11** shows the UV-visible diffuse reflectance spectra of 0.3%Au0.3%Ag/TiO_2 which exhibits a single Plasmon band at 556 nm. This lies between the plasmon bands of Au (578 nm) and Ag (397 nm colloidal). From this we can assume that the metals are indeed alloyed due to the absence of two separate plasmon peaks. Other experiments that would shed more light on the use of bimetallics for this application would be the formation of a more complete set of catalysts with differing Ag:Au metal ratios that include Ag-rich catalysts so that the activity could be plotted as a function of metal ratio.

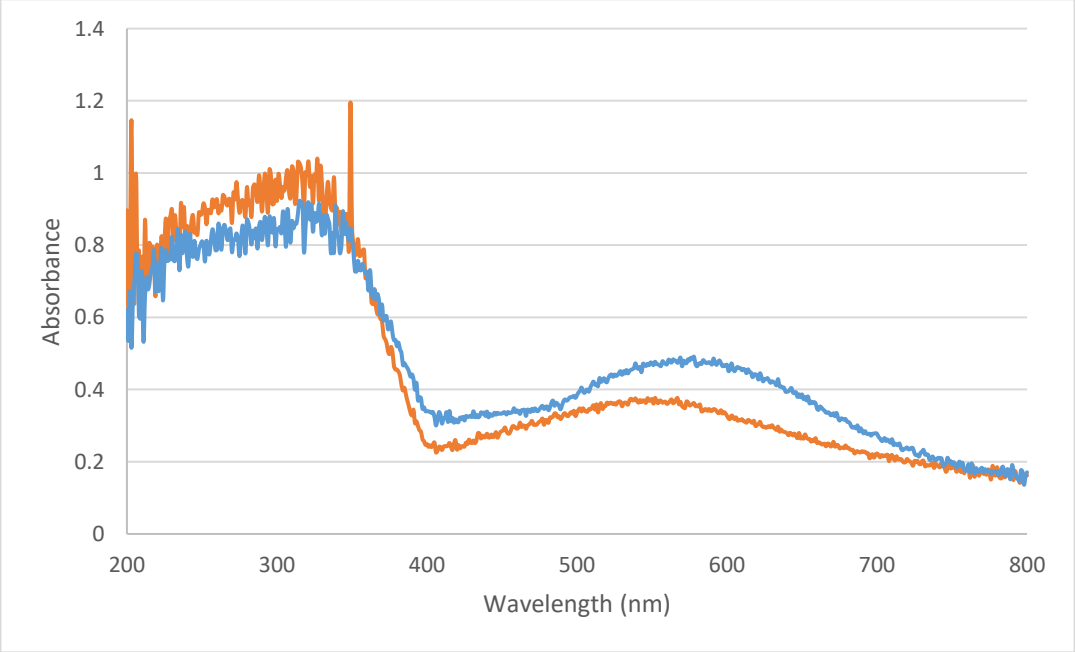

Figure 4.11: UV-Visible DRS spectrum of 0.3%Au0.3%Ag/TiO_2 (red) and 0.6%Au/TiO_2 (blue)

Unfortunately, not enough characterisation data could be acquired to draw any strong conclusions as to why we observe the activities demonstrated in **Figure 4.10** but we can state that there is certainly promise for the use of bimetallic noble-metal/TiO_2 for this application as can be seen by the improvement in selectivity and activity of the bimetallic catalysts over their monometallic equivalent of high (>0.3%) weight loadings.

4.3 Investigations into Potential Poisons

The end application of these catalysts is use in real water systems which will not only contain our target contaminants such as nitrate and short chain organic acids but also various other organic and inorganic pollutants. To test how the catalysts would perform in un-distilled water systems 0.2%Au/TiO_2 was tested using tap water in place of deionised water. Unfortunately the conversion could not be ascertained due to the presence of unidentified peaks overlapping with the nitrate peak during ion chromatography analysis.

In lieu of this, a set of synthetic "polluted waters" was prepared by adding differing amounts of either NaCl or Na_2SO_4 which are the most common inorganic species present in drinking water.

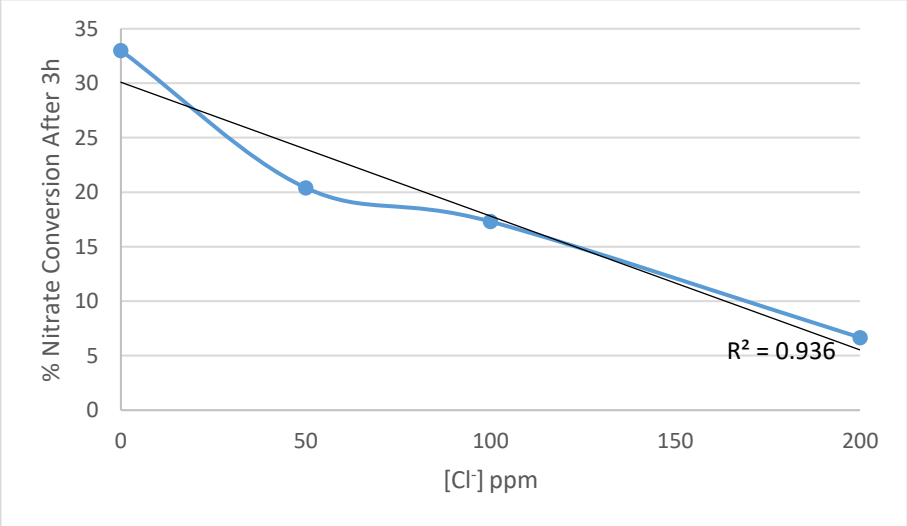

Figure 4.12: Nitrate conversion after 3h reaction time vs Cl^- concentration using a 0.2%Ag/TiO_2 catalyst

Figure 4.12 shows the plot of nitrate conversion after 3h vs the concentration of Cl^- in the reaction solution. From this we see an almost linear decrease in activity with increasing Cl^- concentration which confirms this species does indeed act as a poison in this reaction. This presents a problem as the Water Supply Regulations act in the UK sets a limit on the allowable concentration of Cl^- at 250mg/L and that chorine-compounds are actively added to the water supply for sterilisation purposes. As such these catalysts would struggle to remain effective in waters that have been treated with Cl^- but may be more suited to applications as a pre-treatment step before the addition of chlorine-compounds.

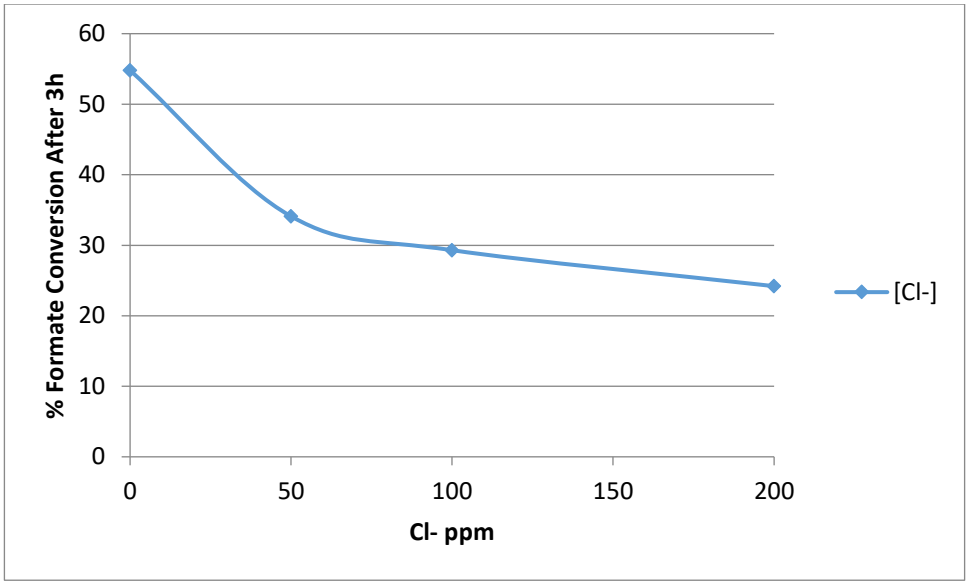

Figure 4.13: Formic acid conversion after 3h reaction time vs Cl- concentration using a 0.2%Ag/TiO_2 catalyst

Figure 4.13 shows the effect of Cl^- on the formate oxidation reaction which mirrors that of the nitrate reduction if a little less linear. The poisoning effect is likely due to competition for adsorption between the like-charged NO_3^- ions and Cl^-. There are some reports in the literature concerning the poisoning effects of Na on the photocatalytic activity of TiO_2-based catalysts [12]. The poisoning effects of Na in these cases is theorised to come from the diffusion of Na into the titania lattice during calcination, resulting in the growth of inactive sodium titanates. Since this reaction is carried out at low temperatures this effect can be ruled out and since Na is cationic in this case we can assume there is no significant adsorption to the partially positively-charged titania surface. The concentration of Cl^- was tracked throughout the reaction by ion chromatography analysis and found very slightly decrease as the reaction goes on, likely due to the adsorption of Cl^- on the titania.

Table 4.17: Cl^- concentration at different points in the photoreduction of nitrate reaction using 0.2%Ag/TiO_2

Time (mins)	[Cl^-] (ppm)
0	52
60	52
120	50
180	50

This effect is amplified when Cl^- is replaced with SO_4^{2-}, with nitrate percent conversion values dropping to only 3.8% at 100ppm SO_4^{2-} and with inactivity occurring at 200ppm SO_4^{2-}.

Table 4.18: Performance of 0.2%Au/TiO_2 for the removal of formic acid and nitrate with varying concentrations of Na

100 ppm SO_4^-				
Time (mins)	**NO_3 (ppm)**	**Formate (M)**	**NO_3 % conversion**	**Formate % conversion**
0	99.4	0.0076	0.0	0.0
60	97.2	0.0072	2.2	5.3
120	97.6	0.0068	1.8	10.5
180	95.6	0.0064	3.8	15.8
200 ppm SO_4^-				
Time (mins)	**NO_3 (ppm)**	**Formate (M)**	**NO_3 % conversion**	**Formate % conversion**
0	98.3	0.008	0	0
60	98.3	0.0068	0	15
120	98.3	0.0066	0	17.5
180	98.3	0.0062	0	22.5

Guillard *et al* demonstrated the preferential order of adsorption for several anion in their 2005 paper [13]. The order they reported was as follows:

Nitrate < chloride < sulphate < phosphate < carbonate

This order is reflected in our experiments and implies that the presence of phosphates and carbonates could cause further problems in real-world water systems.

4.4 Band-Gap Modification

In order to try and improve the visible-light activity of these catalysts it was decided that band-gap modification would be explored via the doping of nitrogen into TiO_2. To do this a sol-gel method was employed in which urea was used as the nitrogen source (see Chapter 2). As described in Chapter 1, the doping of non-metals into titania in this way introduces electronic states between those of the valence and conduction bands of titania, allowing electronic transitions to the conduction band to be facilitated by lower energy photons than in an un-doped sample.

When tested under solar-simulating conditions, the sol-gel-prepared N-TiO_2 catalyst performed poorly (5 % nitrate conversion, 3 h) (**Figure 4.14**). This was determined not to be due to a low surface area and in fact it was shown via BET analysis that the surface area of the sol-gel N-TiO_2 catalyst (120 m^2g^{-1}) was considerably higher than that of P25 (50-58 m^2g^{-1}).

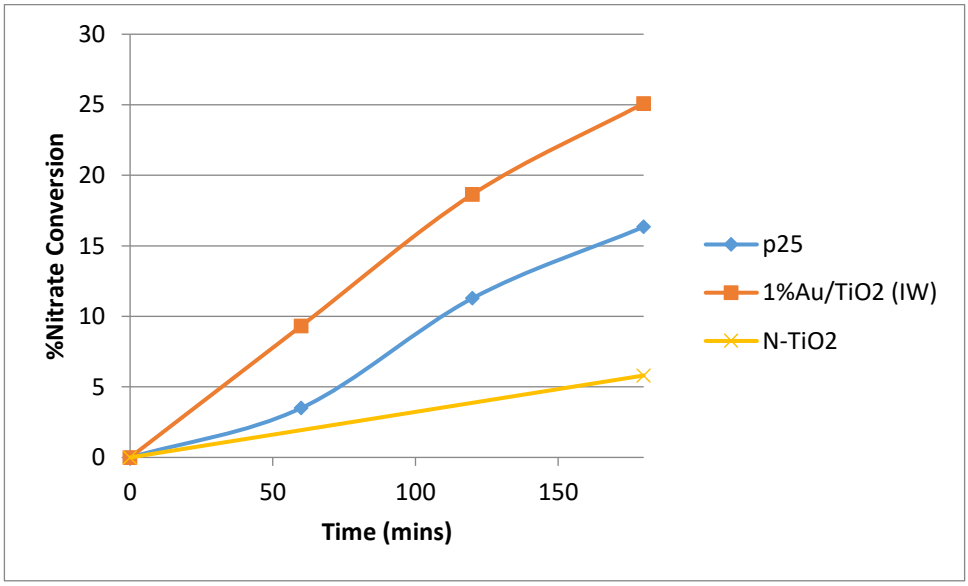

Figure 4.14: Photoactivity for nitrate reduction under solar-simulated light of N-TiO_2 prepared via sol-gel in comparison to P25 and 1%Au/TiO_2

XRD analysis of the sol-gel N-TiO_2 showed the material to consist of titania purely in the anatase phase with no sign of rutile peaks (**Figure 4.15**). A notable decrease in crystallinity is observed in the sol-gel N-TiO_2 over the commercial samples which has been shown in the literature in some cases to be unfavourable for achieving high photoactivities [14]. As mentioned in Chapter 1, mixed phase titania catalysts have been

shown to perform much better than single phase ones for many photoreactions. To confirm if the single-phase nature of the sol-gel N-TiO_2 was hindering the reaction a commercially bought anatase TiO_2 (Sigma-Aldrich) catalyst was used tested, as well as a commercially bought rutile catalyst (Sigma-Aldrich). The BET surface area of the commercial anatase was comparable higher than that of P25 ($80M^2g^{-1}$) but the rutile catalyst was found to have a much lower surface area (<10 M^2g^{-1}).

Table 4.19: Nitrate and formate % conversions of several single-phase catalysts.

Catalyst	% Nitrate converted (3h)	% Formate converted (3h)
Anatase	0	11
0.3% Au/Ana	2	20
Anatase (calcined)	0	14
0.3% Au/Ana (calcined)	4	23

The performance of the single-phase plain-titania catalysts and their 0.3 wt % Au counterparts are given in **Table 9**. From this it can be seen that the plain catalysts are totally inactive for nitrate reduction over the timeframes studied here and only a marginal improvement is seen when they are modified with Au. While a decrease in activity for single-phase systems is expected, the severity with which the activity drops off is surprising.

Before discounting N-doping as a means of improving the visible-light efficiency of these catalysts it is important then to try and synthesise an N-TiO_2 catalyst with a comparable surface area and anatase to rutile ratio to that of P25. Several methods were considered with the most promising being the heat-treatment of P25 under an atmosphere of ammonia [15]. Due to a lack of suitable equipment and the dangerous nature of this preparation a method was settled upon in which TiN was heated in air resulting in partial oxidation and the formation of an N-TiO_2 which will herein be referred to as N-TiO_2(TiN). The simple heating and thus phase-transformation of the sol-gel catalyst was not favourable due to the long aging times of the preparation.

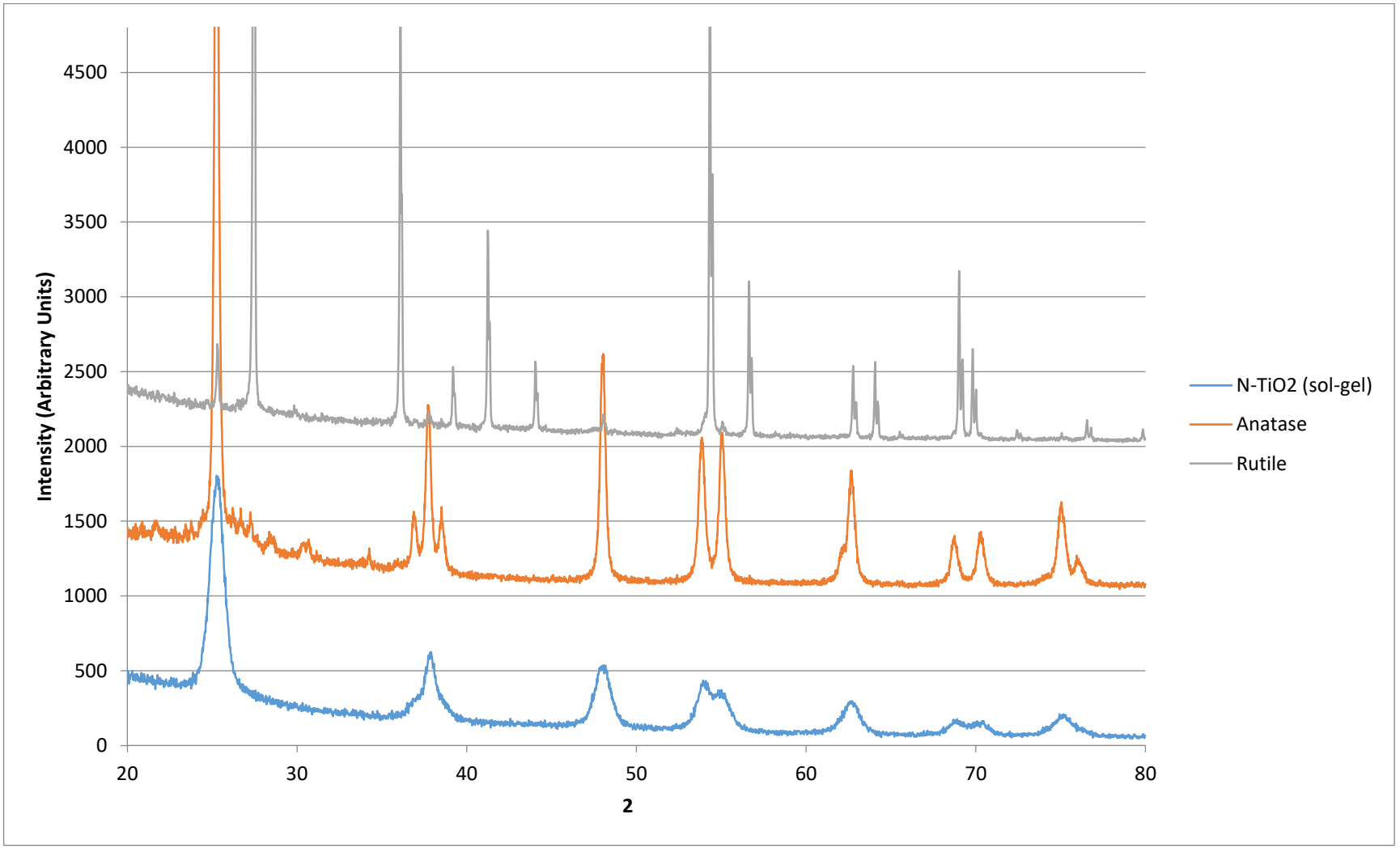

Figure 4.15: XRD analysis of Anatase (Sigma-Aldrich) and N-TiO_2 made via sol-gel synthesis.

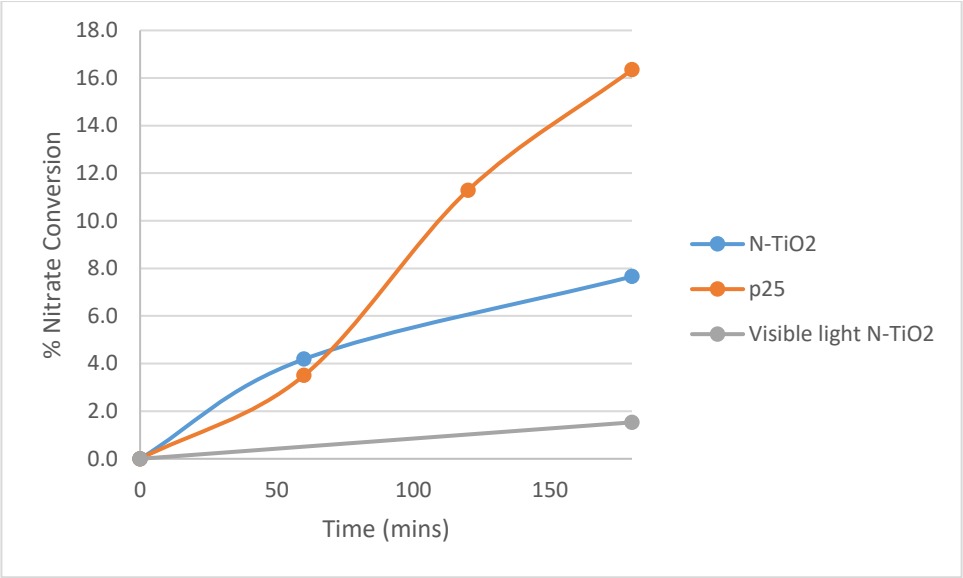

Figure 4.16: Conversions of N-TiO_2 (made from TiN) under solar-simulating (blue) and visible-light (green).

Figure 4.16 shows the activity of N-TiO_2(TiN) compared to plain P25. A slight improvement is seen when using N-TiO_2(TiN) over the sol-gel-prepared catalyst for nitrate photoreduction over 3h of solar-simulated illumination but activities comparable to P25 were not achieved. When tested under visible-only light a small amount of activity was detected (1.8%) but this result was not repeatable and so we must conclude that the doping of nitrogen to TiO_2 in the ways reported here do not result in a visibly active catalyst for the reduction of aqueous nitrates.

XRD analysis of N-TiO_2(TiN) shows a clear transformation from the TiN precursor to TiO_2 but the presence of nitrogen in the lattice structure is not apparent from this analysis alone (**Figure 4.17**). A clear colour change occurs upon heat treatment of TiN from a dark brown (untreated) to a light brown colour (calcined). The presence of nitrogen is inferred by the light brown colour present in N-TiO_2(TiN) compared to that of undoped TiO_2 (bright white powder) and by a red-shift in the absorption edge when analysed via UV-Vis Diffuse Reflectance Spectroscopy (**Figure 4.18**).

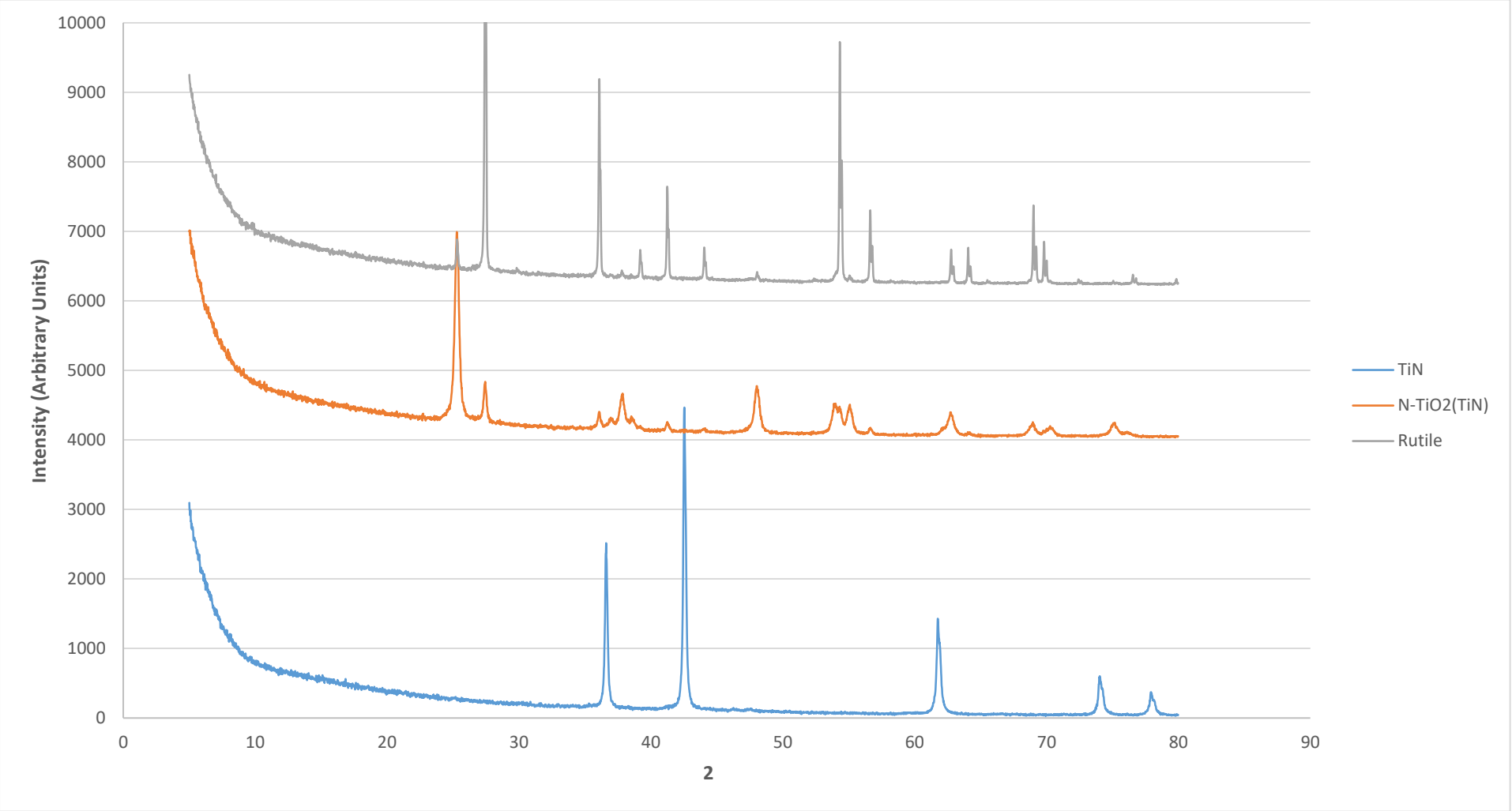

Figure 4.17: XRD analysis of N-TiO_2(TiN) and the starting precursor TiN and commercially bought rutile

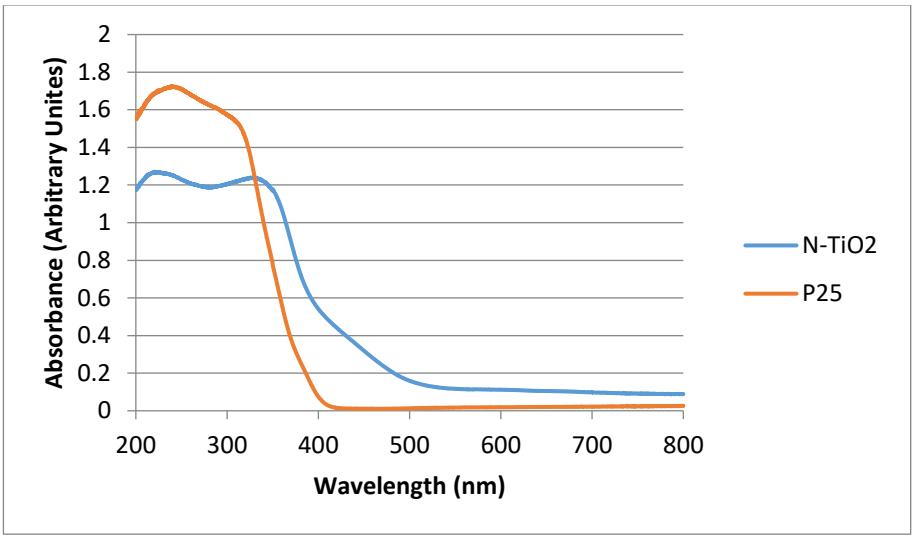

Figure 4.18: UV-visible DRS showing red-shift in adsorption edge of N-TiO_2(TiN) over P25

The XRD analysis also shows clear rutile peaks in the N-TiO_2(TiN) catalyst and a phase % was obtained from the software that showed the catalyst to be 86% anatase and 16% rutile. (**Table 4.10**).

Commercial anatase was also subjected to calcination in order to improve the photoactivity. In-situ XRD was carried out on a sample of commercial anatase to try and observe the temperature at which the phase change occurs.

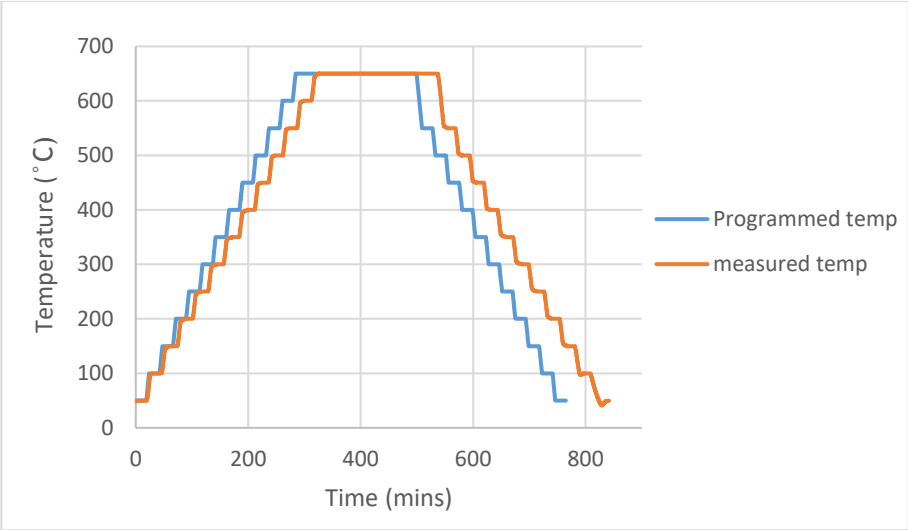

Figure 4.19: Temperature profile of in-situ XRD analysis showing programmed and measured temperatures.

Unfortunately, over the temperatures used during the in-situ XRD experiment there was no observable phase change in the anatase (**Figure 4.21**). What was observed was a slight sharpening of anatase peaks indicating an increase in crystallinity and an increase in crystallite size which is to be expected with extensive heating. It was not possible to reach temperatures above 850˚C due to limitations of the XRD unit cooling system. Nonetheless a final attempt at inducing a phase change in the commercial anatase was undertaken by heating in a tube furnace at 900˚C (**Figure 4.20**).

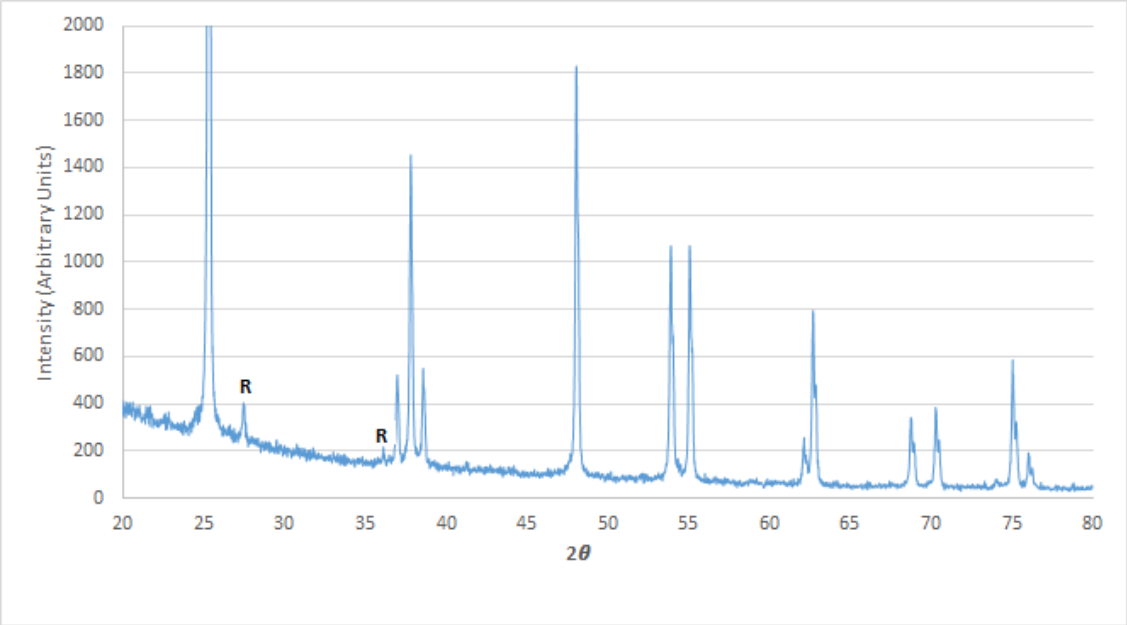

Figure 4.20: XRD analysis of anatase heated to 850 °C showing clear rutile peaks (denoted R).

Despite the introduction of rutile into the catalyst (**Figure 4.21**), the catalyst remained inactive for nitrate reduction on its own and was only very poorly active upon addition of 0.3% weight Au. (**Table 4.9**).

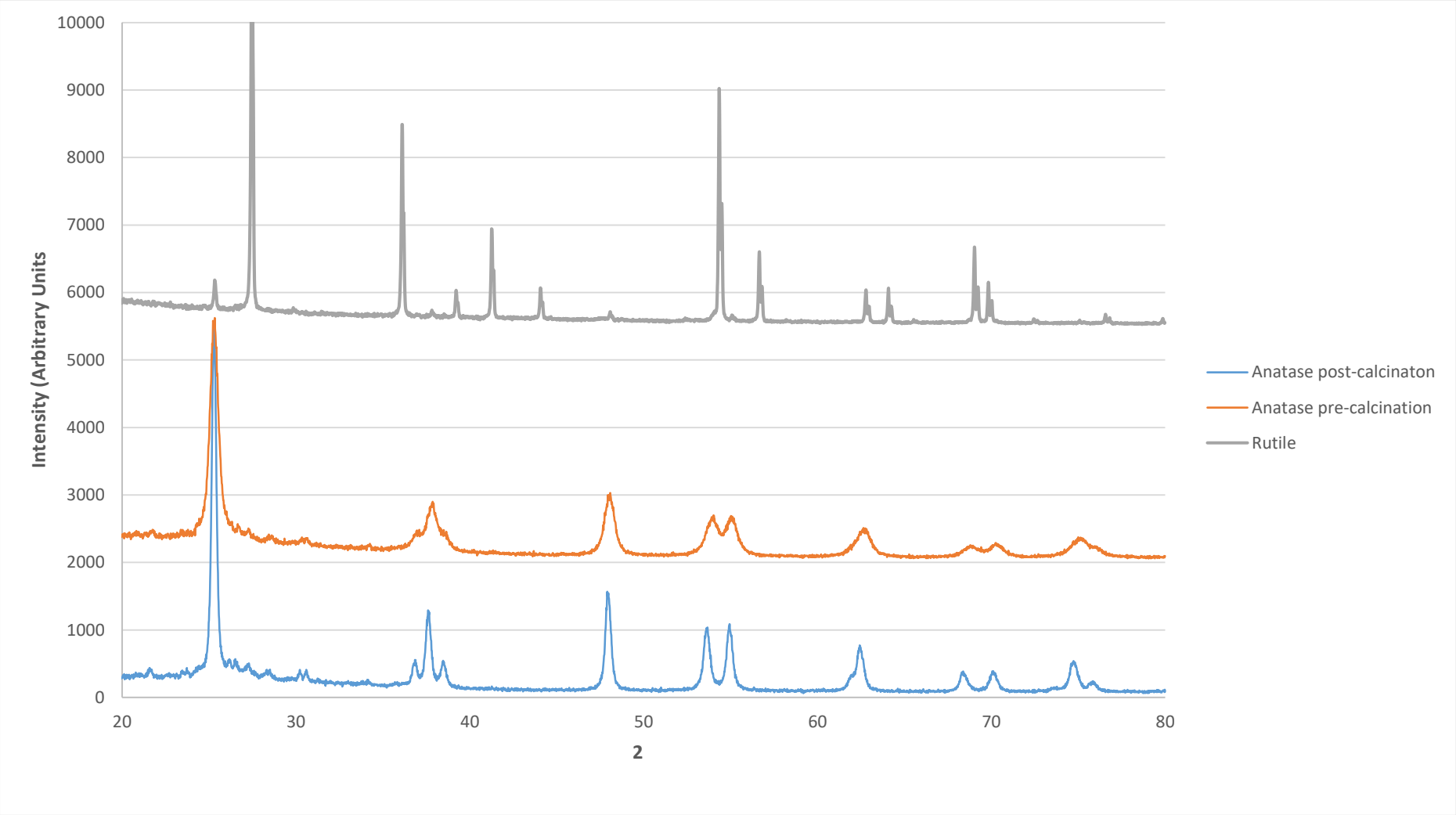

Figure 4.21: XRD analysis of anatase post-calcination and anatase at the end of the in-situ XRD heat-treatment programme

4.5 Conclusions

In conclusion, highly active Ag/TiO_2 catalysts were prepared using the optimised incipient wetness detailed in Chapter 3. The most active of these catalysts proved more active than the most active Au catalyst at similar loadings. The Ag/TiO_2 catalysts showed a tendency to produce significant amounts of nitrite during the early stages of reaction but showed a higher overall selectivity to N_2 after 3 h reaction time.

The activity of these catalysts showed a very similar dependency on metal weight loading to Au/TiO_2 catalysts with an optimum weight loading found to be at 0.4% wt Ag. The "switching off" of catalyst activity at high weight loadings (1% wt) must be due to a blocking of TiO_2 active sites with increased Ag loading by very small Ag nanoclusters as is the case with Au/TiO_2 catalysts as the presence of only large metal nanoparticles could not account for the lack of "baseline" activity associated with plain P25. This idea is supported by EDX analysis of "empty" areas of Ag/TiO_2 that show no visible sign of large particles. The EDX spectra showed the presence of Ag in these areas although sufficient resolution was not achieved to observe them.

Active Pd catalysts were made via the incipient wetness method but only upon reducing under flowing H_2. It was found that the activity of the reduced catalyst was lower than that of plain P25 indicating detrimental amounts of surface coverage by small Pd nanoparticles. Upon subsequent calcination the Pd catalysts were found to be active due to the sintering of small nanoparticles, reducing overlap and exposing TiO_2 surface sites. Active Cu/TiO_2 catalysts were synthesised by this same IW method and found to have activities above that of P25 with literature indicating that Cu exists as an oxide after IW treatment, indicating that TiO_2 can be improved by metal oxides as well as the metals themselves. Highest activity was achieved when Cu/TiO_2 was prepared using reduction rather than calcination showing that metallic deposits are generally more effective and improving the photo-activity of TiO_2.

No visible light activity was observed when using any $M\text{-}TiO_2$ catalyst showing that these catalysts improve the activity of TiO_2 by improving charge-carrier separation and not by extending the range of light available for photocatalysis.

Several bimetallic catalysts were tested with the most promising being AuAg/TiO_2 catalysts, the best-performing of which are more active than the best-performing monometallic equivalents and give 100% selectivity to N_2 at all stages of reaction.

Cl^- and SO_4^{2-} were investigated and found to be poisons for Au/TiO_2 catalysts due to competitive adsorption with nitrate. This limits the application of these systems to water systems that don't contain excessive levels of either of these species.

Efforts were made to improve the visible-light capabilities of TiO_2 by doping with N via two different methods. Partial oxidation of TiN was found to be the most effective method of N doping as the resultant material contained anatase and rutile TiO_2 phases in a ratio comparable to that of P25. The presence of N was inferred by a clear redshift in the adsorption spectra of the doped sample compared to P25 however no reproducible visible-light activity could be achieved.

4.6 References

[1] H-W Chen, Y Ku, Y-L Kuo, *Water Research*, **2007,** 41, 2069-2078

[2] A Zielińska-Jurek, A Zaleska, *Catalysis Today,* **2014**, 230,104–111

[3] A Zielińska-Jurek*, Journal of Nanomaterials*, 2014, 2014, 17

[4] Schneider, M. Wildberger, M. Maciejewski, D.G. Duff, T. Mallat, A. Baiker, *Journal of Catalysis*, **1994**, 148, 2, 625-638

[5] J K. Edwards, J Pritchard, M Piccinini, G Shaw,Q He, A FCarley, C J Kiely, G J. Hutchings *Journal of Catalysis,* **2012**, 292, 227–238

[6] S. Ichikawa, *Energy Convers Manage,* **1995**, 36, 613-616

[7] Z Wang, K Teramura, T Shishido, T Tanaka, *Top Catal*, **2014**, 57:975–983

[8] Naijia Guan, F Zhang,Y Li, X Zhang, Chen, H Zeng*, Langmuir,* **2003***,* 19, 8230-8234

[9] D James, M Bowker, L Millard, J Greaves, J Soares, *Gold Bulletin*, **2004**, 37, 3–4

[10] G J Hutchings, James H. Carter, Sultan Althahban, E Nowicka, S J Freakley, D J. Morgan,,P M. Shah, S Golunski, C J. Kiely.

[11] J Kennedy, W Jones, D J. Morgan, M Bowker, L Lu, C J. Kiely, P P. Wells, N Dimitratos, *ACS Catal*. **2016**, 6, 6623−6633

[12] Y Gogotsi,T Longenbach, M E Kurtoglu, *International Journal of Applied Glass Science*, **2011** , 2 , 108–116

[13] C Guillard, E Puzenat, H Lachheb, A Houas, J -M Herrmann, *Catalysis, Structure & Reactivity,* **2015,** 1, 1-9

[14] V.A. Lebedeva, D.A. Kozlova, I.V. Kolesnika, A.S. Poluboyarinova, A.E. Beceriklib, W. Grünertb, A.V. Garsheva, *Applied Catalysis B: Environmental,* 2016*,* 195, 39–47

[15] W Chen, Y Wang, Z Jin, C Feng, Z Wu, Z Zhang, *Sci China Ser B-Chem***, 2009**, 52, 8, 1164-1170

5.1 Conclusions

This project has shown that M-TiO_2 catalysts prepared by incipient wetness can be far more active than plain titania for the photoreduction of nitrate. XRD and BET analysis confirmed this effect was not due to changes in the TiO_2 support. It has been shown through visible-only experiments that the addition of these metals onto the semiconductor increase photocatalytic efficiency only by minimising charge-carrier recombination rates and not by increasing the range of visible light available to the catalyst via the SPR effect.

Optimisation of the Incipient Wetness method illustrated that the calcination temperature and metal loading were some of the more important variables with catalyst activities increasing to an optimum before decreasing in both cases. TEM and EDX analysis demonstrated that although very large metal nanoparticles exist on the catalyst (up to 50nm) the TiO_2 surface is covered with very small nanoclusters. These nanoclusters are used to explain the observed decrease or "switching off" of activity at higher metal loadings as increasing surface-coverage and increasing metal nanoparticle overlap leads to the blocking of TiO_2 surface sites. Optimal calcination temperatures are explained by the sintering of these nanoclusters to optimal sizes, freeing TiO_2 surface sites. Pd and Cu catalysts were also made via incipient wetness and found that even in their oxide form they can increase the activity of the catalyst to levels higher than that of P25, although not to the same extent as their metallic counterparts.

The potential real-world application of these catalysts was found to be limited by their susceptibility to poisons such as Cl^- and SO_4^- due to competitive adsorption of these anions with the target anion NO_3^-

Some promising results were obtained by using bimetallic catalysts, particularly AuAg/TiO_2, with this catalyst out-performing their monometallic equivalents in terms of both activity and selectivity at high metal loadings. At low metal loadings, anti-synergistic effects were observed between Au and Ag.

Efforts were made improve the visible-light capability of TiO_2 by N doping using a sol-gel method and a method involving the partial oxidation of TiN. XRD and UV-Vis DRS analysis showed this catalyst to have good photocatalytic properties such as a red-shifted adsorption edge and an anatase : rutile ratio similar to that of P25. Unfortunately no visible-only activity was observed reproducibly.

5.2 Future Work

Further TEM investigations in to the nature of the small nanoclusters formed when depositing metal on TiO_2 using IWwould be useful in explaining trends in both calcination temperature and metal loading. Further research into developing N-TiO_2 with the same surface area and phase-composition properties would also be very valuable. An example of this would be the immerging trend of doping P25 directly by heating under an atmosphere of NH_3 [1]. It seems likely then that a combination of N-doping, P25-like structural properties and metal doping could yield activity in the visible regime.

5.3 References

[1] W Chen, Y Wang, Z Jin, C Feng, Z Wu, Z Zhang, *Sci China Ser B-Chem*, **2009,** 52, 8, 1164-1170